Simulation of Ceramic Ware and Kiln Car Temperature Profiles for Analysing the Tunnel Kiln Process in the Production of Bricks and Roof tiles

Denny Mathew Alex

Simulation of Ceramic Ware and Kiln Car Temperature Profiles for Analysing the Tunnel Kiln Process in the Production of Bricks and Roof tiles

Dissertation
zur Erlangung des akademischen Grades

Doktoringenieur
(Dr.-Ing.)

von: M.Sc. Denny Mathew Alex
geb. am: 26.01.1992
in: Mandi, Indien

genehmigt durch die Fakultät für Verfahrens- und Systemtechnik
der Otto-von-Guericke-Universität Magdeburg

Promotionskommission
Prof. Dr.-Ing. Frank Beyrau (Vorsitz, OvGU)
Prof. Dr.-Ing. Eckehard Specht (Gutachter u. Betreuer, OvGU)
Prof. Dr.-Ing. Herbert Pfeifer (Gutachter, RWTH Aachen)
Dr.-Ing. Rigo Giese (Gutachter, IZF Essen e.V.)

eingereicht am: 23.05.2023
Promotionskolloquium am: 29.09.2023

Abstract

A model is developed to simulate the tunnel kiln process. The model of the roof tile tunnel kiln includes the heat transfer between the kiln car and the ware and also between the kiln car and the gas. The model requires the temperatures and mass flow rates of all the inputs like the ware, furniture, kiln car, fuel, and cooling air. The model also requires the output mass flow rate of the LTR and HTR and not the temperatures. The model can calculate the temperature profiles of the ware, the gas, and the kiln car in the tunnel kiln by solving ordinary differential equations. The ordinary differential equations of the ware, gas, and kiln car are solved using the ode solver in MATLAB.

The model simulated the firing curve of the brick and roof tile in two reference tunnel kilns. The simulations showed that the temperature profiles of the kiln car in the brick tunnel kiln and roof tile tunnel kiln are different. The residence time of the kin car in the tunnel kilns is the main reason for the different temperature profiles in the two tunnel kiln cars. The residence time in the roof tile kiln is 16.5 hours whereas in the brick kiln, it is 60 hours. In the brick kiln, the bottommost layer of the kiln car is heated to a temperature of 250°C at the exit of the tunnel kiln. The temperature of the bottommost layer of the kiln car throughout the tunnel kiln remains the same as its inlet temperature in a roof tile kiln. The radiative heat transfer coefficient between the kiln car and the roof tile is higher than between the kiln car and the brick. From the simulation of different arrangements of the bricks on the kiln car, a configuration of the bricks was simulated which had 48% less fuel consumption than another configuration for the same production rate in which the bricks are closely stacked.

The kiln car was found to be a major reason for the energy loss in the tunnel kiln process. The energy savings achieved in a tunnel kiln process without the kiln car can be more than 30%. To reduce the impact of the heavy kiln car on the tunnel kiln process, the idea of using carrier plates as a transportation system is investigated. The carrier plates transport the ceramic ware along the tunnel kiln on fixed ceramic rollers. The two reference tunnel kilns are re-simulated with the

transportation system as carrier plate which has the same physical characteristics as that which is used at the Brick and Tile Research Institute Essen (Institut für Ziegelforschung Essen e.V.). The firing curve of the brick and roof tile are recreated also for different thermal conductivity of the carrier plate. Removing the kiln cars entirely from the existing tunnel kilns is not cost-effective. Hence, another configuration was considered, where the ceramic rollers are fixed on the kiln car and the carrier plate will move on top of the ceramic rollers. This configuration enables the reduction of heat loss through the bottom of the tunnel kiln compared to the configuration without a kiln car.

Zusammenfassung

Es wurde ein Modell entwickelt, um den Tunnelofenprozess zu simulieren. Das Modell des Tunnelofens für Dachziegel umfasst die Wärmeübertragung zwischen dem Ofenwagen und der Ware sowie zwischen dem Ofenwagen und dem Gas. Das Modell benötigt die Temperaturen und Massenströme aller Inputs wie Ware, Transporthilfsmittel, Ofenwagen, Brennstoff und Kühlluft. Das Modell benötigt auch den Ausgangsmassendurchsatz des LTR und HTR und nicht die Temperaturen. Das Modell kann die Temperaturprofile der Ware, des Gases und des Ofenwagens im Tunnelofen durch Lösen der Differentialgleichungen berechnen. Die Differentialgleichungen für die Ware, das Gas und den Ofenwagen werden mit dem Ode-Solver in MATLAB gelöst.

Das Modell simulierte die Brennkurve des Ziegels und des Dachziegels in zwei Referenz-Tunnelöfen. Die Simulationen zeigten, dass die Temperaturprofile des Ofenwagens im Ziegeltunnelofen und im Dachziegeltunnelofen völlig unterschiedlich sind. Die Verweilzeit des Ofenwagens in den Tunnelöfen ist der Hauptgrund für die unterschiedlichen Temperaturprofile in den beiden Tunnelofenwagen. Die Verweilzeit im Dachziegelofen beträgt 16,5 Stunden, während sie im Ziegelofen 60 Stunden beträgt. Im Ziegelofen wird die unterste Schicht des Ofenwagens am Ausgang des Tunnelofens auf eine Temperatur von 250 °C aufgeheizt. Die Temperatur der untersten Schicht des Ofenwagens bleibt während des gesamten Dachziegeltunnelofens die gleiche wie die Eingangstemperatur. Der Strahlungswärmeübergangskoeffizient zwischen dem Ofenwagen und dem Dachziegel ist höher als zwischen dem Ofenwagen und dem Ziegel. Aus der Simulation verschiedener Anordnungen der Ziegel auf dem Ofenwagen wurde eine Konfiguration der Ziegel simuliert, die bei gleicher Produktionsrate 48 % weniger Brennstoff verbraucht als eine andere Konfiguration, bei der die Ziegel dicht gestapelt sind.

Es wurde festgestellt, dass der Ofenwagen ein Hauptgrund für den Energieverlust im Tunnelofenprozess ist. Die Energieeinsparungen, die in einem Tunnelofenprozess ohne Ofenwagen erzielt werden,

können mehr als 30 % betragen. Um die Auswirkungen des schweren Ofenwagens auf den Tunnelofenprozess zu verringern, wird die Idee untersucht, Trägerplatten als Transportsystem zu verwenden. Die Trägerplatten transportieren die keramische Ware entlang des Tunnelofens auf feststehenden Keramikrollen. Die beiden Referenz-Tunnelöfen werden mit dem Transportsystem als Trägerplatte nachgebildet, das die gleichen physikalischen Eigenschaften aufweist, wie sie im Institut für Ziegelforschung Essen e.V. verwendet werden. Die Brennkurve des Ziegels und des Dachziegels wird auch für unterschiedliche Wärmeleitfähigkeiten der Trägerplatte nachgebildet. Der komplette Ausbau des Ofenwagens aus den bestehenden Tunnelöfen ist nicht wirtschaftlich. Daher wurde eine andere Konfiguration in Betracht gezogen, bei der die Keramikrollen auf dem Ofenwagen befestigt sind und sich die Trägerplatte auf den Keramikrollen bewegt. Diese Konfiguration ermöglicht die Verringerung des Wärmeverlusts durch den Boden des Tunnelofens im Vergleich zur Konfiguration ohne Ofenwagen.

Contents

Nomenclature

Latin Symbol

A	Area	m^2
A	Coefficient in radiation	
B	Coefficient in radiation	
C	Coefficient for the kind of flow	
Config	Configuration	
$\dot{E}_b$	Emissive power of a black body	W/m^2
Gr	Grashofs number	
$\dot{H}$	Enthalpy flow	W
L	Mass-related air demand	$\frac{kg_L}{kg_f}$
L_c	Characteristic length	m
$\tilde{L}$	Volume-related air demand	m_L^3/m_f^3
$\dot{M}$	Mass flow rate	kg/s
Nu	Nusselt number	
Pr	Prandtl number	
$\dot{Q}$	Heat flow rate	W
R	Thermal resistance	$(m^2 \cdot K)/W$
Re	Reynolds number	
T	Temperature (Kelvin)	K
O	Mass-related oxygen demand	$\frac{kg_{O_2}}{kg_f}$
$\tilde{O}$	Volume-related oxygen demand	$m_{O_2}^3/m_f^3$
a	Length of rectangle	m
b	Breadth of rectangle	m
c	Specific heat capacity	$J/(kg \cdot K)$
c_p	Specific heat capacity (isobaric condition)	$J/(kg \cdot K)$
d_h	Hydraulic diameter	m
h_u	Specific heating value	J/kg
Δh_{vap}	Vaporization enthalpy of water	J/kg
h	Heat transfer coefficient	$W/(m^2 \cdot K)$
l	Length	m

p	Absolute pressure	bar
p_i	Partial pressure	bar
$\dot{q}$	Heat flux	W/m²
s_{eq}	Beam length	m
t	Time	s
v	Velocity	m/s
x_i	Mass fraction of gas component i	
$\tilde{x}_i$	Volume fraction of gas component i	

Greek symbol

Δ	Difference	
α	Heat transfer coefficient	W/(m²·K)
β_T	Thermal volumetric coefficient	
ε	Emissivity	
φ	View factor	
λ	Air demand	
λ	Thermal conductivity	W/(m·K)
ϑ	Temperature (Celsius)	°C
ρ	Density	kg/m³
ρ	Reflectivity	
σ	Stefan-Boltzmann constant	W/(m²·K⁴)
τ	Transmittivity	
ν	Kinematic viscosity	m²/s
χ	Transient factor	
∞	Flow	

Indices and abbreviations

b	Brick
Cal	Calorific temperature
Cond	Conduction
Conv	Convection
eff	Effective
f	Fuel

g	Gas
G	Gas
HT	High temperature
HTR	High temperature recovery
KC	Kiln car
L	Air
lam	Laminar
LT	Low temperature
LTR	Low temperature recovery
m	Exponent for Reynolds number
m	Number of carbon atoms in hydrocarbon molecule
n	Exponent for Prandtl number
n	Number of hydrogen atoms in hydrocarbon molecule
Rad	Radiation
S	Solid
s	Surface
s	Thickness
TS	Transportation System
turb	Turbulence
Z	Roof tile

1 Introduction

A tunnel kiln is used in the last stage of the production of bricks and roof tiles. As seen in the flowchart in **Figure 1-1**, a tunnel kiln is used in the firing stage, to heat the dried bricks and roof tiles to temperatures more than 900 °C. A tunnel kiln can be described as a rectangular chamber with a height of more than 3 m, a width of more than 6 m, and a length of more than 100 m. The bricks and roof tiles (wares) with the help of support structures called furniture are stacked on top of a kiln car which is guided on rail tracks, to transport the wares through the tunnel kiln.

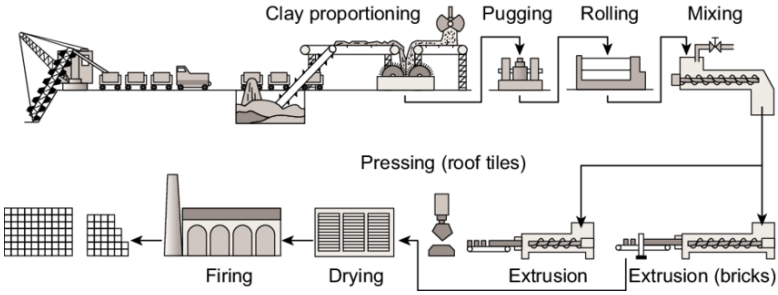

Figure 1-1 Flowchart of a modern brick and roof tile manufacturing plant [1]

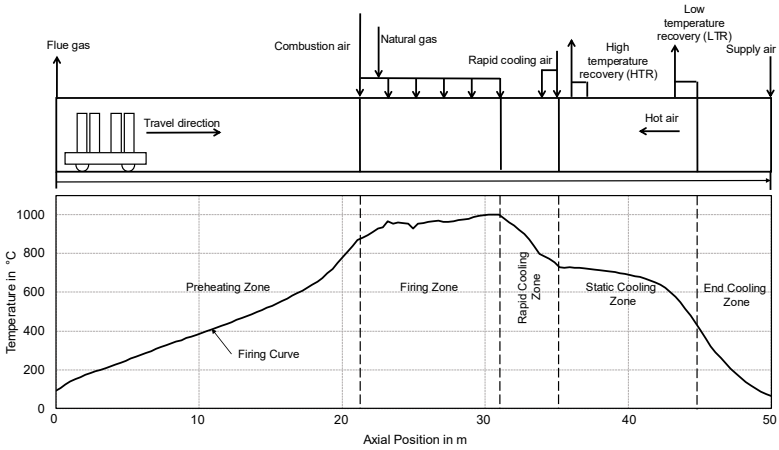

Figure 1-2 Tunnel kiln process and firing curve of the ware

Figure 1-2 shows the process diagram of the tunnel kiln along with the temperature profile of the ware along the kiln. The temperature profile of the ware along the tunnel kiln as shown in Figure 1-2 is known as the firing curve and this temperature profile has to be replicated in each of the ware to maintain the product quality irrespective of the production rate.

In the tunnel kiln, the wares which are to be fired enter through the entrance of the tunnel kiln whereas the air is injected at the exit of the tunnel kiln. The hot air moves in a direction from the exit of the tunnel to the entrance of the tunnel kiln. In the tunnel kiln, there are three predominant zones namely preheating zone, firing zone, and cooling zone. In the preheating zone, the ware is heated up to temperatures of 800 °C by the exchange of heat from the flue gas coming from the firing zone. In the preheating zone, the moisture from the ware comes out when the temperature is around 120 °C and in the temperature range of 300 °C to 500 °C, oxidation of the organic matter takes place if they are present. The crystal water which is combined within the structure of the clay minerals is released when the temperature is between 500 °C and 650 °C. Finally, when the temperature is between 650 °C to 800 °C, the disassociation of the calcite and dolomite takes place to release carbon dioxide which is called process emission. In the firing zone where temperatures are between 950 °C to 1300 °C (depending upon the ware this highest temperature changes), sintering takes place where the breakdown of the lattice structure of the original clay minerals, followed by the formation of new crystalline compounds and glassy phases. The energy in the firing zone is mainly delivered by the combustion of natural gas.

In the cooling zone, wares are cooled by lower-temperature air which is blown from the exit of the tunnel kiln. The cooling zone is divided into three different sub zones namely rapid cooling zone, static cooling zone, and end cooling zone. 1300 °C to 700 °C is the temperature range in the rapid cooling zone where the air at ambient temperature is fed into the tunnel kiln to prevent low valance Fe to be oxidized. In the static cooling zone where the temperature range is around 700 °C to 400 °C, the cooling rate of the product is low to avoid crack formation

due to quartz inversion. In the end cooling zone, the product is cooled from 400 °C to the desired outlet temperature of the product by ambient air which is blown from the exit of the tunnel kiln. Low-temperature recovery (LTR) means the removal of air from the start of the end cooling zone to lower the cooling rate of the product in the static cooling zone. High temperature recovery (HTR) is the removal of air at the starting of the static cooling zone before the addition of ambient air to increase the cooling rate in the rapid cooling zone.

According to a study about different kinds of kilns used for the production of brick in South Asia [2], the quality of the product from the tunnel kiln is superior to the products produced in the other kinds of kiln. In addition to the product quality, tunnel kiln allows high production capacity. The study also found that the tunnel kiln performed better in producing less particulate matter than the other kilns. Tunnel kilns were found to take a much higher amortization period than the other type of kilns in addition to the high specific energy consumption which is also confirmed in a study by Z. Zhang [3]. **Table 1-1** lists the findings about the different kinds of brick-producing kilns in South Asia. I. Gonzalez et al. [4] found that the emissions of fluorine, chlorine, and sulphur are lesser in tunnel kilns than in Hoffman kilns which are operated in the Andalusian region in Spain.

Table 1-1 Quality assessment of various brick making technologies commonly used in South Asia [2]

Kiln Type	Partic-ulate matter	CO	Specific energy consump-tion for firing	Quality of fired product	Ability to fire hollow bricks	Return on Investment
DDK	+	+	+	++	++	++
FCBTK	+	++	++	++	++	++
Zig - zag kiln	++	++	++	++	++	++
Tunnel Kiln	+++	++	++	+++	+++	+
VSBK	+++	++	+++	+	+	++

+++ Denotes the best performance in the category; DDK - Down-Draft Kiln; FCBTK - Fixed chimney Bull's trench kiln; VSBK - Vertical shaft brick kiln.

In Germany, the annual energy requirement of the tunnel kiln is approximately 18 GWh and the total emissions from the German Brick and Tile Industry is about 1.73 million tonnes of CO_2, including the process emission [5]. The different kinds of thermal energy loss from a tunnel kiln are represented as a Sankey Diagram from an analytical perspective and are depicted in **Figure 1-3**. The main energy loss which is considered as the hot air extracted as low temperature recovery and high temperature recovery. This air is directed to the dryer when the dryer is operational. The tunnel kiln operates continuously whereas the dryer is operational during the weekday and hence the dryer cannot use the hot air from the tunnel kiln continuously. Therefore, the hot air from LTR and HTR can be considered as heat loss. The heat lost through the tunnel kiln as flue gas corresponds to the next main loss with heat lost through the walls of the tunnel kiln being about 10% - 14%. The other main losses are the heat lost through the ware and the furniture, the kiln car, and the endothermic reactions inside the ware in the preheating zone.

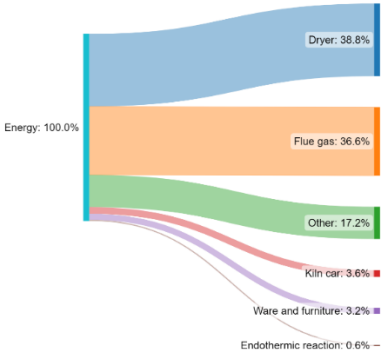

Figure 1-3 Energy loss from a tunnel kiln (Source: Brick and Tile Research Institute Essen)

The advantages of the tunnel kiln such as a highly mechanised system that reduces the labour requirement, low pollution, and most importantly high product quality make tunnel kiln favourable to other types of kilns. Even though the amortization period is high, the

advantages far outweigh the disadvantage. The aim to become carbon neutral by 2050 and the high price of natural gas [6] have caused the need for tunnel kilns to improve their thermal efficiency.

Tunnel kilns are very expensive to build and maintain, hence a scaled-down experimental setup is also expensive. Even if an experimental setup is built, the firing time for a brick is 60 hours whereas, for a roof tile, it is 12 hours to 16 hours which means that for the setup to reach a thermal steady state after parameter change will be very long. To avoid the disadvantages of the expensive experimental setup and long duration to gather experimental data; thermal modeling of the tunnel kiln is preferred. A verified and validated model of the tunnel kiln incorporates all the mechanisms of energy exchange between the ware, the gas, the kiln car, and the ambient air outside the tunnel kiln. The model helps to conduct the energy auditing of the tunnel kiln to determine energy loss through each of the outflows from the tunnel kiln like flue gas, kiln car, ware and furniture, and through LTR and HTR. The model can be further used for the parameter study or finding the influence of new material with new physical properties like low-density material for the furniture on the firing curve to save energy. Since many of the tunnel kilns operate for a long time; more than 40 years and the knowledge about the working is mostly passed from one generation of workers to another generation of workers within the industry through manual trial and error method. This leads to difficulty in training new workers and loss of product and cost the industry time and money. Models can help the workers to understand the working of the tunnel kiln in a virtual environment before working on the actual kiln. Modeling of the tunnel kiln is advantageous for the manufactures of tunnel kilns and its auxiliary units like kiln cars and furniture as well as for the owners of the tunnel kilns.

2 Literature Review

2.1 Models without kiln car

N. Soussi et al. [7] modeled a tunnel kiln producing bricks which is shown in **Figure 2-1** and has a length of 117.45 m. The bricks from the dryer with a moisture content of 4% enter the pre-kiln where the cooling air extracted through E1, E2, E3, E4, E5, and E6 is injected. After the elimination of moisture in the brick because of the temperature increase of the brick in the pre-kiln and preheating zone, the bricks are heated to a temperature of 900°C in the firing zone. In the firing zone, there are 12 groups of top burners with 10 burners in each group. After the firing zone, the bricks undergo a fast and then final cooling to reach the desired exit temperature of 30°C to 60°C.

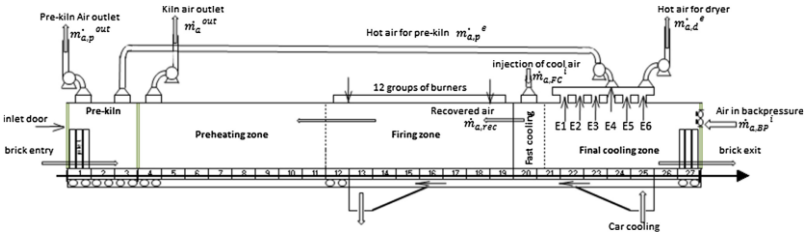

Figure 2-1 Modelled tunnel kiln schematic [7]

The kiln is modeled with ordinary differential equations for the gas and the brick. The gas has different ordinary differential equations in all the different zones in the tunnel kiln. In the pre-kiln and preheating zone, the ordinary differential equation has the heat lost due to the evaporation of water from the brick whereas in the firing zone, the heat released by the combustion of natural gas is added to the ordinary differential equation. In the cooling zone, the heat as a source and sink term is added because of the injection and extraction of cooling air. The ordinary differential equation of the brick has only the heat transferred by convection between the brick and gas and the heat transferred to the kiln interior walls by radiation. The ordinary differential equations are solved using numerical code developed with the SCILAB program and are based on the finite difference method.

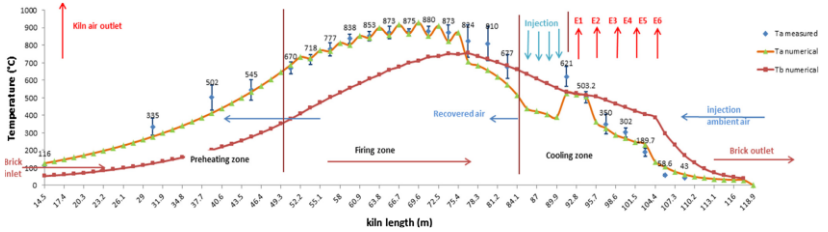

Figure 2-2 Measured and simulated temperature profile [7]

The result from the paper is shown in **Figure 2-2** and is validated with the measured gas temperature and the numerically simulated gas temperature. The simulated temperature values are almost the same as that of the measured values even though the radiative heat exchange between the gas and the brick is neglected.

The preheating zone of a brick producing tunnel kiln was modeled by E. Mancuhan et al. [8]. The ordinary differential equation of the gas in the preheating zone represents the heat loss from the gas as the heat exchange by convection to the brick and wall. The equation contains the heat lost due to evaporation and the heat taken by the evaporated water. The ordinary differential equation of the brick contains the heat gained by the brick through convective heat transfer from gas to brick. The ordinary differential equations are solved by shooting method using the solver in Excel. The initial conditions are the inlet temperature of the brick which is 30°C and the inlet temperature of the gas to the preheating zone from the firing zone which is 750°C. **Figure 2-3** shows the measured temperature of the gas (Tmeasured) and the simulated temperature of the gas (Tg model) and the brick (Tb model). A sudden decrease in the temperature of the gas between 20% and 50% of the dimensionless length is because of the addition of ambient air in the preheating zone.

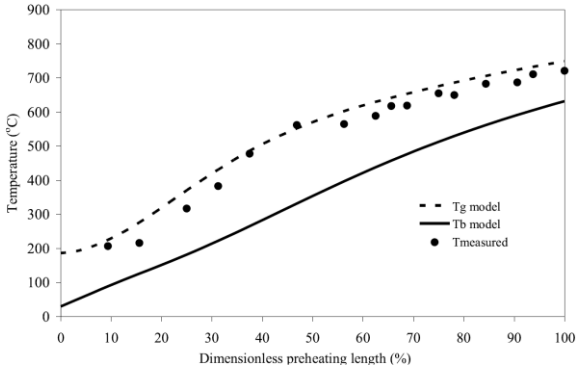

Figure 2-3 Comparison of the measured temperatures to the computed gas and brick temperatures [8]

S. Kaya et al. [9,10] using the same method as E. Mancuhan et al. [8] modeled the cooling zone [9] and firing zone [10] of a brick producing tunnel kiln. In the cooling zone, as seen in the left graph in **Figure 2-4**, the measured temperature (T kiln) especially between 0% to 30% of the dimensionless length does not represent the temperature of the gas or the brick but a mix of the temperatures of gas and brick. For a length of more than 50% of the dimensionless length, the measured temperature tends to be similar to the simulated gas temperature. This is also visible in the 70% to 100% of the dimensionless length in the firing zone as seen in the right graph in Figure 2-4. The error in the measurement of the gas in the tunnel kiln would have aroused because of an exposed thermocouple without radiation shield. The measurement of the thermocouple would have been interfered by the radiation from the brick [11].

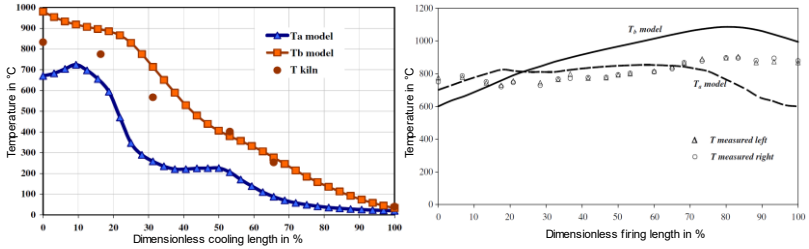

Figure 2-4 Measured and simulated temperatures of gas and simulated temperature of brick in the cooling zone [9] (left) and firing zone [10] (right)

A tunnel kiln producing brick, whose experimental measurements are documented in a master thesis [12], is used for the numerical simulation by M.F. Naccache et al. [13]. The simulation is performed for a two-dimensional horizontal plane of the tunnel kiln in the commercial software Fluent (Fluent Inc.). In the simulation, the temperature of the combustion gas in the firing zone is not calculated but explicitly given in addition to the convective heat transfer coefficient from the external wall of the kiln a value of 10 W/m^{2}K. The study compares only the gas temperature fields in the horizontal plane with the experimental result which is shown in **Figure 2-5**. The numerically simulated temperature along the tunnel kiln at a position near the wall (Case 1 y = 0.55 m) and at a position at the centre of the kiln (Case 2 y = 1.225 m) are depicted in Figure 2-5. The experimental results which are depicted as a red line are obtained with thermocouples located at the right kiln wall. The paper does not explain the reasons for the huge discrepancy between the measured and simulated temperature profiles of the gas.

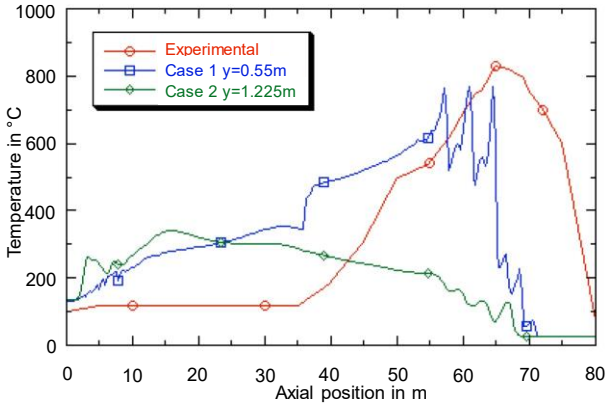

Figure 2-5 Comparison of the numerical result with the experimental result [13]

A.H. Tehzeeb et al. [14] used the tunnel kiln dimensions and flow rates from P. Meng [15] to simulate it using ANSYS CFX. Only one-sixth of the kiln width was simulated and the temperature of the brick was given as an initial condition. In this study, a combination of models was applied to model turbulence, NO emission, radiation, and combustion. A grid independence study for the simulation was missing along with the details on the computational time.

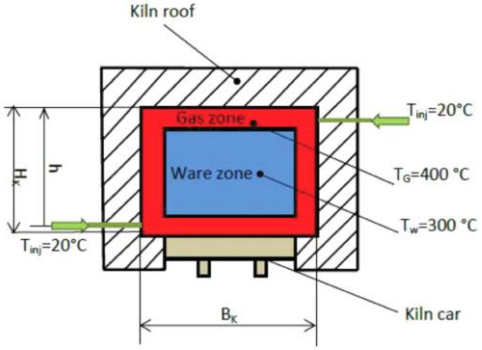

Figure 2-6 Tunnel kiln transverse section between two kiln cars with injection [16]

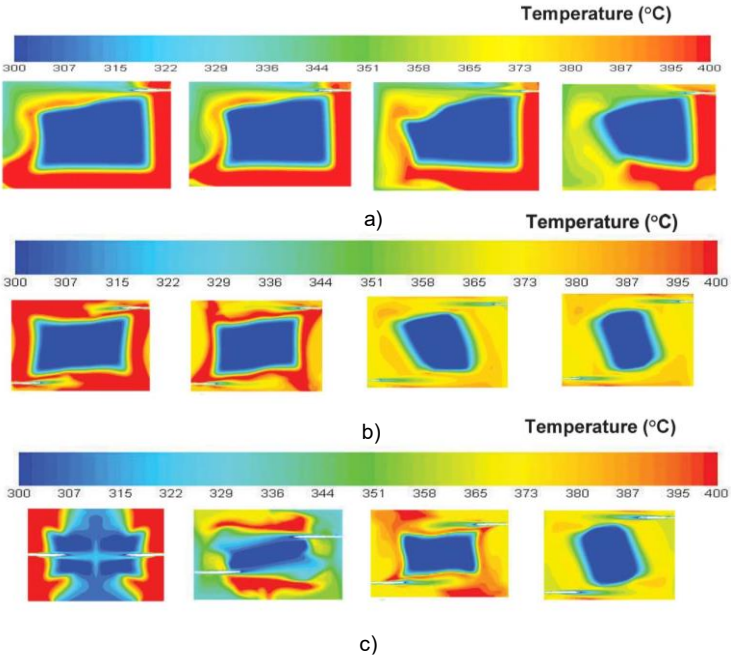

Figure 2-7 Temperature distribution for various injection velocities with **a)** one nozzle **b)** two nozzle and **c)** various nozzle positions [16]

Al-Hasnawi et al. [16] did a CFD simulation using FLUENT for the cross-section of the tunnel kiln as shown in **Figure 2-6**. The gas zone represents the gas that is flowing between the ware and the walls and between the ware and the kiln car. The ware zone represents the gas that flows in between the ware which has a lower velocity than the gas in the gas zone. The nozzles which inject air are kept in between the kiln car gap and on the side walls. The aim was to study the mixing of gas when injected between two kiln cars to create a homogeneous temperature distribution in the vertical direction. When one nozzle is used as seen in **Figure 2-7 a**, an increase in the injection velocity (diagram to the right) leads to uneven temperature distribution along the width of the tunnel kiln. When two nozzles are used as seen in **Figure 2-7 b**, an increase in the injection velocity (diagram to the right) leads to a decrease in the area with a temperature of 300 °C. **Figure**

2-7 c, shows the influence of the position of the two nozzles with the same air injection velocity. The most effective position of the two nozzles is when H_R (H_R=h/H_K; h is the distance of burner from the roof; H_K is the height of the tunnel kiln) is greater than 0.7 (diagram to the right).

H.A. Rafaey [17] did a theoretical study where a one dimensional mathematical model of tunnel kiln is developed to predict the gas and solid temperature profiles in the preheating and firing zone. The ordinary differential equations developed for the gas and the solid are solved using a bvp4c solver in MATLAB. The model simulated temperature profiles of the solid and gas for three different cases. Case A is with zero firing length, Case B is with zero preheating zone and Case C has equal length of preheating and firing zone. The total length of the tunnel kiln remains same in all the three cases which is equal to 50 m. It was found out that the length of the firing zone influences the energy consumption and the firing length should be as short as possible for low energy consumption.

T. Redemann [18] modeled a tunnel kiln producing roof tile using Euler's method to solve the differential equations for the tunnel kiln. The model was validated with industrial measurements but the kiln car mass was approximated as a thermally active mass of the kiln car. Approximately 37% of the mass of the kiln car was added to the mass of the roof tiles and cassette. The model did not include the thermal interactions like radiation between the kiln car and the roof tile and also convection and radiation between the kiln car and gas.

S. Vogt and K. Nover [19] calculated the overall heat transfer coefficient between the gas and the brick setting on the kiln car in the tunnel kiln. The effective heat transfer coefficients were calculated for different kinds of settings of bricks on the kiln car. As seen in the left diagram in **Figure 2-8**, the effective heat transfer coefficient was calculated with models for convection by Abbakumov [20], gas radiation by Elgeti [21], and heat conduction by Jeschar [22]. The actual and modeled effective heat transfer coefficients along the tunnel kiln with compact brick setting are shown on the right side of Figure

2-8. The maximum variation in the modeled value to the actual effective heat transfer coefficient is 20% and the difference is more predominant in the firing zone and the cooling zone. Abbakumov [23] empirically showed that the best setting of bricks on a kiln car is a 7 to 8 column setting with a column thickness of 1 standard brick.

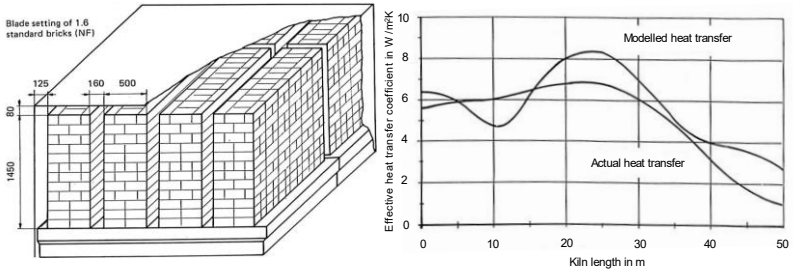

Figure 2-8 Compact setting pattern (left); Comparison of actual and model heat transfer the compact setting (right) [19]

2.2 Models with kiln car

V. P. Nicolau and A. P. Dadam [24] developed a model which is based on the application of mass and energy conservation equations in the integral form for a tunnel kiln. The numerical code was implemented using the FORTRAN language. The model included the heat conduction and radiation between the ware and the kiln car in addition to the convection between the gas and the kiln car. The heat conduction through the kiln car was also considered along with the heat transfer between the gas and the ware and the heat transfer from inside the tunnel kiln to the outside air through the kiln walls. The model was validated with the gas temperatures for an industrial tunnel kiln as shown in the left side of **Figure 2-9**. The inner temperature profile of the ware along the tunnel kiln for different internal area ratios A_{int} is shown on the right side of Figure 2-9. The internal area ratio is the ratio between the inner load area which is the load's internal area in contact with the internal flow to the external area of the setting. For small A_{int} = 0.001, the central point inside the setting takes at least 10 m to initiate the heating process and the cooling takes longer where the outlet temperature is around 350 °C. The temperature profile of the kiln car

along the tunnel kiln was not depicted in the paper even though the model takes into account the interaction of the ware and gas with the kiln car.

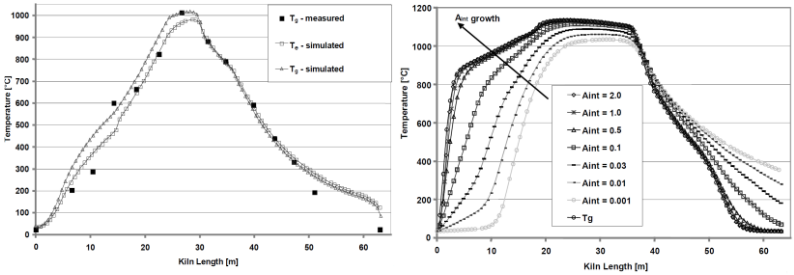

Figure 2-9 Validation of the model with gas temperature in the tunnel kiln (left); Temperature distribution inside the load for different internal air ratios (right) [24]

R. Oba et al. [25] simulated a tunnel kiln producing white tiles using natural gas as fuel. The numerical code was developed in FORTRAN and is based on the finite volume method. The heat transfer which is considered in the model is depicted in **Figure 2-10**. The heat is transferred from the ceramic load to the furniture which is also the kiln car by conduction. The model neglects the convective and radiative heat transfer between the gas and kiln car. The solid-to-solid radiation between the kiln car and the ceramic load is also not taken into consideration. The model was not validated with a measurement from industry but simulated the temperature profiles of the gas and ware for two different mass flow rates of fuel. Even though the heat conduction through the kiln car is included in the model, an explanation or depiction of the kiln car temperature profile was not presented in the paper.

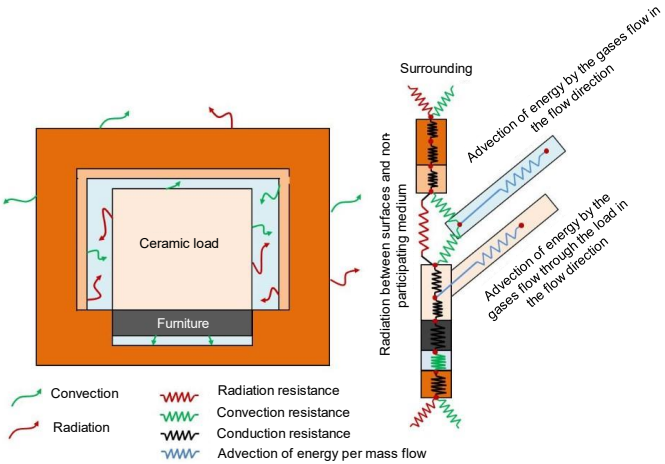

Figure 2-10 Heat transfers and thermal resistances in a transverse section of the furnace [25]

R. Oba et al. [26] modeled a tunnel kiln producing roof tiles using the method explained in the paper by the same author R. Oba [25]. In the model, the Navier-Stokes equation was not solved instead a flow is prescribed in the kiln through a known velocity field. This simplification was done to reduce the computational cost because of the large dimension of the tunnel kiln. Another assumption of the model was that the radiation effect of the gas inside the gas was not taken into account. **Figure 2-11** compares the simulated temperature of the gas and load with the measured temperature of the gas. The maximum difference in the measured and simulated temperature of the gas is about 33% and is in the firing zone.

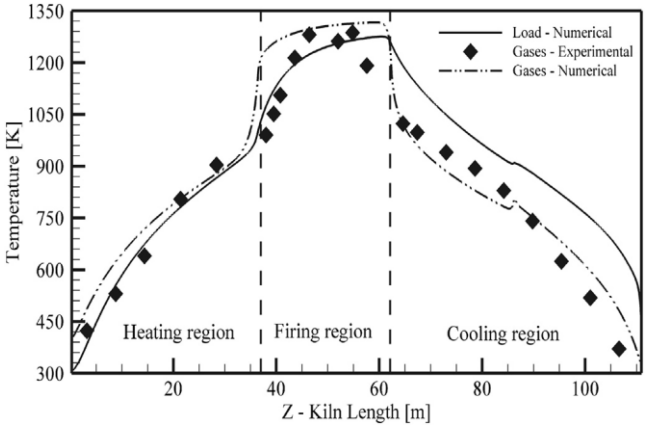

Figure 2-11 Simulated temperature profile of the load and gas along the tunnel kiln with the measured mean gas temperature near the load surface [26]

B. Yu [27] proposed a mathematical model based on the transient heat conduction in the wares and the lining bricks of kiln cars. The gas temperature and the oxygen concentration in the tunnel kiln for the program were given as known quantities. The heat stored by the ware and the lining brick of the kiln car for a 72 m tunnel kiln with 40 kiln cars was investigated in the paper. Three different types of lining bricks of the kiln car were considered in the study and they are depicted in the left figure of **Figure 2-12**. The right side of Figure 2-12 shows that at the exit of the tunnel kiln, the amount of heat storage in lining brick structure 1 is much more than that in the other structures, 2 and 3. This means that when the car is pushed out from the kiln, much more energy will be wasted using a lining brick structure 1 than using the other structures. The validation of the model was done with respect to the measurements from the tunnel kiln mentioned in another paper [28].

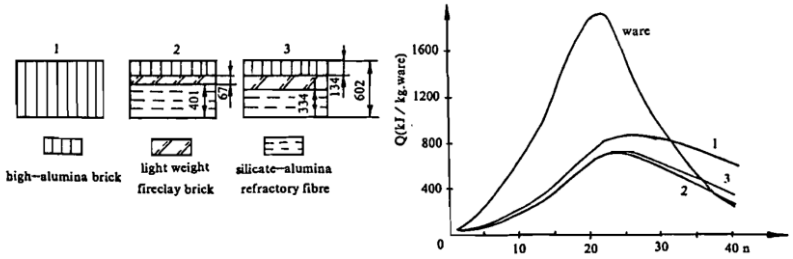

Figure 2-12 Three kinds of lining brick for kiln car (left); Heat storage of different brick linings for kiln car and ware for various kiln car positions (right) [27]

A theoretical study on the thermal behaviour of the tunnel kiln car was done by H. Hagens et al.[29]. **Figure 2-13** shows the amount of heat stored by a two-course kiln car as a function of the thickness (S_1) of the top layer of the kiln car, at the points in time $t=t_D/2$ and $t=t_D$. The curves are based on the sinusoidal time history of the surface temperature of a kiln car with a peak temperature of 1000 °C and a kiln passage time, t_D, of 40 hours. The two kinds of materials used are defined by the physical characteristics where material A has a thermal conductivity of 2 W/m·K and density of 2000 kg/m^3 whereas material B has a thermal conductivity of 0.2 W/m·K and density of 200 kg/m^3. Two cases have been theoretically studied where the thickness of the top layer was changed from 0 to the kiln car thickness of 0.6 m. Case I (heavy material at the top) was when material A was the top layer and Case II (heavy material at the bottom) was when material B was the top layer. As seen in Figure 2-13, when the thickness (S_1) of the top layer increases, the heat storage increases in case I (heavy material at the top) and decreases in case II (heavy material at the bottom). For cases I and II when the thickness is at 0.15, the heat stored by the two different kiln cars is the same at the exit of the kiln, $t=t_D$. At the point in time $t=t_D/2$, however, the heat content of the case I car is more than five times that of the case II car. It means that the case I car accumulates and releases more energy than the case II car. This shows that the thermal evaluation of the kiln car cannot be solely on the exit energy losses of the kiln car.

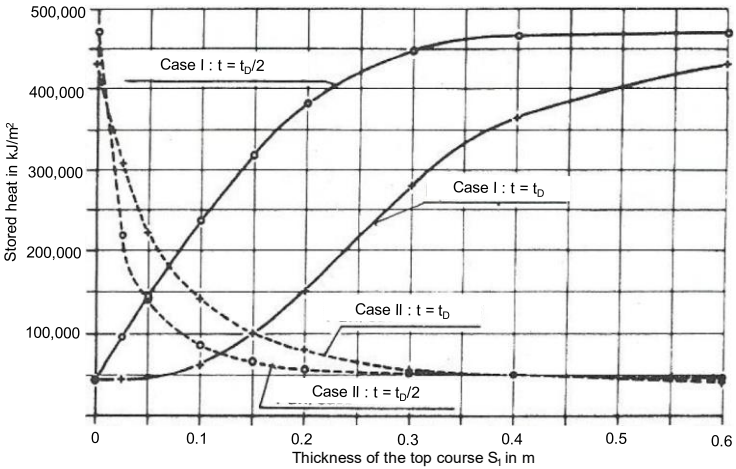

Figure 2-13 Amount of heat stored by a two-course tunnel kiln car with an adiabatic underside, as a function of the upper layer thickness S_1 [29]

While modeling the tunnel kiln process, 30% to 60% of the mass of the kiln car is considered to be taking part in the tunnel kiln process and the specific heat capacity is also considered as a temperature independent. H. Hagens et al. [30] explained why considering a part of the mass of the tunnel kiln car into the mass of the ware and the furniture while modeling the tunnel kiln is not the right way to study the influence of the kiln car on the process. The theoretical and actual heat storage of the kiln car is shown on the left side of **Figure 2-14** and the ratio of the actual heat storage and the theoretical heat storage is shown on the right side of the same figure. It can be seen that at the end of the firing zone (Time > 8 hours), the ratio γ becomes more than 1. This happens when the mean temperatures in the kiln car exceed the mean temperature in the tunnel kiln chamber. This shows that taking a constant factor for the mass of tunnel kiln car for the energy balance of a tunnel kiln leads to false results.

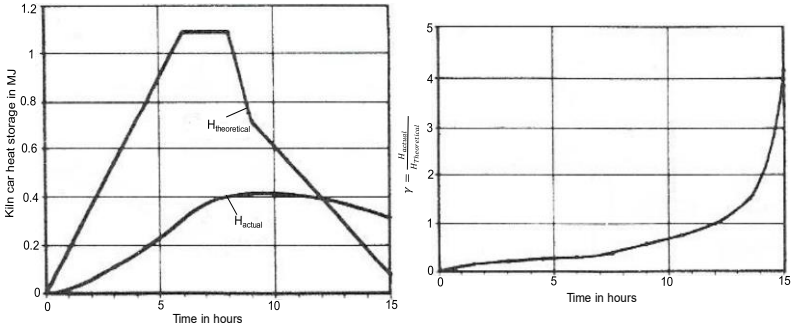

Figure 2-14 Theoretical heat storage $H_{theoretical}$ and actual heat storage H_{actual} in the tunnel kiln car (left); Time-dependent ratio γ of the actual to theoretical heat storage in the tunnel kiln car (right) [30]

H. Hagens [31] created a computer program that can predict the temperature inside the tunnel kiln car during its operation in the tunnel kiln. The measured data of the temperature inside the kiln car of the tunnel kiln is the input for calculating the temperature of the gas in the tunnel kiln. For the same tunnel kiln with a different kiln car design, the calculated temperature of the gas is used to predict the temperature of the kiln car with the new design. As shown in **Figure 2-15**, the lightweight kiln car (B) absorbs less heat in the preheating zone as compared to a heavy kiln car (A). In the cooling zone, the lightweight kiln car (B) gives less heat to the air than the heavy kiln car (A). This shows that the interaction between the kiln car and the process is more important for the design of the kiln car than the overall energy balance.

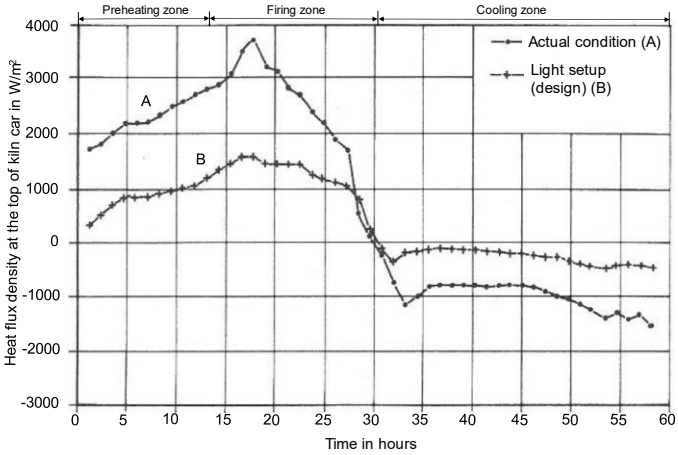

Figure 2-15 Change of the heat flux density through the top of the kiln car after optimization of the car design [31]

Y. Zhang et al. [32] simulated the temperature profiles inside the kiln car along its journey through the tunnel kiln. Partial differential equations were derived for the kiln car which was solved using the finite difference method in MATLAB. The input for solving the partial differential equation was the gas temperature profile along the tunnel kiln. The gas temperature is used for the calculation of the convective heat transfer and the radiative heat transfer between the kiln car and the gas. The temperature profiles inside the kiln car for different depths along the kiln car are shown in **Figure 2-16**. The temperature profile for x = 0.45 m is the temperature of the top of the kiln car. This profile is almost similar and equal to the gas temperature profile in the preheating and firing zone but not in the cooling zone. The temperature of the bottom layer of the kiln car which is shown by the profile x = 0 m, gradually increases its temperature in the preheating and firing zone. This is because of the heat conduction from the top of the kiln car and in the cooling zone, the temperature remains constant and comes out with a temperature of 700 K. Even though the model is able to simulate the inside temperature of the kiln car, the model has the disadvantage that it needs the gas temperature profile as the input. The second disadvantage is that the heat transfer between the ceramic ware and

the kiln car is not included in the model. Depending upon the ceramic ware which is produced, the radiative heat transfer between the kiln car and ware will be different.

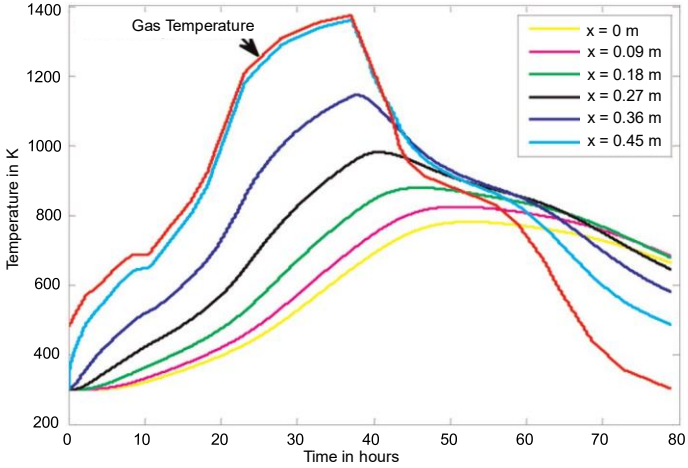

Figure 2-16 Calculated axial temperature profile for different depths in tunnel kiln car as it moves through the tunnel kiln [32]

2.3 Conclusion from literature review

From the literature review, it can be seen that in the models of the tunnel kiln, the kiln car is approximated as an additional mass flow rate to the ware. The heat exchanges between the kiln car with the gas and the ware are neglected in these models. Even when the kiln car is considered, then the temperature of the gas has to be given as a starting input condition to get the thermal behaviour of the kiln car. In this work, the model incorporates the heat exchange between the kiln car, ware and furniture, and gas separately. The input variables in this model are the mass flow rates of the ware, furniture, and kiln car and their respective inlet temperatures. The model also requires the inlet mass flow rate and temperatures of the supply air, rapid cooling air, combustion air, and fuel. The information required from the outlet flows is the outlet mass flow rates of LTR and HTR.

3 Modeling the Heat Transfer and Combustion

3.1 Geometry Simplifications

Figure 3-1 shows a typical setting of roof tiles. Each roof tile is kept on a H-cassette and they are together stacked to form the configuration on the kiln car. Each stack has a total of 16 rows of roof tile and cassette which are stacked one on top of the other and 17 columns along the breadth of the kiln car. In total, there are 4 stacks on the kiln car, where two stacks are near to each other whereas the rest of the stacks are far from the first two stacks to create a gap known as a firing dyke. A firing dyke is the separation between the first two stacks and the last two stacks on the kiln car and it's needed so as to allow the flame from the burners to be directed in the gap rather than hitting the roof tiles.

Figure 3-1 Actual setting of roof tiles and cassettes on kiln car (Photo: BMI Technical Services GmbH)

The geometric design is difficult to describe mathematically. For a more general description of the firing process, the design of the roof tile has to be simplified. The combination of roof tile on the H-cassette can be simplified as a rectangular plate that has the same dimensions as the combination along length, breadth, and height. The 3-D scan of the

roof tile on the cassette is shown in **Figure 3-2** and the simplification of the roof tile on the cassette as a rectangular plate is also shown in the same figure. The ratio of the surface area of the actual roof tile and H-cassette combination to the simplified rectangular plate is 2.1. This simplification changes the setting on the kiln car as flat long plates which are stacked on top of each other with a gap of 55 mm which is equal to the gap in the actual setting as seen in **Figure 3-3**.

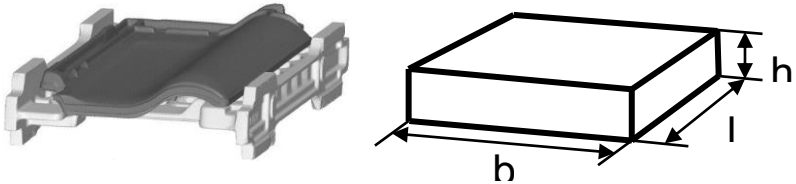

Figure 3-2 Simplification of roof tile and cassette as a rectangular plate

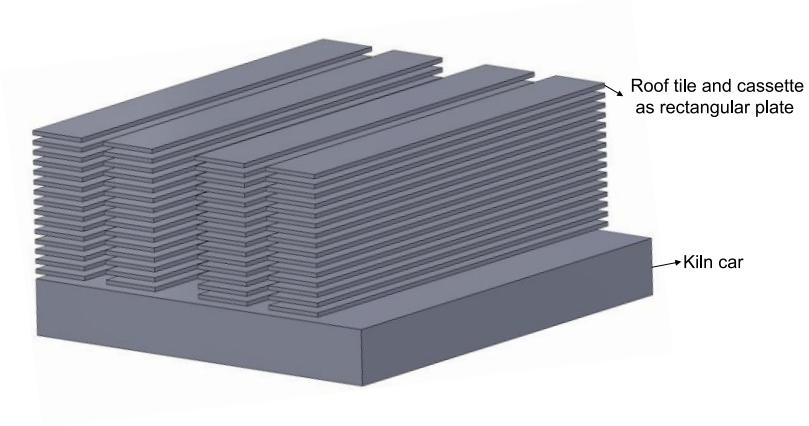

Figure 3-3 Simplified setting on the kiln car

The side view and front view of a typical kiln car are depicted in **Figure 3-4**. The base of the kiln car is the steel chassis which can be considered the backbone of the kiln car. The temperature at this location should not exceed more than 400 °C to avoid the deformation of the steel due to buckling. Insulation layers on top of the steel chassis

avoid the heat from the gas atmosphere to penetrate to the bottom of the kiln car thereby avoiding the bottom steel chassis from heating up as it moves through the tunnel kiln. The top of the insulation layers is covered with cover plates which provide a stable surface for the placing of a base frame and the roof tiles along with the cassettes are kept on the base frame.

Each different components of the kiln car have a single function and each component work independently of each other. In order to model the heat conduction through the kiln car as it moves along the tunnel kiln, the different components can be simplified as different material layers. Each material layer has the properties of that component which has a major part in providing structural stability or insulation. The length and width of the material layer will be that of the kiln car whereas the thickness is that of the component. **Figure 3-5** shows the simplification of the kiln car into different material layers such that the total mass of the kiln car should remain constant. The 1st material layer has the properties of the cover plate which is the predominant material on top of the kiln car. The 2nd, 3rd, and 4th material layers have the properties of insulation material 1, 2, and steel chassis, respectively.

The kiln car in the tunnel kiln manufacturing roof tile where the measurement was carried had a different construction as shown in Figure 3-4. The kiln car is simplified as explained above and the information regarding the different material layers is given in **Table 3-1**.

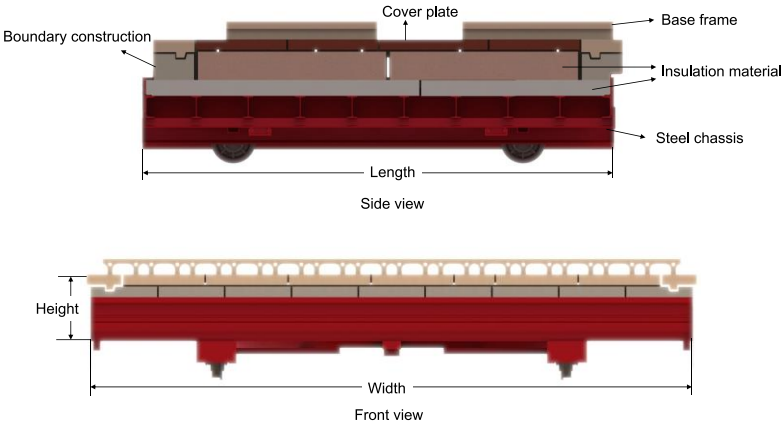

Figure 3-4 Construction of kiln car [33]

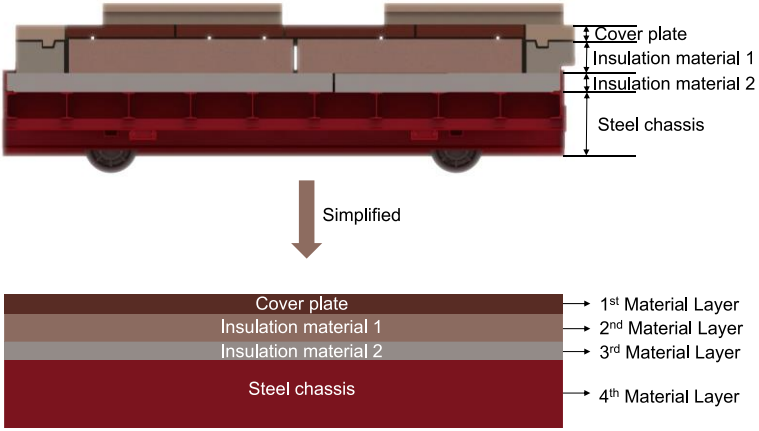

Figure 3-5 Simplification of the kiln car geometry for modelling (side view)

Table 3-1 Characteristics of the different material layers of kiln car in the roof tile producing tunnel kiln

Material Layer	Thickness of each layer compared to the total thickness of kiln car [%]	Thermal conductivity [W/(m·K)]	Density [kg/m^3]
1st	7	1.5	1200
2nd	23	0.8	1100
3rd	20	0.25	400
4th	8	0.18	64
5th	14	0.4	1100
6th	28	0.8	1000

3.2 Convective Heat Transfer

3.2.1 Forced Convection

Convection is the heat transfer through a fluid due to the movement of the fluid. The movement can be induced due to an external force or naturally by means of a buoyancy effect. Convection due to external force is called forced convection whereas convection due to natural means is known as free or natural convection. Consider a body with a surface temperature of T_s and a fluid with a temperature of T_∞ flows over the body with a velocity, then the heat transfer from the surface to the fluid can be represented by Newton's law of cooling as given in (3-1)

$$\dot{q}_{conv} = h(T_s - T_\infty). \tag{3-1}$$

Here h is the convective heat transfer coefficient in W/(m^{2}K). Nusselt number is a dimensionless number that is defined as the ratio of heat transfer through a fluid layer as a result of convection to conduction across the same fluid layer. Nusselt number is considered as the dimensionless convective heat transfer coefficient

$$Nu = \frac{hL_c}{\lambda}. \tag{3-2}$$

The Nusselt number comprises the convective heat transfer coefficient h, the characteristic length of the geometry L_c, and the thermal conductivity of fluid k, which is calculated as the average temperature of the fluid and surface. The dimensionless Nusselt number can be represented as a function of two dimensionless numbers; the Reynolds number and the Prandtl number. Depending upon the geometry the Nusselt number can be expressed as a simple power-law equation with the Reynolds number and Prandtl number

$$Nu = CRe_L^m Pr^n. \tag{3-3}$$

The value of m is 0.5 for laminar flow and 0.8 for turbulent flow. The value of n is in the range of 0.4 and the value of C depends on the kind of flow (laminar or turbulent) and whether the flow is over a plate or through a duct. In the cooling zone of the tunnel kiln, the cooling air comprises of non-radiating gases unlike carbon dioxide and water vapour in the firing zone and preheating zone. Hence in the cooling zone, the only mode of heat transfer between the cooling air and fired ceramic ware is by convection. This section explains how the convective heat transfer coefficient is calculated by considering forced convection between the ware and gas and kiln car.

Zhu [34] had shown that the heat transfer coefficient for a flow in between the roof tiles can be calculated with the Nusselt number equation for a flow over a plate. CFD calculation was used to calculate the heat transfer coefficient for flow through roof tiles which are simplified as plates with length 'l' and breadth 'b' equal to the roof tile. The heat transfer coefficient calculated with CFD is compared to the heat transfer coefficient which is calculated with the Nusselt number equation for flow over a plate as given by Pohlhausen [35] and Specht [36]

$$Nu_{lam} = 0.664 \cdot Re_{lk}^{0.5} Pr^{0.33} \tag{3-4}$$

$$Nu_{turb} = \frac{0.037 \cdot Re_{lk}^{0.8} \cdot Pr^{0.43}}{1 + 2.443 \cdot Re_{lk}^{-0.1} \cdot \left(Pr^{\frac{2}{3}} - 1\right)} \cdot \tag{3-5}$$

When the Reynolds number is below 10^5, the flow is laminar and the Nusselt number equation is Nu_{lam} and when it is above 10^5, the flow is turbulent and the equation is (3-5). The Reynolds and Prandtl numbers are calculated with the help of the following equations

$$Re_{lk} = \frac{\overline{w} \cdot l_k}{\nu(T_s)} \tag{3-6}$$

$$Pr = \frac{\nu_G(T_s) \cdot \rho_G(T_s) \cdot c_{pG}(T_s)}{\lambda_G(T_s)} \tag{3-7}$$

$$T_S = \frac{T_{S,Surface} + T_G}{2}. \tag{3-8}$$

It was seen that the heat transfer coefficient calculated with CFD when the roof tiles are approximated as plated and the heat transfer coefficient calculated with the Pohlhausen Nusselt number equation is almost the same. The heat transfer coefficient calculated with the Nusselt number is multiplied by the ratio of the area of the roof tile and cassette combination to the area of the plate to get the heat transfer coefficient for over roof tile. When this is compared to the CFD result of the heat transfer coefficient for flow over roof tile, it showed that the values are similar to that calculated with the Nusselt number equation for flow over a plate.

The Nusselt number for flow over a plate is chosen as the Nusselt number equation [36]. And equation (3-11) is used in the transition range from laminar flow to the turbulent flow

$$Nu_{lam} = 0.664 \cdot Re_{lk}^{0.5} Pr^{0.33} \tag{3-9}$$

$$Nu_{turb} = 0.037 \cdot Re_{lk}^{0.8} \cdot Pr^{0.43} \tag{3-10}$$

$$Nu = \sqrt{Nu_{lam}^2 + Nu_{turb}^2}. \tag{3-11}$$

3.2.2 Free Convection

Density differences and the gravitational field act to produce a buoyancy force, which causes a flow. This flow is called free or natural convection. The density difference can be caused by a difference in

temperature or concentration in the fluid. In the tunnel kiln free convection can be the mode of heat transfer from the roof tiles to the gas or from the outside walls and top wall of the kiln to the ambient atmosphere. For the free convection from roof tiles to the gas, the Nusselt number used for calculating the convective heat transfer coefficient depends on the surface of the roof tile. When the free convection takes place from the top surface of the roof tile, the Nusselt number equations (3-12) and (3-13) are used as given in VDI Heat Atlas [37]. When $Gr \cdot Pr \cdot f_2$ is greater than $7 \cdot 10^4$ then the Nusselt number equation (3-13) for the turbulent flow should be used. The Nusselt number for free convection from the bottom of the roof tile is equation (3-14). Since the top and bottom surfaces of the roof tile exchange heat with the gas in the tunnel kiln, the top and bottom Nusselt numbers are added to take into account the effect of heat exchange through both the top and bottom surface (3-15)

$$Nu_{Top,lam} = 0.766 \cdot (Gr \cdot Pr \cdot f_2)^{\frac{1}{5}} \tag{3-12}$$

$$Nu_{Top,turb} = 0.15 \cdot (Gr \cdot Pr \cdot f_2)^{\frac{1}{3}} \tag{3-13}$$

$$Nu_{Bottom} = 0.6 \cdot (Gr \cdot Pr \cdot f_1)^{\frac{1}{5}} \tag{3-14}$$

$$Nu_{Free} = Nu_{Top} + Nu_{Bottom} \tag{3-15}$$

$$f_2 = 0.4\,. \tag{3-16}$$

Gr is the Grashof number and in free convection, it replaces the Reynolds number. The Grashof number is given in (3-17) where β_T is known as the thermal volumetric coefficient of expansion. β_T can be approximated as the inverse of the average absolute temperature of the body taking part in free convection and the fluid. L is the characteristic length and is calculated with the equation (3-18) for a rectangular body. Pr for gases is equal to 0.7

$$Gr = \frac{g \cdot L^3 \cdot \beta_T \cdot \Delta T}{\nu^2} \tag{3-17}$$

$$L = \frac{a \cdot b}{2 \cdot (a + b)}\,. \tag{3-18}$$

The Nusselt number for calculating the heat transfer coefficient when heat is lost from the outside side walls of the tunnel kiln due to free convection to the atmosphere is given as (3-19) [37]

$$Nu = \left[0.825 + 0.387 \cdot (Gr \cdot Pr \cdot f_1)^{\frac{1}{6}}\right]^2 \tag{3-19}$$

$$f_1 = 0.34\,. \tag{3-20}$$

3.2.3 Superposition of Free and Forced Convection

To determine which type of convection is predominant for the heat transfer from the solid to the fluid, Archimedes number is used

$$Ar = \frac{Gr}{Re^2} = \frac{g \cdot L \cdot \beta_T \cdot \Delta T}{\overline{w}^2}\,. \tag{3-21}$$

When the Archimedes number is less than 0.2 then the convection type is forced convection and when the Archimedes number is greater than 10 then the convection type is free convection. When the Archimedes number is between 0.2 and 10 then the flow is in the transition zone and influences of both free and forced flows should be considered as given by Churchill [38]. The equation (3-22) is used when the free and forced convection are perpendicular to each other as is the case for the roof tile and the vertical wall outside the tunnel kiln

$$Nu = \left(Nu_{free}^4 + Nu_{forced}^4\right)^{\frac{1}{4}}\,. \tag{3-22}$$

3.3 Conduction in Ware

The heating of the ware in the firing zone is transient. To determine the resistance by conduction, a solution of Fourier's differential equation

$$\frac{\partial T}{\partial t} = \frac{\lambda_S}{\rho_S \cdot c_S}\left(\frac{\partial^2 T}{\partial x^2}\right) \tag{3-23}$$

assuming an infinitely extended plate is necessary for the one-dimensional case is necessary. Here are λ_S the thermal conductivity, ρ_S the density and c_S the heat capacity of the ware.

As shown in **Figure 3-6**, the surface and the core have different temperatures. Thus, during heating, the core always lags behind the surface. After the thermal start, constant temperature differences develop between the environment, the surface, and the core of the ware. The heat flux at the surface of the ware is

$$\dot{q} = (\alpha_{conv} + \alpha_{rad}) \cdot \left(T_G - T_{S,Surface}\right) \tag{3-24}$$

and is equal to the heat dissipated into the core. For the determination of the effective heat transfer coefficient, the averaged (caloric) temperature of the ware $T_{S,Cal}$ can be used and is as follows

$$\alpha_{eff} = \frac{\dot{q}}{\left(T_G - T_{S,Cal}\right)}. \tag{3-25}$$

This effective heat transfer coefficient includes convection, radiation, and heat conduction in the ware. If this is to be estimated without having to solve the differential equation mentioned above, the below expression can be used

$$\alpha_{eff} = \frac{1}{\left(\frac{1}{\alpha_{conv} + \alpha_{rad}} + \frac{0.5 s_s}{\chi \cdot \lambda_S}\right)}. \tag{3-26}$$

The transient factor χ for a plate is about 3 [39]. This approximate solution was derived analytically and is valid, if the thermal start is complete and the ambient temperature, in this case the gas temperature, changes linearly. Especially in the preheating zone, the capacitance ratio of gas flow and product is about one, so linear and parallel temperature profiles are approximated.

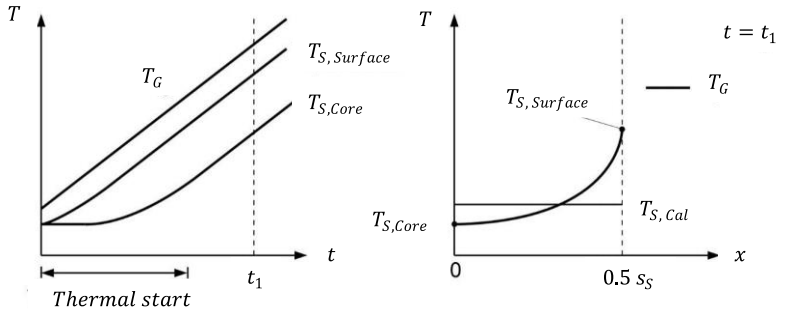

Figure 3-6 Transient heat conduction [39]

3.4 Radiation

In a tunnel kiln, the gas in the firing and preheating zone exchange heat with the ware and the kiln car by radiation in addition to convection because of the presence of water vapour and carbon dioxide. The ware and the kiln car exchange heat throughout the tunnel kiln by solid-to-solid radiation.

The radiation energy emitted by a black body per unit time and per unit surface area was determined experimentally by Joseph Stefan in1879 and is expressed as

$$\dot{q}_b(T) = \sigma T^4 \tag{3-27}$$

where $\sigma = 5.67 \times 10^{-8}$ W/m²K⁴ is the Stefan-Boltzmann constant and T is the absolute temperature of the surface in K.

A black body absorbs the maximum amount of the total incident radiation and the same is valid for the emitted radiation. All natural bodies reflect or transmit a certain fraction of the incident radiation. They absorb (and emit according to Kirchoff's law: the emissivity of the body is equal to its absorptance) a smaller heat flux than a black body and is given by

$$\dot{q} = \varepsilon \sigma T^4 \tag{3-28}$$

where ε is the emissivity of the body with $0 < \varepsilon < 1$. The above equation is valid for gray bodies where the emissivity is independent of the wavelength.

3.4.1 Equivalent Thickness of Transparent Bodies

The radiation in a transparent medium beams in different directions, as illustrated in **Figure 3-7** for a rectangular space. As a consequence, the beams have different lengths. Only in a hemisphere do beams from a central source have the same length, as indicated in the right part of the figure. For all other geometries, an average length must be determined by integrating all lengths of the individual beams. This average distance is referred to as equivalent beam thickness. It represents the radius of a hemisphere, which has the same absorptance as the actual body.

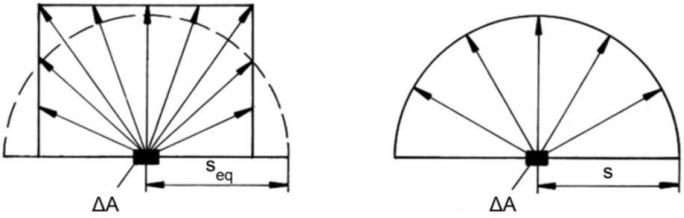

Figure 3-7 Determination of the equivalent beam layer thickness [39]

Equivalent length can be approximated for any body shape with the equation

$$s_{eq} = 0.9 \cdot \frac{4 \cdot V}{A} \tag{3-29}$$

where V represents the volume of the body and A is the area of the body exchanging radiation.

3.4.2 Emissivity of Ceramics

From **Figure 3-8** it can be seen that the emissivity of the ceramics decreases with an increase in the temperature in contrast to metals. Materials containing carbon such as SiC tend to show a stable value of emissivity with respect to an increase in the temperature.

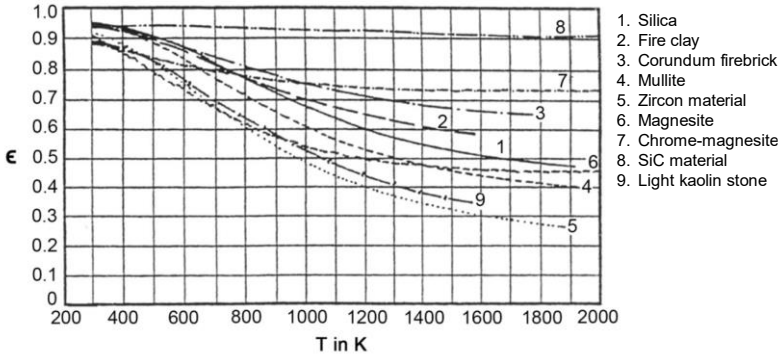

Figure 3-8 Emissivity of selected ceramics [39]

3.4.3 Emissivity of CO_2 and H_2O

While solid-to-solid radiation is continuously released over all the wavelengths, gases are permeable to thermal radiation in the largest part of the spectrum and don't radiate in these regions. They radiate only in limited wavelength ranges called bands. The molecules of basic gases like H_2, O_2, N_2, and Ar don't emit and absorb radiation.

For technical calculations, the heat flow emitted over the entire wavelength range is of interest and thus the average overall wavelength is used for emissivity. This in turn is calculated from

$$\varepsilon(T) = \frac{\int_0^\infty \varepsilon_\lambda(\lambda) \cdot I(\lambda, T) \cdot d\lambda}{\sigma \cdot T^4} \tag{3-30}$$

where $I(\lambda, T)$ is the intensity of the radiation which is a function of the wavelength λ and temperature T .The total integral is however conveniently replaced by the sum of integrals over the radiant bands, as the space between the bands of the emissivity is negligible

$$\varepsilon_{Gi} = \frac{1}{\sigma \cdot T^4} \cdot \sum_k \int_{\lambda_{k1}}^{\lambda_{k2}} \varepsilon_{\lambda_i} \cdot I_\lambda d\lambda \tag{3-31}$$

where $\lambda_{k1}$and λ_{k2} are the limits of the k-th band for the gas i.

The emissivity of carbon dioxide and water vapor are shown in **Figure 3-9** and **Figure 3-10** as a function of its temperature. From the figures

the emissivity can be approximated for CO_2 at temperatures above 1300 K, and for H_2O at temperatures above 700 K with the equation

$$\varepsilon = A \cdot \exp(-B \cdot T) \tag{3-32}$$

and the two quantities A and B depend on the product of the partial pressure and layer thickness of the gas p·s and are given in **Table 3-2**. The emissivity of the gas mixture with CO_2 and H_2O can be calculated with the following equation.

$$\varepsilon_G = \varepsilon_{CO_2} + \varepsilon_{H_2O} - \varepsilon_{CO_2} \cdot \varepsilon_{H_2O} \tag{3-33}$$

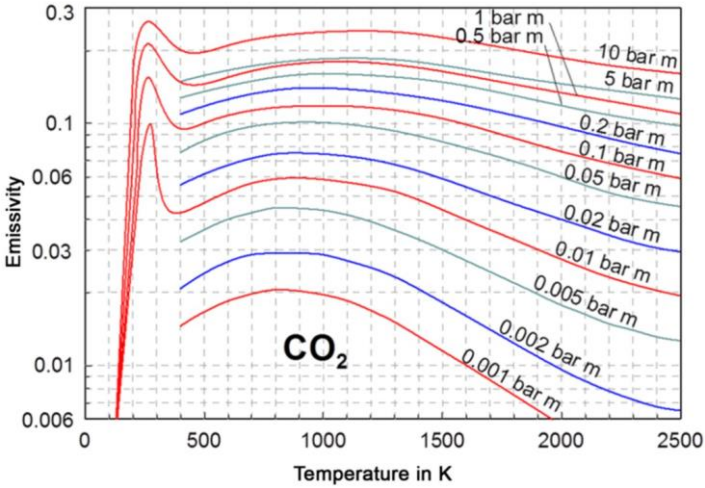

Figure 3-9 Emissivity of carbon dioxide [39]

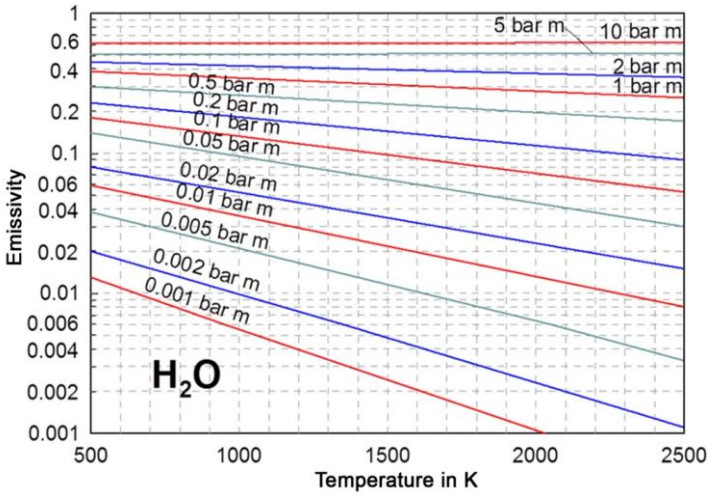

Figure 3-10 Emissivity of water vapor [39]

Table 3-2 Approximations to calculate the emissivity of CO2 and H2O [39]

Gas	A	B	P·s [bar ·m]	T [K]
CO_2	$0.36\cdot(p\cdot s)^{0.20}$	$3.4\cdot10^{-4}\cdot(p\cdot s)^{-0.19}$	>0.002 <0.1	> 1300
	$0.28\cdot(p\cdot s)^{0.084}$	$4.1\cdot10^{-4}\cdot(p\cdot s)^{-0.11}$	>0.1 <10	
H_2O	$0.69\cdot(p\cdot s)^{0.46}$	$3.7\cdot10^{-4}\cdot(p\cdot s)^{-0.22}$	>0.002 <0.1	> 700
	$0.41\cdot(p\cdot s)^{0.23}$	$2.1\cdot10^{-4}\cdot(p\cdot s)^{-0.46}$	>0.1 <2	

3.4.4 Radiative Heat Transfer Coefficient

The sum of the radiative heat flow and the convective heat flow gives the total heat flow from the gas to the ware or to the kiln car. The radiative heat flux from gas to solid can be written as

$$\dot{q} = \varepsilon_{eff} \cdot \sigma \cdot (T_G^4 - T_S^4). \tag{3-34}$$

To make the heat flux equation similar to the heat flux equation of convection a radiative heat transfer coefficient can be determined

$$\alpha_{rad} \cdot (T_G - T_S) = \varepsilon_{eff} \cdot \sigma \cdot (T_G^4 - T_S^4). \tag{3-35}$$

ε_{eff} is the effective emissivity. The radiative heat transfer coefficient can be written as

$$\alpha_{rad} = \varepsilon_{eff} \cdot \sigma \cdot T_G^3 \left(1 + \frac{T_s}{T_G} + \left(\frac{T_s}{T_G}\right)^2 + \left(\frac{T_s}{T_G}\right)^3\right). \tag{3-36}$$

The radiative heat transfer coefficient can be approximated as

$$\alpha_{rad} \approx 4 \cdot \varepsilon_{eff} \cdot \sigma \cdot \left(\frac{T_G + T_S}{2}\right)^3. \tag{3-37}$$

The above equation can also be used for calculating the radiative heat transfer coefficient between the gas and the solid or between two solid bodies.

3.4.5 Effective Emissivity between Two Walls

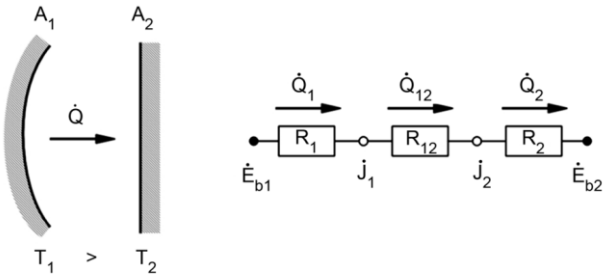

Figure 3-11 Radiation exchange between two walls [40]

Figure 3-11 shows radiative heat exchange between two walls of the area A_1 and A_2 with temperatures T_1 and T_2 where $T_1 > T_2$. The thermal resistance network is also shown in the same figure where R_1 and R_2 are known as net resistance this hinders the radiation because of a real, non-black surface. R_{12} is called transmission resistance or geometric resistance and the equations are given below

$$R_1 = \frac{\rho_1}{A_1 \cdot \varepsilon_1} \tag{3-38}$$

$$R_{12} = \frac{1}{A_1 \cdot \varphi_{12}} \tag{3-39}$$

$$R_2 = \frac{\rho_2}{A_2 \cdot \varepsilon_2} \tag{3-40}$$

where ρ is the reflectivity of the wall and ε is the emissivity of the walls.

The heat flow from wall 1 to wall 2 is

$$\dot{Q} = \frac{\dot{E}_{b1} - \dot{E}_{b2}}{R_1 + R_{12} + R_2}. \tag{3-41}$$

$\dot{E}_{b2}$ is the emissive power of a black body at the same temperature and is given by

$$\dot{E}_b = \sigma \cdot T^4. \tag{3-42}$$

Appling Kirchoff's law to the equation and substituting the resistance equations will result in the heat flow from wall 1 to wall 2 be

$$\dot{Q} = \frac{A_1 \cdot \sigma \cdot (T_1^4 - T_2^4)}{\frac{1}{\varepsilon_1} - 1 + \frac{1}{\varphi_{12}} + \frac{A_1}{A_2} \cdot \left(\frac{1}{\varepsilon_2 - 1}\right)}. \tag{3-43}$$

The heat flow equation can be written with the effective emissivity as

$$\dot{Q} = \varepsilon_{eff} \cdot A_1 \cdot \sigma \cdot (T_1^4 - T_2^4) \tag{3-44}$$

where,

$$\frac{1}{\varepsilon_{eff}} = \frac{1}{\varepsilon_1} - 1 + \frac{1}{\varphi_{12}} + \frac{A_1}{A_2} \cdot \left(\frac{1}{\varepsilon_2 - 1}\right). \tag{3-45}$$

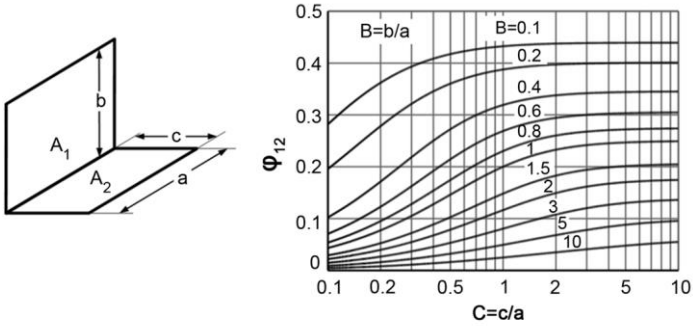

Figure 3-12 View factor between two perpendicular plates [39]

φ_{12} is called the view factor and has to be calculated taking into consideration the orientation of the two bodies with each other. In the roof tile kiln, to calculate the view factor from the roof tile to the kiln car, the roof tile and the kiln car can be approximated as two parallel plates and hence the view factor is one. In the brick kiln, the brick on the kiln car can be considered as two rectangles that are perpendicular to each other with a common base and **Figure 3-12** can be used to calculate the view factor from the kiln car to the brick φ_{21}. Reciprocity rule can be used to calculate the view factor from the brick to the kiln car φ_{12}.

For the effective emissivity for the heat flow from the gas to the ware or kiln car, the (3-46) can be used and is represented as

$$\frac{1}{\varepsilon_{eff}} = \frac{1}{\varepsilon_G} - 1 + \frac{1}{\varphi_{GS}} + \frac{A_G}{A_S} \cdot \left(\frac{1}{\varepsilon_S - 1}\right) \cdot \tag{3-46}$$

The view factor φ_{GS} between the gas and the ware or the kiln car becomes 1. In addition to the view factor becoming 1, the area ratio $\frac{A_G}{A_S}$ also becomes 1 and the effective emissivity equations can be simplified as

$$\frac{1}{\varepsilon_{eff}} = \frac{1}{\varepsilon_G} + \frac{1}{\varepsilon_S} - 1 \cdot \tag{3-47}$$

ε_S is the emissivity of the ware when the radiation is between the ware and the gas but when the radiation is between the kiln car and the gas, ε_S becomes the emissivity of the top layer of the kiln car.

3.5 Modeling of Combustion

The heating requirement of the tunnel kiln is primarily met by the combustion of natural gas in Germany. The crude natural gas which is extracted from the gas fields can be differentiated into two groups depending upon the concentration of hydrogen sulfide and organic sulfur compounds. Sweet natural gas is devoid of hydrogen sulfide and organic sulfur whereas sour natural gas contains up to 20% by volume. The hydrogen sulfide and organic sulfur compounds are removed and then natural gas from different sources is mixed to maintain a constant quality. Natural gas is divided into two different kinds depending on the concentration of methane. Natural gas with a high concentration of methane is termed natural gas H, whereas natural gas with a low concentration of methane is termed natural gas L.

The chemical enthalpy is converted into heat by the oxidation of the carbon and hydrogen contained in the fuel. As shown in **Figure 3-13**, when the gas is cooled to 0 °C after combustion, then the resulting water is present as a liquid. The enthalpy converted in this process is called the upper heating value H_o. After the combustion, the gas is drawn off with temperatures above the dew point so that the water is vaporous. As a result, the condensation enthalpy is not converted into heat and then the converted chemical enthalpy of the fuel is known as the lower heating value h_u. The equation for calculation of lower heating value is given below with x_{H_2O} being the proportion of water in the gas.

$$h_u = H_o - x_{H_2O} \cdot \Delta h_{vap} \tag{3-48}$$

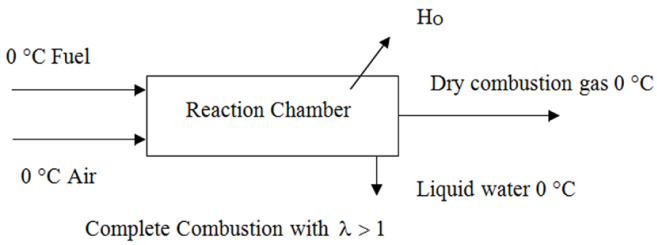

Figure 3-13 Determining the heating value [39]

Natural gas L and natural gas H have different concentrations of methane, ethane, hydrocarbons, carbon dioxide, and nitrogen. The composition of the natural gas L, natural gas H, and hydrogen along with the lower heating value of the respective fuel is mentioned in **Table 3-3**.

Table 3-3 Composition and lower heating value of fuels [39]

Fuel	Concentration [% vol]						
	CH_4	C_2H_6	$\sum C_nH_m$	H_2	CO	CO_2	N_2
Natural Gas L	82	3	0	-	-	1	14
Natural Gas H	93	3	2	-	-	1	1
Hydrogen	-	-	-	100	-	-	-
Lower heating value	Natural Gas L		Natural Gas H		Hydrogen		
[MJ/kg]	38.3		47.3		120		
[MJ/m^3]	31.8		37.4		10.8		

The overall reaction equation of each component of the fuel with oxygen is given below.

$$CH_4 + 2O_2 \rightarrow CO_2 + 2H_2O \tag{3-49}$$

$$C_2H_6 + \frac{7}{2}O_2 \rightarrow 2CO_2 + 3H_2O \tag{3-50}$$

$$C_nH_m + \left[n + \frac{m}{4}\right]O_2 \rightarrow n \cdot CO_2 + \frac{m}{2}H_2O \tag{3-51}$$

$$H_2 + \frac{1}{2}O_2 \rightarrow H_2O \tag{3-52}$$

$$CO + \frac{1}{2}O_2 \rightarrow CO_2 \tag{3-53}$$

The calculation of the specific oxygen demand $[\frac{m_{O_2}^3}{m_f^3}]$ of the gaseous is done with the equation

$$\tilde{O} = \sum \tilde{x}_{if} \cdot \nu_i - \tilde{x}_{O_2 f} \tag{3-54}$$

where,

$\tilde{x}_{if}$ $[\frac{m_i^3}{m_f^3}]$ is the content by volume of component i in fuel.

ν_i [Mol O_2/Mol$_i = \frac{m_{O_2}^3}{m_i^3}$] is the stoichiometric number of i for complete oxidation.

$\tilde{x}_{O_2 f}$ is the content by volume of O_2 contained in the fuel.

The specific air demand $[\frac{m_L^3}{m_f^3}]$ depends on the concentration of O_2 in the air ($\tilde{x}_{O_2 L}$) and generally, the concentration of O_2 is approximately 21% by volume.

$$\tilde{L} = \frac{\tilde{O}}{\tilde{x}_{O_2 L}} \tag{3-55}$$

The mass-related air demand $[\frac{kg_L}{kg_f}]$ is calculated using the density of the air ρ_L and the density of the fuel ρ_f.

$$L = \tilde{L} \cdot \frac{\rho_L}{\rho_f} \tag{3-56}$$

$$\rho_f = \sum \tilde{x}_{if} \cdot \rho_i \tag{3-57}$$

where ρ_i is the density of the individual components of the fuel.

The air demand which is also the stoichiometric air demand is the minimum amount of air required for the complete combustion of the

fuel. The ratio of actual air supplied for combustion to the stoichiometric air demand is known as excess air number λ.

$$\lambda = \frac{Actual\ air\ input}{Stoichiometric\ air\ demand} \tag{3-58}$$

After the complete combustion of the fuel, the combustion gas comprises of carbon dioxide, water vapor, nitrogen, and oxygen, and the specific concentration of the gases $\tilde{v}_i$ can be calculated with the following equations.

$$\tilde{v}_{O_2} = (\lambda - 1) \cdot \tilde{L} \cdot \tilde{x}_{O_2 L} \tag{3-59}$$

$$\tilde{v}_{N_2} = \lambda \cdot \tilde{L} \cdot \tilde{x}_{N_2 L} + \tilde{x}_{N_2 f} \tag{3-60}$$

$$\tilde{v}_{CO_2} = \tilde{x}_{CO_2 f} + \tilde{x}_{CH_4 f} + \tilde{x}_{CO f} + \sum n \cdot \tilde{x}_{(C_n H_m) f} \tag{3-61}$$

$$\tilde{v}_{H_2O} = \tilde{x}_{H_2 f} + 2 \cdot \tilde{x}_{CH_4 f} + \sum \frac{m}{2} \cdot \tilde{x}_{(C_n H_m) f} + \lambda \cdot \tilde{L} \cdot \tilde{x}_{H_2 O L} \tag{3-62}$$

The burners in the tunnel kiln are either located on the roof or at the side. The burners release the combustion gas which will be mixed with the gas that is already present in the tunnel kiln and hence raises the temperature of the gas further. For a burner that is located at the end of the firing zone, the combustion gas will be mixed with the high temperature air which is coming from the cooling zone. This process where the combustion gas mixes with the gas in the tunnel kiln happens at all the locations of the burners as shown in **Figure 3-14**.

Mass balance at the burner position will result in the mass flowrate of the gas with high temperature.

$$\dot{M}_{Gas_{HT}} = \dot{M}_{Gas_{LT}} + \dot{M}_f + \dot{M}_L \tag{3-63}$$

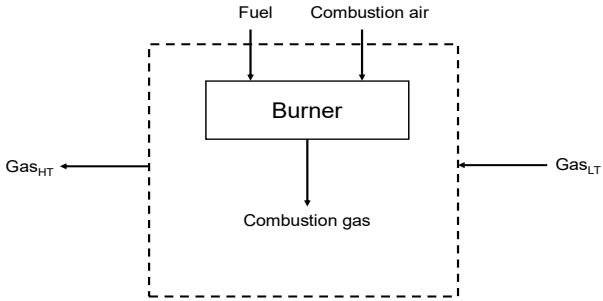

Figure 3-14 Mixing of the combustion gas with the gas in the tunnel kiln at the burner position

The overall energy balance (3-64) at the mixing position can be used to calculate the final temperature of the gas after mixing with the combustion gas and gas in the tunnel kiln.

$$\dot{M}_{Gas_{LT}} \cdot c_{pGas_{LT}}\big|_{T_0}^{T_{Gas_{LT}}} \cdot \vartheta_{Gas_{LT}} + \dot{M}_f \cdot \left(c_{pf}\big|_{T_0}^{T_f} \cdot \vartheta_f + h_{u\,f}\right) + \dot{M}_L \cdot c_{pL}\big|_{T_0}^{T_L} \cdot \vartheta_L = \dot{M}_{Gas_{HT}} \cdot c_{pGas_{HT}}\big|_{T_0}^{T_{Gas_{HT}}} \cdot \vartheta_{Gas_{HT}} \tag{3-64}$$

By rearranging the above equation, the temperature of the final gas can be evaluated with the equation which is given below

$$\vartheta_{Gas_{HT}} = \frac{\dot{M}_{Gas_{LT}} \cdot c_{pGas_{LT}}\big|_{T_0}^{T_{Gas_{LT}}} \cdot \vartheta_{Gas_{LT}} + \dot{M}_f \cdot \left(c_{pf}\big|_{T_0}^{T_f} \cdot \vartheta_f + h_{u,f}\right) + \dot{M}_L \cdot c_{pL}\big|_{T_0}^{T_L} \cdot \vartheta_L}{\dot{M}_{Gas_{HT}} \cdot c_{pGas_{HT}}\big|_{T_0}^{T_{Gas_{HT}}}} \tag{3-65}$$

where,

$$c_{pGas_{LT}}\big|_{T_0}^{T_{Gas_{LT}}} = \sum_i x_{iGas_{LT}} \cdot c_{piGas_{LT}}\big|_{T_0}^{T_{Gas_{LT}}} \tag{3-66}$$

$$c_{pf}\big|_{T_0}^{T_f} = \sum_i x_{if} \cdot c_{pif}\big|_{T_0}^{T_f} \tag{3-67}$$

$$c_{pL}\big|_{T_0}^{T_L} = \sum_i x_{iL} \cdot c_{piL}\big|_{T_0}^{T_L} \tag{3-68}$$

$$c_{pGas_{HT}}\big|_{T_0}^{T_{Gas_{HT}}} = \sum_i x_{iGas_{HT}} \cdot c_{piGas_{HT}}\big|_{T_0}^{T_{Gas_{HT}}} \tag{3-69}$$

and $c_{pi}\big|_{T_0}^{T}$ is the mean specific heat capacity between the reference temperature ($T_0 = 273K$) and the corresponding temperature of the respective gases. The mean specific heat capacity can be calculated by equation (3-70)

$$c_{pi}\big|_{T_0}^{T} = \frac{1}{T - T_0} \cdot \int_{T_0}^{T} c_{pi}(T) \cdot dt = \frac{c_{pi}(T_0)}{n+1} \cdot \left[\frac{(T/T_0)^{1+n_{ci}} - 1}{T/T_0 - 1} \right]. \quad (3\text{-}70)$$

4 Mathematical Model of the Tunnel Kiln Process

4.1 Differential Equation for the Tunnel Kiln Process

The temperature of the ceramic as it moves along the tunnel kiln increases in the preheating zone, reaches a maximum at the firing zone and cools down in the cooling zone. Depending upon the cooling rate the different regions in the cooling zone are divided into rapid cooling, static cooling, and end cooling zone. The rate of cooling is high, low, and medium in the rapid cooling zone, static cooling zone, and end cooling zone, respectively. The profile of the temperature fluctuations that the ceramic undergoes along the tunnel kiln is called the firing curve. The main aim of modeling the tunnel kiln process is to recreate the firing curve of the ceramic along the tunnel kiln with the help of mathematical equations.

From the end of the tunnel kiln, the cooling air takes the heat from the fired ceramic and heats up as it flows to the firing zone. In the firing zone, the air is mixed with the combustion gas to heat the ceramic to the firing temperature. Finally, in the preheating zone, the gas heats the non-fired ceramic and cools down. The gas is exhausted at the entrance of the tunnel kiln as flue gas. The direction of the flow of gas is opposite to the direction of the ceramic which shows that the tunnel kiln can be approximated as a counter-current heat exchanger. Therefore, the modeling of a tunnel kiln can be done similarly to the modeling of counter-current heat exchanger.

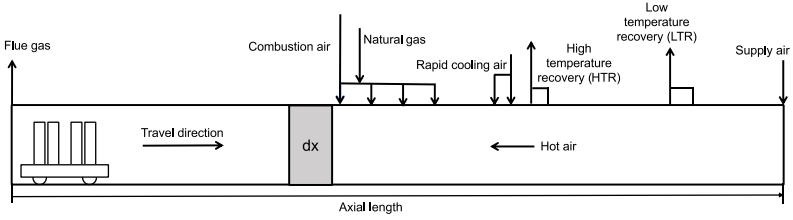

Figure 4-1 Tunnel kiln with small section ‘dx’

In the tunnel kiln, the unburnt ceramics are kept on the kiln car with supports called furniture. The ceramics and the furniture will be

together mentioned as solid from now onwards. Inside the heat exchanger, heat is exchanged between a hot fluid and a cold fluid but in the tunnel kiln, the heat is exchanged between the gas, the solid, and the kiln car. According to the analogy with a heat exchanger, the enthalpy change of a fluid is equal to the net heat transferred to the fluid for a small section is given by the following equation (4-1).

$$d\dot{H}_f = d\dot{Q} \tag{4-1}$$

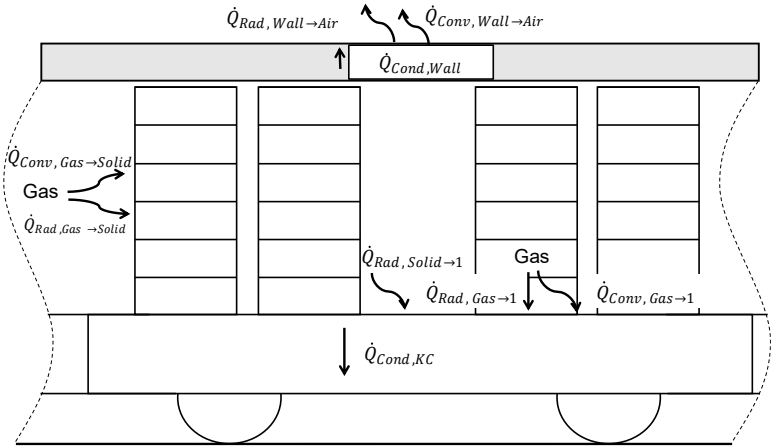

Figure 4-2 Heat transfer in the tunnel kiln in the preheating zone

This principle is applied to a small section 'dx' in the tunnel kiln for the preheating zone as shown in **Figure 4-1** for each heat-exchanging medium in the tunnel kiln (solid, kiln car, and gas). **Figure 4-2** shows principally the heat exchange between the three mediums in the preheating zone. The enthalpy change of the gas is the heat flow to the solid ($\dot{Q}_{Gas\rightarrow Solid}$) and the kiln car ($\dot{Q}_{Gas\rightarrow KC}$) and also through the walls of the tunnel kiln to the ambient air $\left(\dot{Q}_{Gas\rightarrow Ambient\ Air}\right)$. The enthalpy change of the solid is the heat flow to the kiln car $\left(\dot{Q}_{Solid\rightarrow KC}\right)$ and the heat flow from the gas. The enthalpy change of the kiln car is the heat flow from the gas and solid. Applying equation (4-1) and combing it with the above explanation helps to formulate the equations (4-2), (4-3), and (4-4).

$$\dot{m}_{Gas} c_{p,Gas} \frac{dT_{Gas}}{dx} = -\left(-\dot{Q}_{Gas \rightarrow Solid} - \dot{Q}_{Gas \rightarrow KC} - \dot{Q}_{Gas \rightarrow \text{Ambient Air}}\right) \quad (4\text{-}2)$$

$$\dot{m}_{Solid} c_{Solid} \frac{dT_{Solid}}{dx} = \dot{Q}_{Gas \rightarrow Solid} - \dot{Q}_{Solid \rightarrow KC} \quad (4\text{-}3)$$

$$\dot{m}_{KC} c_{KC} \frac{dT_{KC}}{dx} = \dot{Q}_{Gas \rightarrow KC} + \dot{Q}_{Solid \rightarrow KC} \quad (4\text{-}4)$$

In equations (4-2), (4-3), and (4-4), the enthalpy change of the gas is given on the left-hand side of the equation and the heat flow is on the right-hand side. The negative sign on the right- hand side in equation (4-2) is to take into account the direction of the flow of gas which is opposite to the solid and kiln car.

4.2 Differential Equation for Kiln Car

The ordinary differential equation for the kiln car which is derived in the previous part considers the kiln car to be a single entity. The kiln car is divided into different material layers and each material layer can be divided into numerical layers. As seen in **Figure 4-3**, the heat which the top part of the kiln car receives from the gas and the solid is conducted till the bottom of the kiln car because the bottom of the kiln car is assumed to be adiabatic. Layer 1 receives heat from the gas through convection and radiation and from the solid by radiation. The heat from layer 1 is conducted to the next layer 2 and this will happen till layer n.

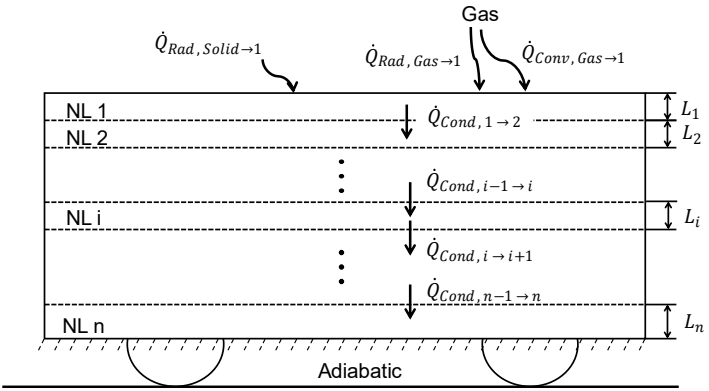

Figure 4-3 Heat conduction through the kiln car in the preheating zone

Ordinary differential equation for layer 1:

$$\dot{M}_1 c_1 \frac{dT_1}{dx} = \left[\dot{Q}_{Gas\to KC^1} + \dot{Q}_{Solid\to KC^1} - \dot{Q}_{KC^1\to KC^2}\right] \tag{4-5}$$

Ordinary differential equation for layer ‘i’:

$$\dot{M}_i c_i \frac{dT_i}{dx} = \left[\dot{Q}_{KC^{i-1}\to KC^i} - \dot{Q}_{KC^i\to KC^{i+1}}\right] \tag{4-6}$$

Ordinary differential equation for layer ‘n’:

$$\dot{M}_n c_n \frac{dT_n}{dx} = \left[\dot{Q}_{KC^{n-1}\to KC^n}\right] \tag{4-7}$$

The number of numerical layers is decided by doing a grid independence study. Hence the single ordinary differential equation for the kiln car is divided into many differential equations to find the temperature profile of the kiln car as it moves through the tunnel kiln.

4.3 Heat Transfer in Tunnel Kiln

In section 4.1, the differential equations were created based on the heat flow rate from gas to the solid (ware and furniture), gas to the first numerical layer of the kiln car, and from the solid to the first numerical layer of the kiln car. This section will explain how to calculate the heat flow rate using the thermal resistance network. The thermal resistance

network of the preheating zone in a tunnel kiln is depicted in **Figure 4-4**.

In analogy to electrical circuits, in heat transfer, temperature difference is considered as the potential difference and heat flow is considered as current. The resistance to the flow of heat can be derived from the equation

$$\dot{Q} = \frac{T_{High} - T_{Low}}{R}. \tag{4-8}$$

In the preheating zone, the temperature of the gas is higher than the solid and the kiln car. The heat flow happens because of the difference in the temperature between the gas, solid, and the kiln car. From the gas to the solid, the heat flows through two parallel paths; one represents the convective heat transfer and the other represents the radiative heat transfer. The flow of heat from the gas to the kiln car also follows two different paths similar to the heat flow between the gas and the solid. The heat flow from the solid to the kiln car consists of only solid-to-solid radiation and hence has only one path from the solid to the kiln car. Inside the tunnel kiln, the flow of gas is unrestricted between the wall and the stacks of the roof tiles on the kiln car and hence the inner wall temperature is assumed to be that of the gas. The heat flows through a single path which means heat is conducted through the wall and then follows two paths; one is convection and the other is radiation to the ambient air. The heat from the top of the kiln car is conducted towards the bottom of the kiln car through the different material layers of the kiln car and follows a single path because there is only a single mode of heat transfer.

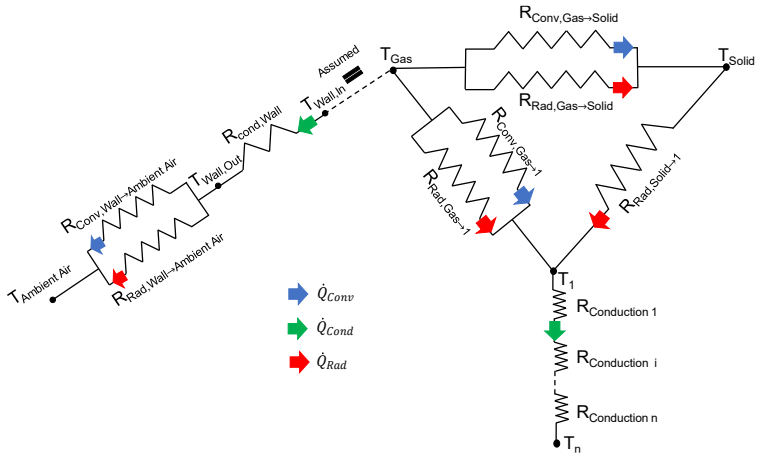

Figure 4-4 Thermal resistance network of heat transfer inside the preheating zone of a tunnel kiln

Heat flow rate between Gas and Solid:

$$\dot{Q}_{Gas\rightarrow Solid} = \dot{Q}_{Conv,Gas\rightarrow Solid} + \dot{Q}_{Rad,Gas\rightarrow Solid} \tag{4-9}$$

$$\dot{Q}_{Conv,Gas\rightarrow Solid} = \alpha_{Conv,Gas\rightarrow Solid} \cdot A_{Solid} \cdot (T_{Gas} - T_{Solid}) \tag{4-10}$$

$$\dot{Q}_{Rad,Gas\rightarrow Solid} = \alpha_{Rad,Gas\rightarrow Solid} \cdot A_{Solid} \cdot (T_{Gas} - T_{Solid}) \tag{4-11}$$

Heat flow rate between Gas and Kiln car (1st numerical layer):

$$\dot{Q}_{Gas\rightarrow 1} = \dot{Q}_{Conv,Gas\rightarrow 1} + \dot{Q}_{Rad,Gas\rightarrow 1} \tag{4-12}$$

$$\dot{Q}_{Conv,Gas\rightarrow 1} = \alpha_{Conv,Gas\rightarrow 1} \cdot A_{Kiln\ car} \cdot (T_{Gas} - T_1) \tag{4-13}$$

$$\dot{Q}_{Rad,Gas\rightarrow 1} = \alpha_{Rad,Gas\rightarrow 1} \cdot A_{Kiln\ car} \cdot (T_{Gas} - T_1) \tag{4-14}$$

Heat flow rate between Solid and Kiln car (1st numerical layer):

$$\dot{Q}_{Solid\rightarrow 1} = \dot{Q}_{Rad,Solid\rightarrow 1} \tag{4-15}$$

$$\dot{Q}_{Rad,Solid\rightarrow 1} = \alpha_{Rad,Solid\rightarrow 1} \cdot A_{Kiln\ car} \cdot (T_{Solid} - T_1) \tag{4-16}$$

Heat flow rate through the kiln car:

$$\dot{Q}_{Cond,1\to2} = \left(\frac{\lambda_1}{L_1/2} + \frac{\lambda_2}{L_2/2}\right) \cdot A_{Kiln\ car} \cdot (T_1 - T_2) \tag{4-17}$$

$$\dot{Q}_{Cond,1\to2} = \dot{Q}_{Cond,i-1\to i} \tag{4-18}$$

$$\dot{Q}_{Cond,i-1\to i} = \left(\frac{\lambda_{i-1}}{L_{i-1}/2} + \frac{\lambda_i}{L_i/2}\right) \cdot A_{Kiln\ car} \cdot (T_{i-1} - T_i) \tag{4-19}$$

$$\dot{Q}_{Cond,1\to2} = \dot{Q}_{Cond,i-1\to i} = \dot{Q}_{Cond,n-1\to n} \tag{4-20}$$

$$\dot{Q}_{Cond,n-1\to n} = \left(\frac{\lambda_{n-1}}{L_{n-1}/2} + \frac{\lambda_n}{L_n/2}\right) \cdot A_{Kiln\ car} \cdot (T_{n-1} - T_n) \tag{4-21}$$

Heat flow rate between gas and outside ambient air:

$$\dot{Q}_{Gas\to Ambient\ Air} = \dot{Q}_{Cond,Wall} = \dot{Q}_{Conv,Wall\to Ambient\ Air} + \dot{Q}_{Rad,Wall\to Ambient\ Air} \tag{4-22}$$

$$\dot{Q}_{Cond,Wall} = \left(\sum_i \frac{\lambda_i}{L_i}\right) \cdot A_{Wall} \cdot \left(T_{Gas} - T_{Wall,out}\right) \tag{4-23}$$

i refers to the different kinds of material in the wall structure.

$$\dot{Q}_{Conv,Wall\to Ambient\ Air} = \alpha_{Conv,Wall\to Ambient\ Air} \cdot A_{Wall} \cdot (T_{Wall,out} - T_{Ambient\ Air}) \tag{4-24}$$

$$\dot{Q}_{Rad,Wall\to Ambient\ Air} = \alpha_{Rad,Wall\to Ambient\ Air} \cdot A_{Wall} \cdot (T_{Wall,out} - T_{Ambient\ Air}) \tag{4-25}$$

4.4 Grid Independence of the Solution

Figure 4-5 shows how the temperature of the roof tile changes when the material layer is divided into different numbers of numerical layers. As the number of numerical layers per material layer increases, the change in the temperature of the roof tile becomes less; when the number of numerical layers is increased from 35 to 60, the increase in

the temperature of the roof tiles at dimensionless position 0.39 is 0.33 %. The time for the simulation with 35 numerical layers for each material layer is around 10 minutes. Each material layer is divided into 35 numerical layers and hence the number of differential equations which represent the kiln car is 210. Along with the ordinary differential equation for gas and solid, a total of 212 ordinary differential equations have to be solved to get the temperature profile of gas, solid, and the kiln car.

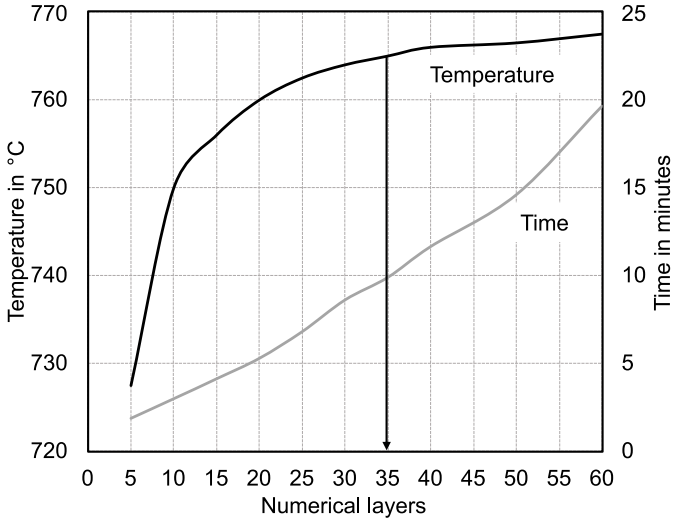

Figure 4-5 Temperature of roof tile at the position 0.39 for different numbers of numerical layers

4.5 Calculation Method

In the tunnel kiln, the mass flowrate of the gas is not constant along the entire length of the kiln. At the end of the tunnel kiln cooling air is given in and some of the air is sucked out in the end cooling zone to reduce the cooling rate of the solid in the static cooling zone. In the rapid cooling zone, cooling air is added to the system and some of the hot air is extracted from the tunnel kiln to increase the cooling rate of the solid that is coming from the firing zone. In the firing zone, the hot air is mixed with combustion gas coming out from the different top and

side burners located at different positions in the firing zone. This shows that the mass flowrate is not constant (**Figure 4-6**) along the tunnel kiln.

To solve the ordinary differential equations, the kiln is segmented into sections where the mass flowrate of the gas remains constant. Starting the calculation from the entrance of the tunnel kiln, the initial conditions are the inlet temperatures of the solid, the different layers of the kiln car, and the outlet temperature of the gas. The inlet temperature of the solid and the kiln car are the data obtained from the experimental measurements but the value of the outlet temperature of the gas (T_{G0}) is an unknown. To start the calculation process, an assumed value for the outlet temperature of the gas (T_{G0}) is considered, and in the initial section where the mass flowrate of the gas remains constant, the ordinary differential equations are solved with MATLAB 'ode23t' solver. The solver gives the temperature profiles of the gas, solid, and the different layers of the kiln car. To solve the ordinary differential equation of the next section, the results from the previous sections are used as initial conditions for the next section. This process continues till the end of the kiln and at the end, the calculated inlet temperature of the supply air is compared with the experimental temperature. When the temperatures do not match (**Figure 4-7**), linear regression is done to find the outlet temperature of the gas (T_{G0}) such that the calculated inlet temperature of the supply air (T_{Gl}) is equal to the actual value (T_{Gl}^{*}).

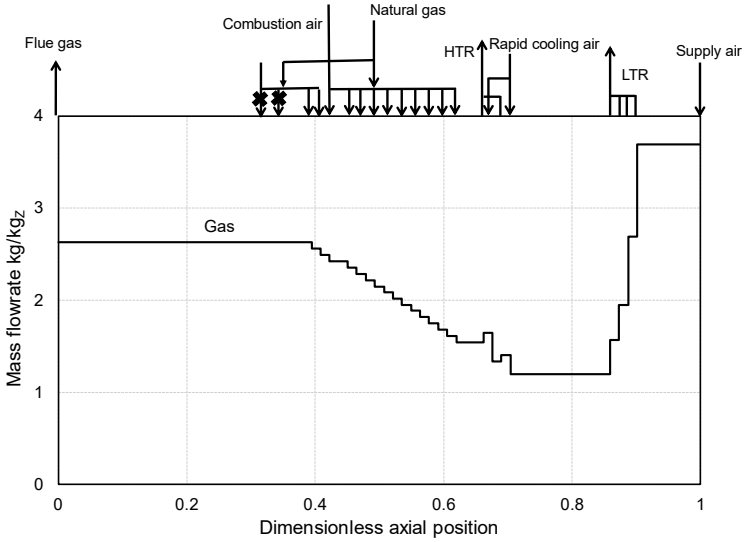

Figure 4-6 Mass flowrate (normalised) of gas in the tunnel kiln

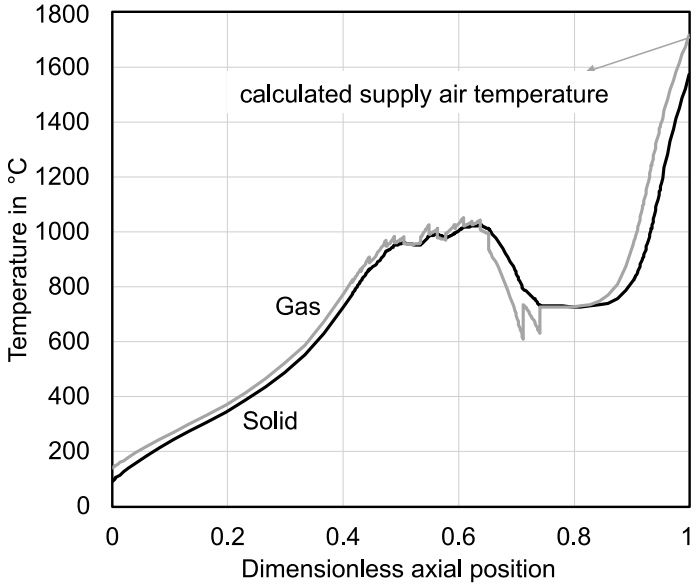

Figure 4-7 Calculated supply air temperature

When the starting assumed temperature of the outlet gas (T_{G0}) is high, then the calculation will go into very high values (**Figure 4-8**). To avoid this instability, when the calculated gas temperature (T_{Gx}) becomes more than 2000 °C, the program will try to find a lower outlet temperature of the gas as a starting value by linear regression, so that the value of the gas will remain less than 1500°C at that position. When the assumed temperature of the gas (T_{G0}) is less, then the calculated temperature (T_{Gx}) will be also less (Figure 4-8), then the program is manually terminated and should be again started with an increased outlet temperature of the gas. The algorithm of the program is shown in **Figure 4-9**.

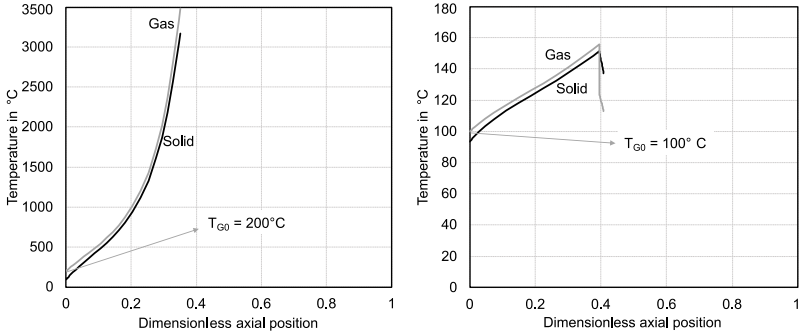

Figure 4-8 Assumed high (left) and low (right) outlet temperature of flue gas

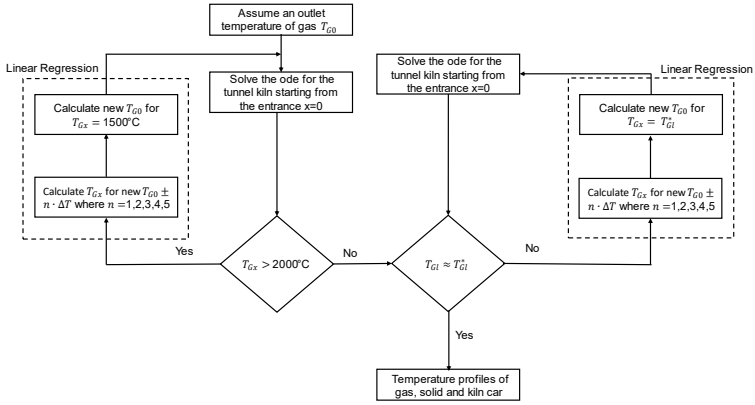

Figure 4-9 Algorithm of the program

5 Model Validation

5.1 Reference Tunnel Kiln

The temperature profile of the kiln car, as it moves through the tunnel kiln, is necessary for developing the process model. Experimental data of a tunnel kiln producing roof tile including the kiln car temperature profile was available from Brick and Tile Research Institute Essen. The total time for the kiln to come out of the tunnel kiln after going in through the entrance is about 16 hours. The mass flow rates are indicated in **Figure 5-1** with respect to per kilogram of the roof tile produced.

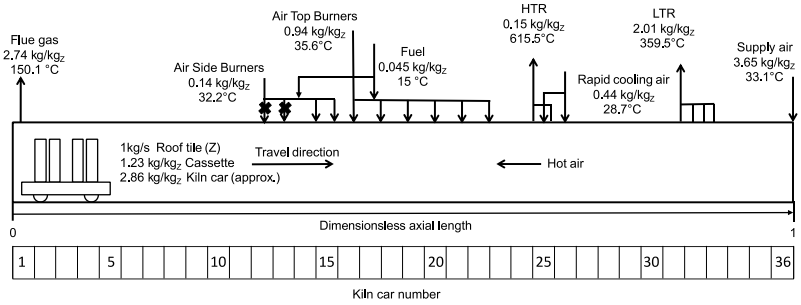

Figure 5-1 Process scheme of the reference tunnel kiln producing roof tiles

Each roof tile is kept on a cassette (H-cassette) and they are stacked on top of each other. The whole stack is kept on the kiln car. The kiln car with the stack moves from the entrance of the tunnel kiln from the left to the exit of the kiln which is at the right end as shown in Figure 5-1. The cooling air at a temperature of 33.1 °C enters the kiln from the exit of the kiln (right side) and travels in a direction opposite to the direction of the kiln car thereby cooling the roof tiles through convection. An amount of 2.01 kilogram of air per kilogram of roof tiles is extracted from the kiln car positions 31 and 32.5 to reduce the cooling rate of the roof tile to avoid cracks due to quartz inversion. A fresh supply of air at a temperature of 28.7 °C is injected at the kiln car location of 25.5 and 24.5 to increase the cooling rate of the roof tile. The hot air mixes with the combustion gas in the firing zone to reach a maximum gas temperature of 1010 °C. The hot gas flows to the

entrance of the kiln and heats the green roof tile and is extracted at the kiln car location of 0.5.

Figure 5-2 shows the experimentally measured temperature profile of roof tile at different positions in a stack and also the top temperature of the kiln car denoted as 3c in the figure. The temperature of the roof tile at the top (1), middle (2), bottom (3), and right side (4) as the roof tile passes through the entire tunnel kiln along with the gas temperature (2b and 3b), Cassette temperature (2a) and the top part of the kiln car (3c). The temperature difference between the top and bottom roof tile in the preheating zone is around 150 K and it shows clearly that the gas temperature distribution in the vertical direction is non-homogeneous. In the cooling zone, the temperature of the gas in the middle of the stack (2b) is almost 50 K more than at the bottom of the stack (3b), whereas, in the preheating zone, the temperature difference is more than 50 K.

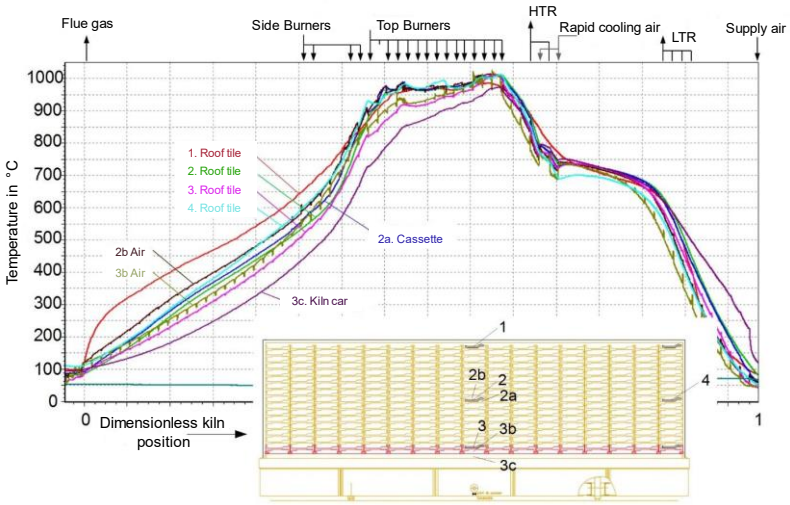

Figure 5-2 Measured axial temperature profile for various positions in the stack

5.2 Validated Model

The average temperature of the roof tiles in each of the 16 rows on a stack is compared with the simulated temperature of the solid (roof tile and cassette) to validate the model. **Figure 5-3** shows the simulated temperature of the gas, solid and the average measured temperature of the roof tiles along the kiln. In the preheating zone, the maximum variation between the simulated and measured temperature of the roof tile is around 25 K. The highest average measured temperature of the roof tile in the firing zone is almost 1001 °C whereas the simulated temperature of the roof tile is approximately 1020 °C. In the cooling zone, the main difference in the profile of the measured and simulated temperature of the solid lies mainly at the end of the tunnel kiln and the difference in the temperatures is 20 K.

As seen in Figure 5-2, the measured temperature of the roof tile in the top (1), middle (2) and bottom (3) of the stack is not the same. In the preheating zone, the top roof tiles are approximately 150 K higher than those in the bottom layer, where as in the firing zone, the bottom roof tiles have the highest temperature of 1010 °C and the top roof tiles have 975 °C. The roof tiles in the top layer are around 50 K higher than those in the bottom layer in the rapid cooling zone and in the static cooling zone, the temperature difference between them is almost 5 K. In the end cooling zone, the temperature of the top layer roof tiles is 50 K higher than the bottom layer roof tiles. This means that the temperature of the gas in the vertical direction is non-homogeneous but in the model, the gas is assumed to have a homogeneous temperature distribution to reduce the complexity of the calculation. The exact gas flow velocities along the vertical direction and the temperature profile of the gas are not known. Therefore, it is standard practice to derive the 1-dimensional temperature distribution of the gas and solid along the tunnel kiln.

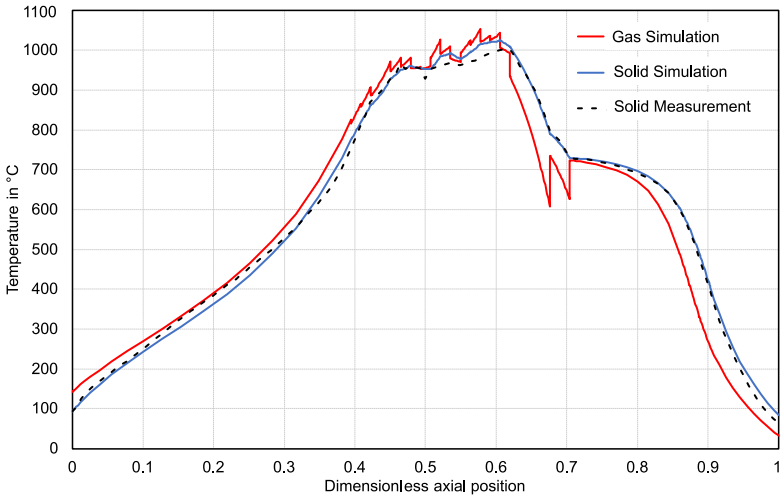

Figure 5-3 Measured and simulated axial temperature in the reference tunnel kiln

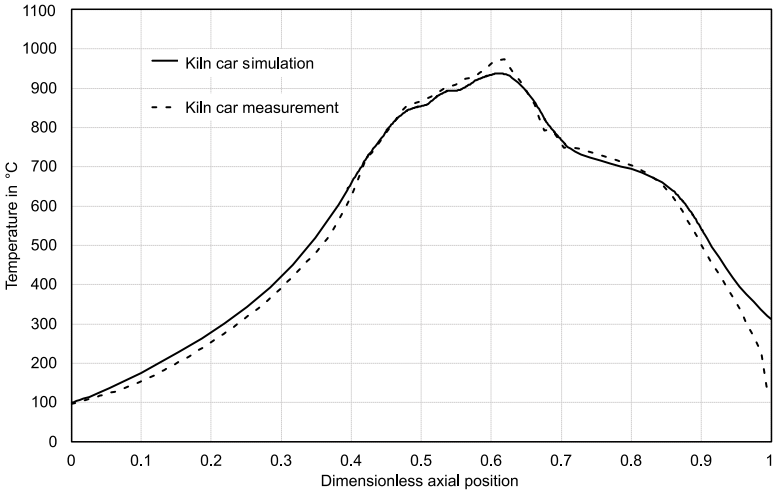

Figure 5-4 Measured and simulated temperature of kiln car in the reference tunnel kiln

Figure 5-4 depicts the measured temperature profile of the first layer of the kiln car and the simulated average temperature profile of the first

layer of the kiln car. In the preheating zone, the simulated kiln car temperature is more than the measured value by approximately 20 K whereas in the firing zone, the measured temperature is 40 K more than the simulated temperature profile. The simulated gas temperature is considered as the average gas temperature in the tunnel kiln and does not consider the vertical temperature distribution of the gas in the kiln. Hence, the simulated temperature will be higher than the gas temperature in the bottom layer of the stack and this results in the higher simulated temperature of the kiln car, where the heat from the gas is given to the kiln car in the preheating zone.

At the end of the firing zone, the average gas temperature becomes lower than the gas temperature in the bottom layer of the stack leading to a lower simulated temperature of the kiln car than the measured value. In the cooling zone especially in the end cooling zone, the simulated temperature profile deviates from the measured kiln car temperature profile and the highest simulated and measured temperatures at the exit of the tunnel kiln are 310 °C and 120 °C respectively. There are two reasons why the simulated temperature is higher than the measured temperature profile of the first layer of the kiln car. The first reason as explained before is because of the non-homogeneous temperature distribution of the gas which is evident from the higher temperature of the top layer roof tiles than the bottom layer roof tiles. This suggests that the gas at the bottom layer of the roof tile is lower than the simulated average temperature of the gas. The second reason is the orientation of the supply air at the end of the cooling zone. The supply air is fed into the cooling zone by blowing in the air at 33.1 °C from the top side of the tunnel kiln. This supply air impinges onto the first layer of the kiln car causing a sudden decrease in the temperature.

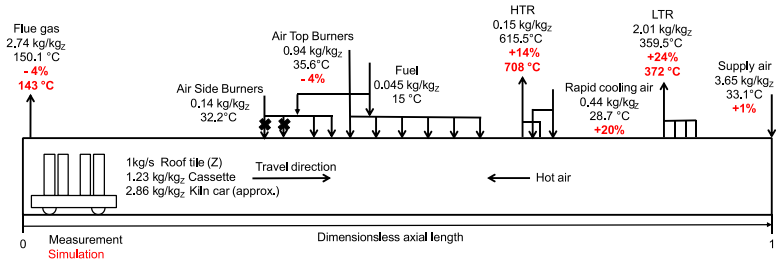

Figure 5-5 Mass flowrate of different inlets and outlets of gas in the reference tunnel kiln; black: Measured value, red: Values used for simulation

The maximum variation in the values of the mass flow rates used for the simulation and the measured value is 24% for LTR. As seen in **Figure 5-5**, the measured temperature of the HTR is 615,5 °C whereas the simulated temperature of the HTR is 708 °C. The difference of 4% between the measured value mass flow rate and simulation value of the exhaust gas shows that the amount of gas in the preheating and firing zone in the simulation and in the reference kiln is almost the same. The simulated outlet temperature of the exhaust gas is 143 °C which is almost 7 K less than the measured value. The variation in the measured mass flow rate of the primary combustion air and the supply air compared to the value used in the simulation is very small and hence it can be understood that the variation at HTR, LTR, and rapid cooling air is due to experimental errors. It should also be taken into account that the mass flows in the tunnel kiln can never be measured very exactly. Mostly, air flows are given by the power profiles of the blowers. The temperature in the flue gas is not homogenous. The temperature is measured only at one position and cannot be the average value.

5.3 Simulation Results

As already mentioned in the modeling section that each material layer is divided into 35 numerical layers. The temperature variation of each of the numerical layers along the tunnel kiln is depicted in **Figure 5-6**. The temperature profiles of numerical layers which belong to the same material layer are coloured similarly. The numerical layers corresponding to the first or top material layer are coloured grey;

orange represents the second material layer; yellow is the third material layer; red depicts the fourth material layer; black corresponds to the fifth material layer and brown is the sixth or the bottommost material layer.

The first material layer is the layer that is heated up faster than the second in the preheating zone by the heat from the hot gas coming from the firing zone. The spikes in the temperature profile on the topmost numerical layer from position 0.4 to 0.6 show the burner position where the energy is fed into the kiln by the burning of natural gas. From position 0.6 to 1, which is the cooling zone; the temperature of the first layer decreases which shows that the heat is transferred from the first layers of the kiln car to cooling air in the cooling zone. The topmost numerical layer of the first material layer has a lower temperature than the bottom numerical layer of the first material layer. The second material layer also decreases its temperature, showing a reversal in the heat transfer direction compared to the preheating zone. At the end of the tunnel kiln, it can be seen that the top half of the second layer has a lower temperature than the bottom half of the second material layer. The first numerical layer of the third material layer increases its temperature gradually in the preheating zone and firing zone; reaches its peak temperature in the cooling zone and stays almost constant till the end of the cooling zone. The temperature of the other numerical layers of the third material layer also increases slowly in the kiln and at the end of the cooling zone comes out of the cooling zone with temperatures in the range of 500 °C to 280 °C. The trend of the fourth and fifth material layers is similar to the third material layer and the bottommost material layer has the least change in the temperature.

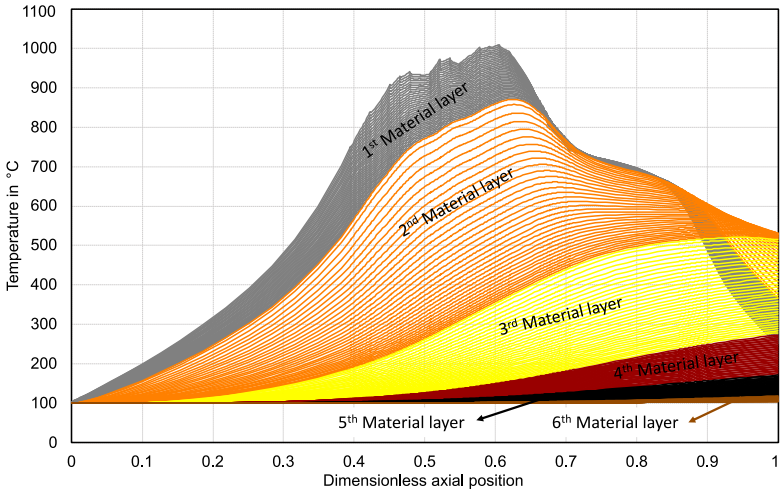

Figure 5-6 Simulated temperature profile of different material layers of kiln car along the tunnel kiln

The convective and radiative heat transfer coefficient between the gas and the solid is shown in **Figure 5-7**. Starting from the right of the graph because the gas flows from the end of the tunnel kiln to the entrance of the tunnel kiln, the convective heat transfer coefficient increases. The locations where there is a sudden drop in the convective heat transfer coefficient depict the locations where the cooling air is extracted from the kiln. The sudden increase depicts the locations where the air is injected in the cooling zone and the burning of natural gas in the firing zone. In the preheating zone, the convective heat transfer coefficient decreases because of the decrease in the gas temperature as the heat from the gas is transferred to the solid and the kiln car. The radiative heat transfer coefficient from the gas to the solid is zero from position 0.62 to 1. This represents the cooling zone and in the cooling zone, only air is present. In the firing and preheating zone, there are triatomic gases like carbon dioxide and water vapor which emit thermal radiation. In the firing zone the radiative heat transfer coefficient increases because of the combustion of the natural gas from the last burner to the first burner. As the temperature of the gas reduces

in the preheating zone the radiative heat transfer coefficient also decreases.

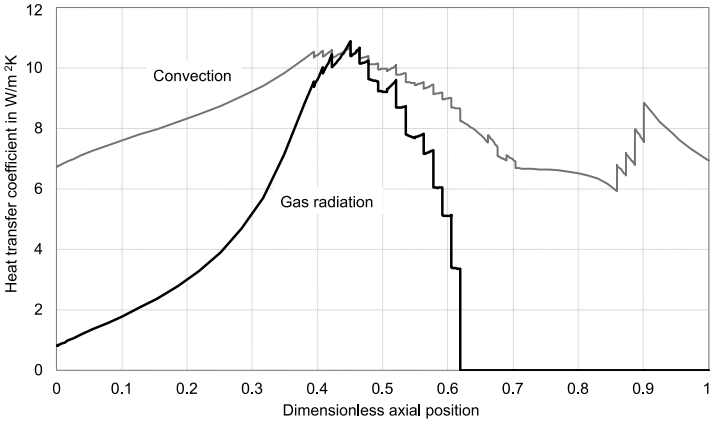

Figure 5-7 Convective and radiative heat transfer coefficient between the gas and solid in the tunnel kiln

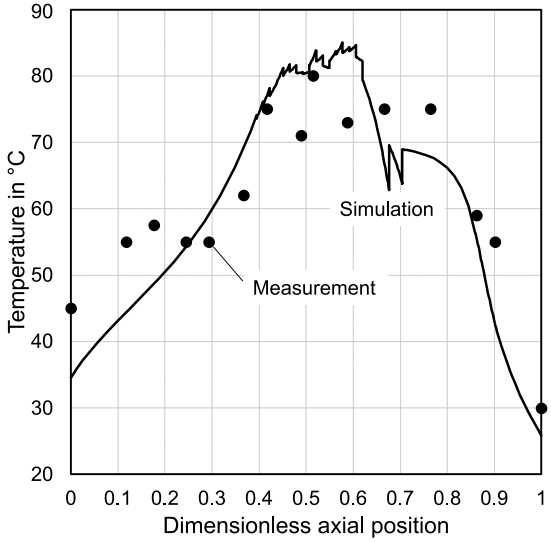

Figure 5-8 Axial temperature profile of the outside wall of the reference tunnel kiln

The simulated and measured outer wall temperature of the kiln is shown in **Figure 5-8**. The simulated outer temperature profile has the same profile shape as that of the gas temperature profile as seen in Figure 5-3. The heat transfer from the gas in the kiln to the outside atmosphere through the kiln wall is calculated for determining the outer wall temperature. This is the reason for the sudden decrease in the outer wall temperature at positions 0.68 and 0.7 and these are the locations where the rapid cooling air is injected.

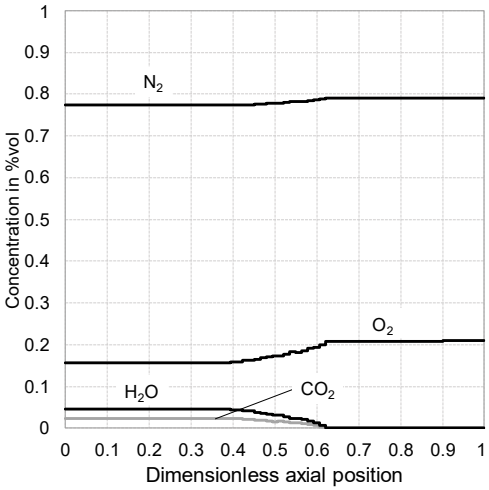

Figure 5-9 Axial profile of the gas concentration in the kiln (simulated)

The volume concentrations of carbon dioxide and water vapour in the exhaust gas calculated from the simulation are approximately 2.4% and 4.6% respectively and the graph is depicted in **Figure 5-9**.

6 Simulating Tunnel Kiln Process for Brick and Roof Tile

6.1 Firing Curve

The tunnel kilns operating in the ceramic industry for manufacturing brick and roof tile are not the same in terms of their dimensions and production capacity. Even if the production capacity and the dimensions remain the same, there can be differences in the process parameter under which the kiln is operating or different kinds of kiln cars for carrying the ware through the tunnel kiln. When a process model for a validated tunnel kiln is used for studying, the variation of process parameters such as change in the mass flow of the ware, then this result is only valid for this particular tunnel kiln. This constraint makes it necessary to create a generic tunnel kiln process for the production of brick and roof tile so that studying the results from the simulation will lead to a better understanding of the tunnel kiln process.

The start of designing a generic tunnel kiln process is with the firing curve of the ware. The firing curve of the ceramic describes the heating rate and cooling rate in addition to the time for which the temperature of the ware should be kept at the sintering temperature. Vasic et al. [41] determined the firing curve of montmorillonite and hydromica brick clays by dilatometry and the temperature profiles of the ceramic from different industrial tunnel kilns obtained from Brick and Tile Research Institute were used to determine the firing curve of brick and roof tile.

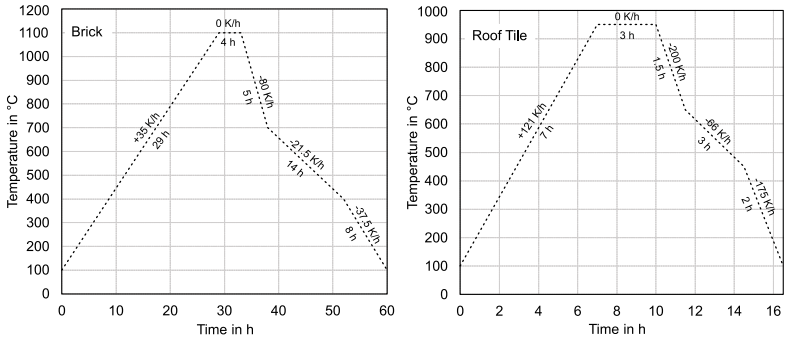

Figure 6-1 Firing curve of brick (left) and roof tile (right)

The graphs in **Figure 6-1** show the theoretical temperature profile the brick and the roof tile should follow to get the desired product quality. For bricks, the time from heating to cooling takes about 60 hours whereas for roof tile it is 16.5 hours. The firing curve also shows the heating rate and the cooling rate at different zones in the tunnel kiln. The highest cooling rate of 80 K/h for bricks and 200 K/h corresponds to rapid cooling. The lowest cooling rate of 21.5 K/h and 66 K/h for brick and roof tile respectively is the cooling rate in the static cooling zone because at temperatures of 573 °C the cooling rate has to be low to avoid crack formation due to quartz inversion. The maximum time-consuming part in the firing zone is the preheating phase which is about 29 hours for the brick and 7 hours for the roof tile and this corresponds to the preheating zone in the tunnel kiln where the moisture in the greenware is evaporated and the organic matter is burnt off.

6.2 Brick Tunnel Kiln

The brick tunnel kiln is designed to have a production capacity of 60 tonnes/day and the brick has a length, breadth, and height of 200 mm, 100 mm, and 70 mm respectively. The kiln car is considered to have a length of 3 m and a breadth of 3.7 m. The information regarding the different material layers in the kiln car are given in **Table 6-1** and the height of the kiln car is 0.68 m and the mass of a kiln car is about 10 tonnes. A single kiln car can transport around 2688 bricks and the arrangement of the bricks on the kiln car is shown in **Figure 6-2**. The information from the firing curve (Figure 6-1), required production capacity, and the mass of bricks on each kiln car can be used to find the length of each zone in the tunnel kiln and the calculated total length of the tunnel kiln is 60 m. The residence time of a kiln car in the tunnel kiln is 60 hours and every 3 hours a kiln car with unburnt bricks should be fed into the tunnel kiln. The height of the tunnel kiln from the top of the kiln car is 1.08 and the breadth is considered to be 3.8 m.

Table 6-1 Different material layers of the kiln car

Material layer	Thickness [m]	Thermal conductivity [W/m·K]	Density [kg/m^3]
1st	0.17	1.5	1550
2nd	0.15	0.25	400
3rd	0.06	0.18	64
4th	0.1	0.4	2013
5th	0.2	0.8	2200

After determining the length of each zone, the positions of the different inlets and outlets of air and burner positions can be fixed to get the firing curve. **Figure 6-3** shows the process scheme of the tunnel kiln that produces bricks. The positions of the different inlets and outlets of air and the burner position in the firing zone are depicted with respect to the kiln car number. Using the mass flow rate and the temperature given in the process scheme and the inlet temperature of the unfired brick and the kiln car as 100 °C, the firing curve can be simulated will the help of the ordinary differential equations as explained in section 4.

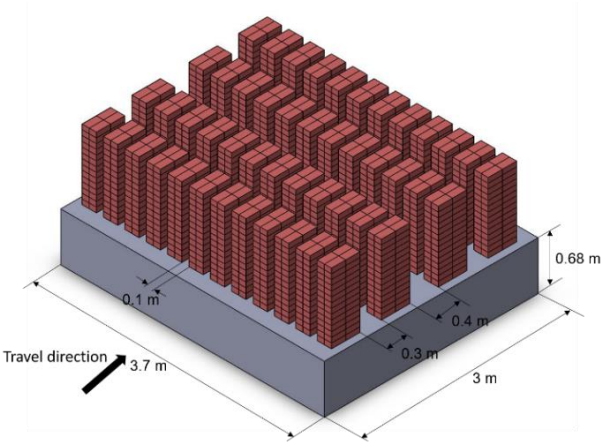

Figure 6-2 Brick arrangement on the kiln car

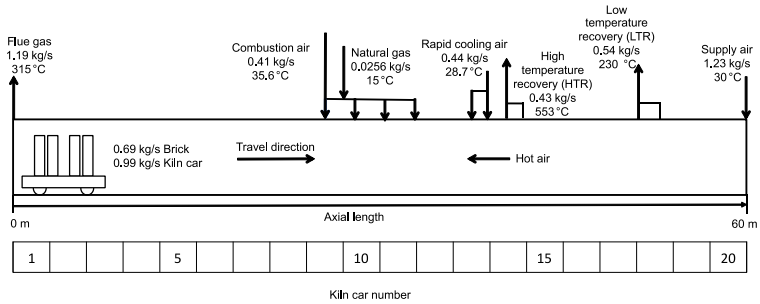

Figure 6-3 Process diagram of tunnel kiln for brick production

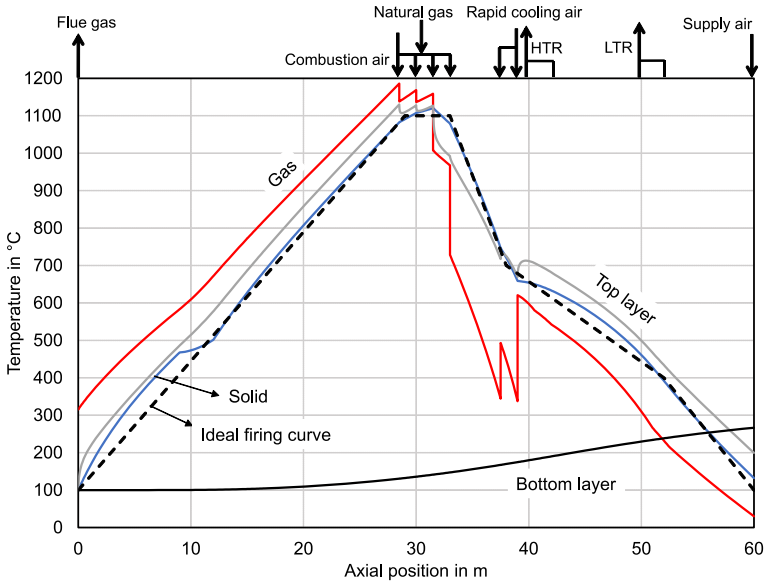

Figure 6-4 Simulated axial temperature profiles in the brick kiln

The simulated temperature profiles of the brick (solid), gas, and the top and bottom numerical layers are shown in **Figure 6-4**. The solid temperature has a maximum temperature difference of 70 K at the start of the preheating zone but follows the ideal temperature profile in the rest of the section of the kiln. At positions from 9 m to 12 m in the preheating zone, the solid temperature profile flattens because of the endothermic reactions happening inside the bricks. In the tunnel kiln,

the gas flows from the end of the kiln to the start of the kiln. In the cooling zone at positions 36 m and 39 m, cooling air at a temperature of 28.7 °C is added which causes the temperature to decline drastically as seen in the graph. In the firing zone, the rapid increase in the temperature is because of the addition of combustion gas and in the preheating zone, the temperature of the gas decreases because of the heat transfer to the brick and the kiln car and the outlet temperature corresponds to about 315 °C. The temperature profile of the top numerical layer of the kiln car has the same trend as that of the temperature profile of gas and the temperature of the bottommost numerical layer increases gradually in the preheating zone and reaches a maximum outlet temperature of 280 °C. The specific energy consumption of the tunnel kiln is 1.4 MJ/kg not including the energy consumption of the dryer.

6.3 Roof Tile Tunnel Kiln

The kiln is designed to have a production capacity of 180 tons per day and the roof tile has length of 450 mm and breadth of 350 mm. The cassette which holds the roof tile can be assumed to have the same length and breadth as the roof tile and the combined height of the roof tile and the cassette is 30 mm. **Figure 6-5** shows the simplified version of how the roof tiles and cassettes are arranged on the kiln car. There are 4 stacks on the kiln car and each stack has 14 layers in the vertical direction which is separated by a gap of 40 mm. In each layer, there are 10 roof tiles and cassettes and this layer is simplified as a flat plate. A single kiln car can transport 560 roof tiles through the tunnel kiln. The total height of the kiln from the top of the kiln car is 1.08 m and the breadth is 3.8 m. The total length of the tunnel kiln is 102 m which is calculated with the information from the ideal firing curve (Figure 6-1), the mass of roof tile on each kiln car and the required production capacity. The residence time of a kiln car in the tunnel kiln is 16.5 hours and every 28 minutes a kiln car with unburnt roof tile should be fed into the tunnel kiln. The kiln car considered for the roof tile tunnel kiln is the same as that of the brick tunnel kiln.

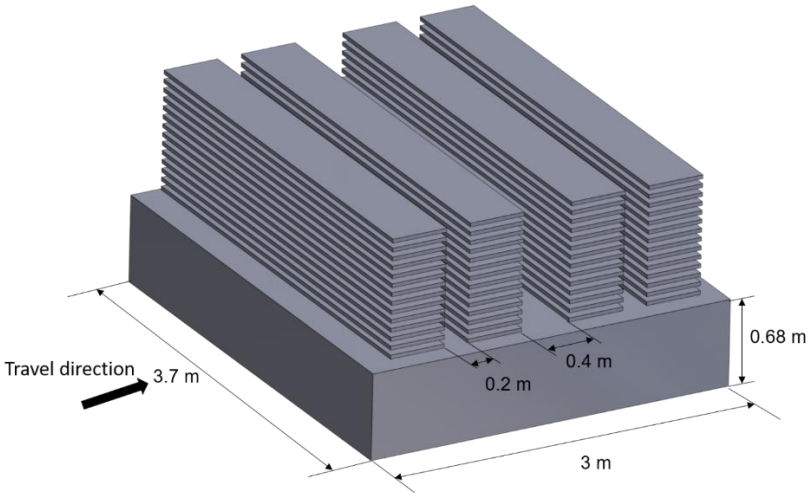

Figure 6-5 Roof tile (simplified) on the kiln car

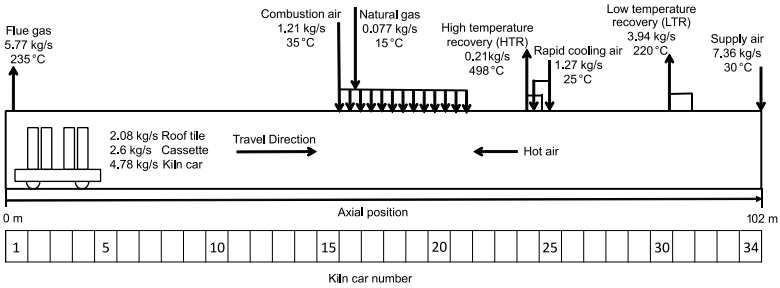

Figure 6-6 Process diagram of tunnel kiln for roof tile production

Figure 6-6 depicts the positions and mass flowrate of the inlets and outlets of air and the burners' positions in the firing zone. Using the mass flowrates in Figure 6-6 and the inlet temperature of the roof tile, cassette, and kiln car as 100 °C and from the method explained in section 4, the temperature profiles of the gas, roof tile and cassette (solid) and the kiln car are simulated.

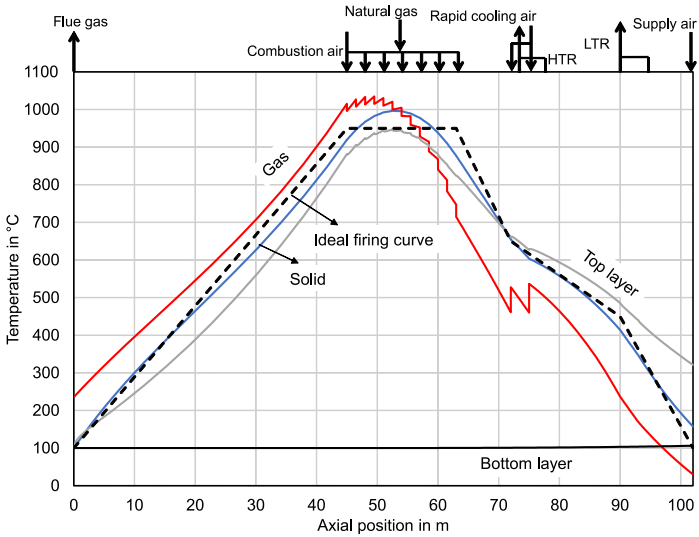

Figure 6-7 Simulated axial temperature profiles in the roof tile kiln

The simulated temperature profiles are shown in **Figure 6-7** and the temperature profile solid describes the temperature profile of the roof tile and cassette together because of the simplification of their configuration on the kiln car as plates. The solid temperature profile has a maximum temperature difference of 50 K to the ideal firing curve in the firing zone and attains a maximum temperature of 1000 °C. As explained previously the gas flows from the end of the tunnel kiln to the entrance of the tunnel kiln. Hence, the sudden decrease in the gas temperature is because of the rapid cooling air and the sudden increase in the temperature of the gas is because of the addition of combustion gas into the tunnel kiln. The temperature of the bottommost numerical layer remains almost the same as the temperature at which it entered and it is 100 °C. The specific energy consumption of the tunnel kiln is 1.56 MJ/kg excluding the energy consumption of the dryer.

6.4 Kiln Car Temperature Profile

The temperature profiles of the different material layers of the tunnel kiln producing bricks and roof tiles are shown in **Figure 6-8** and **Figure 6-9** respectively. Each line in the graph shows the temperature profile of the numerical layer and each material layer in the kiln car is divided into 35 numerical layers. The inlet temperatures of all the material layers are kept at 100 °C because the kiln car in some tunnel kilns directly comes from the dryer and then to a separate preheating chamber before entering the tunnel kiln.

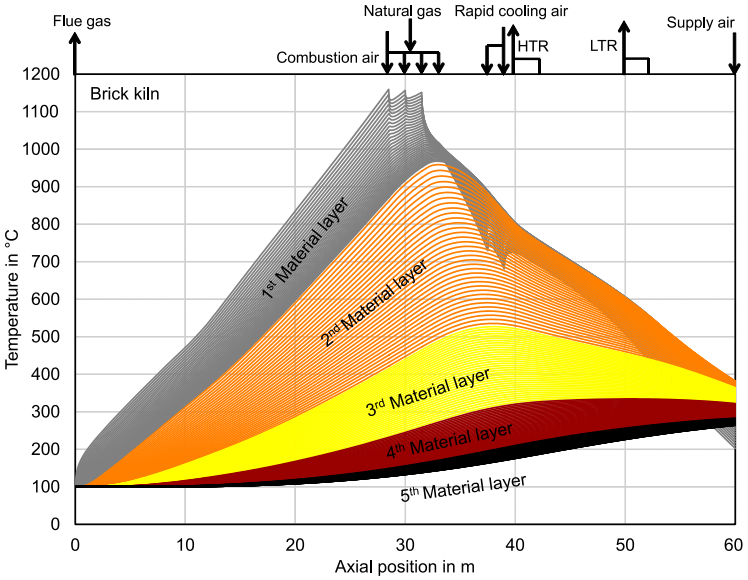

Figure 6-8 Temperature profile of various material layers in kiln car of brick kiln

From Figure 6-8, we can see that the first material layer of the kiln car reaches a temperature of more than 1000 °C. The spikes in the temperature profile of the first numerical layers show the places of the burners where the combustion of natural gas is occurring. Then the decrease in the temperature of the first numerical layers of the first material layer than the second material layer happens in the rapid

cooling zone. In the rapid cooling zone, the sudden drop in the temperature is because of the injection of the rapid cooling air at those positions. The first material layer temperature decreases more than the second material layer and finally comes out of the tunnel kiln with a temperature less than that of the other four material layers. The reason for the decrease in the temperature of the first layer than the other layers in the cooling zone is that the first material layer is exposed to the cooling air and the first layer losses heat more to the cooling air by convection than by conduction to the bottom layers. In the preheating zone, the first layer gets heat from the gas and this heat is conducted to the second material layer which will increase its temperature and the heat will be further conducted downwards till the bottom material layer. The temperature of the fifth material layer does not increase in the preheating zone but as more heat is conducted from the top material layers, its temperature keeps on increasing even in the cooling zone. In the brick tunnel kiln, the outlet temperature of the different material layers will be between 200 °C and 400 °C.

Within the first material layer of the kiln car in the roof tile tunnel kiln, the temperature difference reaches a maximum value of more than 400 K in the firing zone and it is about 300 K for the kiln car in the brick tunnel kiln. The temperature difference within the second material layer is about 350 K and 450 K for the kiln car in the roof tile and brick tunnel kiln respectively. The first layer of the kiln car in the roof tile tunnel kiln cools down faster than the other bottom material in the cooling zone because of the heat transfer to the cooling air by convection. There is only an increase in the temperature of the fifth material layer by 10 K. To understand the difference between the temperature profiles of the kiln car in brick and roof tile producing tunnel kilns, the residence time of the kiln cars in both the tunnel kilns has to be considered. In the brick producing tunnel kiln, the residence time of the kiln car is 60 hours whereas, in the roof tile kiln, it is 16.5 hours. The high residence time of the kiln car in the brick tunnel kiln causes the kiln car to absorb heat from the gas in the preheating zone. This is the reason for the high temperature of the first material layer. But in the cooling zone, even though the first material layer cools down faster than the other material

layers, the last material layer increases its temperature which means that the heat is conducted from the material layers above it. This is not the case with the kiln car in the roof tile tunnel kiln where the temperature increase of the last material layer is about 10 K as compared to almost 200 K in the brick tunnel kiln. The percentage of the energy coming out with the kiln car to the total outlet energy is about 30% and 20% for the roof tile and brick tunnel kiln respectively. The high residence time of the kiln car in the brick kiln allows the heat from the kiln car to be transferred to the cooling air in the cooling zone than the kiln car in the roof tile kiln. This is also the reason for the high outlet temperature of the layers of kiln car in roof tile kiln than brick kiln.

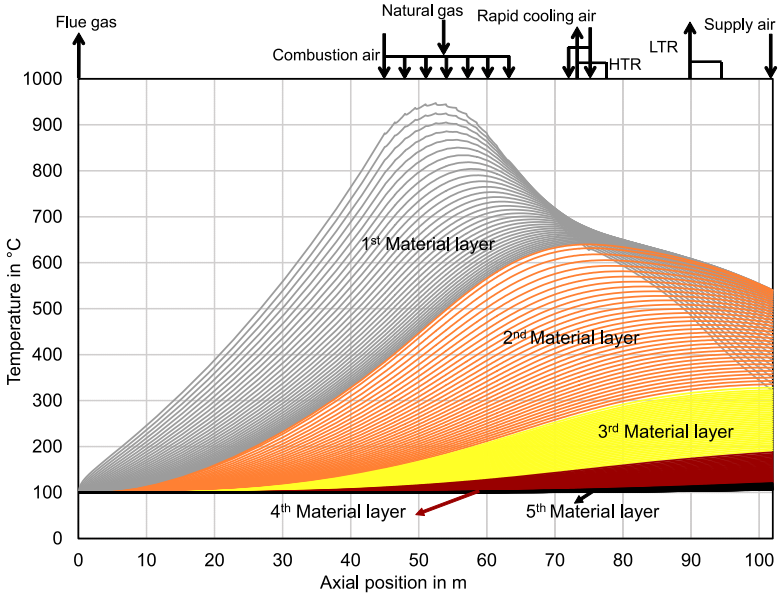

Figure 6-9 Temperature profile of various material layers in kiln car of the roof tile kiln

6.5 Heat Transfer Coefficient of Kiln Car

The overall heat transfer coefficient between the gas and the first layer of the kiln car of the brick and roof tile tunnel kiln is shown in **Figure 6-10**. In the tunnel kiln, the gas flows from the end of the tunnel kiln to the entrance of the tunnel kiln. The overall heat transfer coefficient from 1 to 0.61 position for the roof tile kiln and from 1 to 0.55 position for the brick kiln represents the convective heat transfer coefficient because it is the cooling zone. The peaks in the overall heat transfer coefficient from the position 0.61 in roof tile tunnel kiln and 0.55 in the brick kiln represent the increase in temperature of the gas due to the combustion of natural gas. The overall heat transfer coefficient from this position to the entrance of the tunnel kiln (position 0) represents the combination of the radiative heat transfer coefficient and convective heat transfer from the gas to the kiln car. The volume occupied by the gas for the length of the kiln car is more for the brick kiln than the roof tile kiln. This increases the beam length of the gas and hence the effective emissivity of the gas increases and this increases the radiative heat transfer coefficient between the gas and the first layer of the kiln car in brick kiln than in roof tile kiln. This is the reason for the high temperature of the first numerical layer than the brick as shown in Figure 6-4 whereas for the roof tile kiln, the roof tile has a higher temperature than the first numerical layer of the kiln car (Figure 6-7).

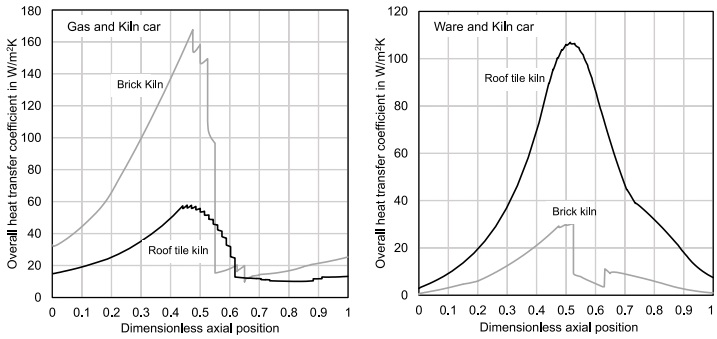

Figure 6-10 Overall heat transfer coefficient between gas and kiln car (left); Overall heat transfer coefficient between ware and kiln car (right)

The overall heat transfer coefficient between the ware and the first layer of the kiln car is shown in Figure 6-10 and is composed of only the solid to solid radiative heat transfer. In the roof tile kiln, the roof tile and the cassette lie parallel to the kiln car and hence the heat transfer can be considered as heat transfer between two parallel plates and the view factor used for calculating the radiative heat transfer coefficient becomes 1. In the brick kiln, the view factor from the top of the kiln car to the brick is calculated by approximating the two surfaces as two perpendicular rectangles with a common edge and the view factor is calculated to be 0.38. This is the reason for the low radiative heat transfer coefficient between the brick and kiln car compared to the roof tile and kiln car. The sudden drop in the radiative heat transfer coefficient between the brick and the kiln car at position 0.52 is because the temperature of the first layer becomes lower than the brick as seen in Figure 6-4. When the change in the temperature happens, the view factor from the brick to the first layer of the kiln car has to be calculated using the reciprocity rule and the view factor is around 0.12. At position 0.62, the temperature of the first layer becomes more than the brick and the view factor also increases which causes the sudden increase in the radiative heat transfer them.

6.6 Influence of the Kiln Car Properties

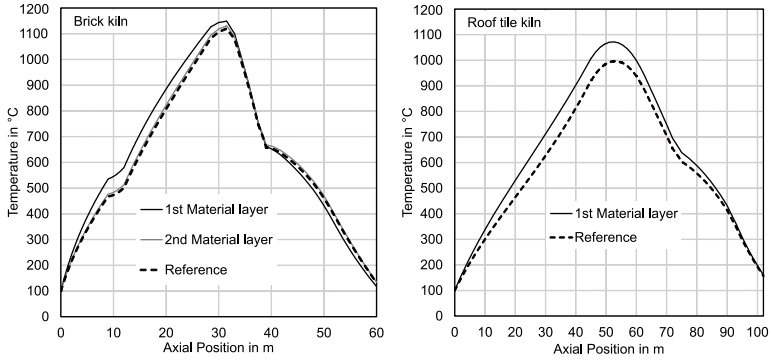

Figure 6-11 Change in the temperature profile of the brick (left) and roof tile (right) when the material property (density and conductivity) is changed to 70% for each layer

The kiln car is composed of five different material layers with different physical properties. The physical properties studied are the density and conductivity of the material layer. The reduction of density and conductivity means the mass of the kiln car is reduced and the kiln car is thermally insulated. An increase in the density and conductivity creates a heavy and thermally conductive kiln car. The density and conductivity of each layer are separately changed from 70% to 130% and the temperature profiles of the brick and roof tile are simulated. **Figure 6-11** shows the temperature profile of the brick and roof tile when the density and conductivity of each layer is 70% of the initial value (reference). For brick as well as roof tile kiln, the highest temperature in the firing zone increases by 30 K and 90 K respectively when the density and conductivity of the first material layer are reduced to 70%. There is a slight increase in the temperature profile of the brick when the density and conductivity of the second layer are reduced to 70% but not for the roof tile. The change in the density and conductivity of the other bottom material layers did not change the temperature profile of the brick and roof tile from the reference temperature profile. This shows that the first material layer of the kiln car influences the temperature profile of the ware in the tunnel kiln.

6.7 Reducing the Thickness of Kiln Car

The idea of reducing the thickness of the kiln car is to reduce the mass of the kiln car and hence reduce the ability of the amount of heat getting stored in the kiln car. The thickness of the current kiln car is 68 cm and two different thickness of the kiln car is considered. First, the kiln car is only 50% of the initial thickness which means the thickness of each material layer in the kiln car is also 50% and the total thickness of the kiln car is 34 cm. This value is considered to find the effect of the mass of the kiln car on the tunnel kiln process. Second, the kiln car is only 1% of the initial thickness and this thickness corresponds to 0.68 cm. Since this thickness is negligible compared to the other dimensions of the tunnel kiln, this can be considered as the case when the tunnel kiln process is without a kiln car.

Table 6-2 Mass flowrate change for the various gas inlets and outlets in percentage

Ware	Brick		Roof tile	
Thickness of kiln car	50	1	50	1
Supply air	0	-28	0	-5
LTR	0	-35	0	0
HTR	0	-45	0	0
Rapid cooling air	-10	-35	0	0
Natural gas	-10	-40	-12	-35
Combustion air	-10	-40	-12	-35

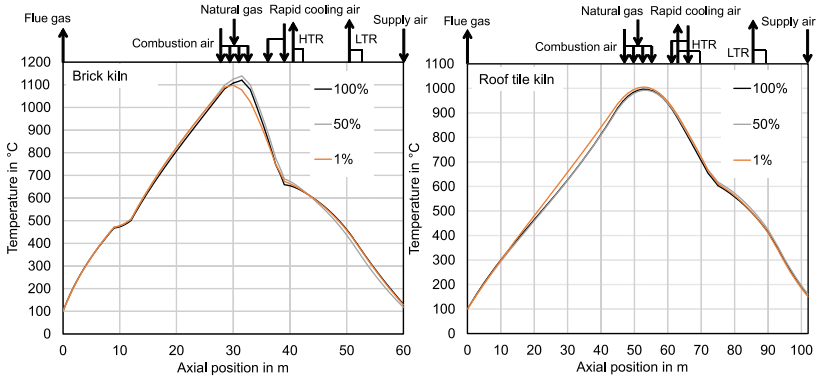

Figure 6-12 Simulated firing curve of brick and roof tile for various thicknesses of kiln car

When the thickness of the kiln car is changed, the temperature profile of the ware along the tunnel kiln should be the same as the firing curve, so that the quality of the product will not be affected. When the mass of the kiln car is reduced, the amount of fuel required to reach the sintering temperature is also reduced. The excess air number used in brick kiln and roof tile kiln is 1.2 and hence the combustion air will also reduce with the reduction in the amount of fuel. **Table 6-2** states the percentage change in the mass flow rates of air and fuel for different inlets and outlets to recreate the firing curve of brick and roof tile when the thickness of the kiln car is reduced. The recreated firing curve of the bricks and roof tile is shown in **Figure 6-12** and all the recreated firing curves are similar to the firing curve when the thickness of the

kiln car is 100%. 40% and 35% in fuel can be reduced in brick kiln and roof tile kiln respectively by the complete exemption of kiln car from the tunnel kiln process.

6.8 Different Kinds of Brick Arrangements

To understand the effects of the brick arrangement on the tunnel kiln process while keeping the production rate constant, three different arrangements are studied including the arrangement shown in Figure 6-2. This arrangement will be mentioned as configuration 2 in this section. For configuration 1 which is shown in **Figure 6-13**, a pillar of bricks is composed of 8 bricks and this configuration can be considered as a compact setting. For configuration 3 as seen in **Figure 6-14**, a pillar of brick is composed of only 1 brick and this can be viewed as a loose setting. Configuration 2 belongs to the case which is in between the compact and loose setting. In all the configurations, the number of bricks on the kiln car is 2688 and the firing dyke length is 0.4 m.

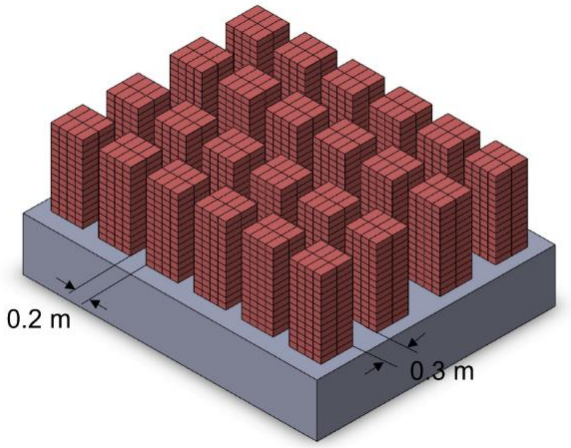

Figure 6-13 Configuration 1

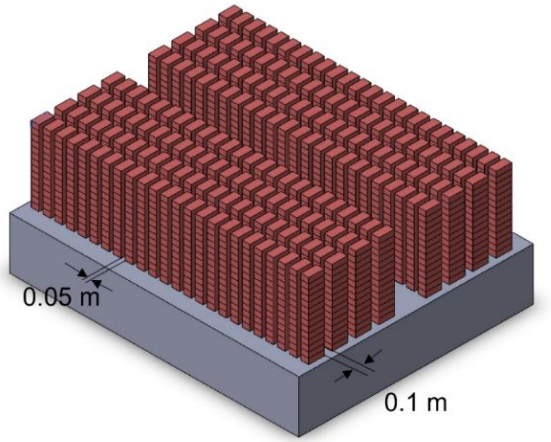

Figure 6-14 Configuration 3

Change in the mass flowrates which should be used to get the firing curve for all the different configurations when compared to configuration 1 is shown in **Figure 6-15**. Configuration 3 requires less than 48 % fuel compared to the compact setting and there is a considerable decrease in LTR and HTR. The decrease in the extraction of air from the cooling zone reduces the energy which is taken out of the tunnel kiln and given to the dryer and since the dryer does not require energy throughout the week. This will enable the dryer and the tunnel to be decoupled and the air which is extracted from the cooling zone can be given as preheated combustion air for the burners in the firing zone. The decrease in the energy requirement is mainly because of the decrease in the conductive resistance of the setting which increases the overall heat transfer coefficient between the brick and the gas. The conductive resistance as given in equation (3-26) is

$$R_{Cond} = \frac{0.5 s_s}{\chi \cdot \lambda_S} \cdot \tag{6-1}$$

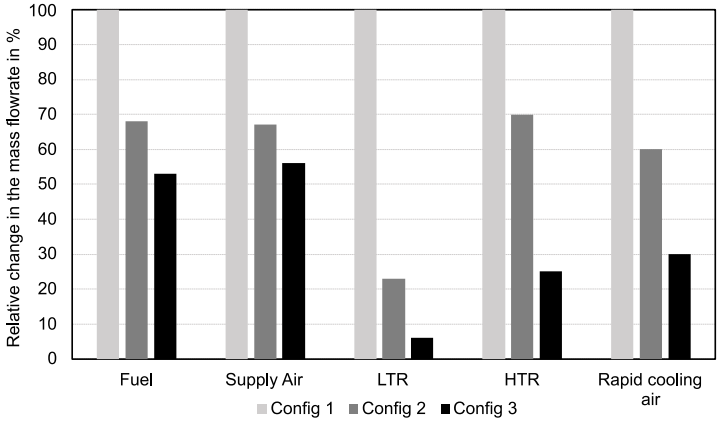

Figure 6-15 Influence of the configuration on the mass flowrate of gas on various inlets and outlets

The conductive resistance for configuration 1 and configuration 2 is 0.067 $m^2 \cdot K/W$ and 0.033 $m^2 \cdot K/W$, respectively. The conductive resistance for configuration 3 is one-fourth that of configuration 1 and the value is 0.0167 $m^2 \cdot K/W$. The surface area of the bricks which is available for the heat exchange between the gas also increases when the stacks have a loose arrangement. The value for the surface area of the bricks per unit length of the tunnel kiln for configuration 1 is 13.82 m^2/m. The arrangement with the loosely arranged bricks of configuration 2 and configuration 3 has the surface area to be 20.09 m^2/m and 38.91 m^2/m, respectively. The ordinary differential equation of the gas which is derived by combing the equations (4-2), (4-10) and (4-11) gives rise to the equation in (6-2).

$$\frac{dT_{Gas}}{dx} = -\frac{1}{\dot{M}_{Gas} c_{pGas}} \cdot \left[\begin{array}{c} -\alpha_{Gas \to Solid} \frac{A_{Solid}}{L} (T_{Gas} - T_{Solid}) - \alpha_{Gas \to 1} \frac{A_{KC}}{L} (T_{Gas} - T_1) \\ - 2\alpha_{Gas \to Air} \frac{A_{Wall}}{L} (T_{Gas} - T_{Air}) \end{array} \right] \tag{6-2}$$

As can be from equation (6-2), when the area available for heat exchange increases, to maintain the same temperature gradient in the cooling zone, the mass flow rate of the gas has to be reduced. This is

the reason for the reduced amount of supply air for configuration 3 as compared to configuration 1.

7 Carrier Plate as Kiln Car

7.1 New Transportation Concept

According to the new transportation system [42], where carrier plates on stationary rollers are used instead of kiln cars, will help avoid the energy loss through the heavy kiln cars. **Figure 7-1** shows the new concept of a transportation system with carrier plates on rollers. The idea is to retrofit the current tunnel kilns with the new transportation system instead of using the kiln cars to transport the ware and furniture along the kiln. The rollers are placed inside the tunnel kiln at a stationary position on a supporting plate which distributes the load evenly over the ground. Carrier plates carry the ware and are pushed over the rollers such that only this plate and ware travels through the kiln.

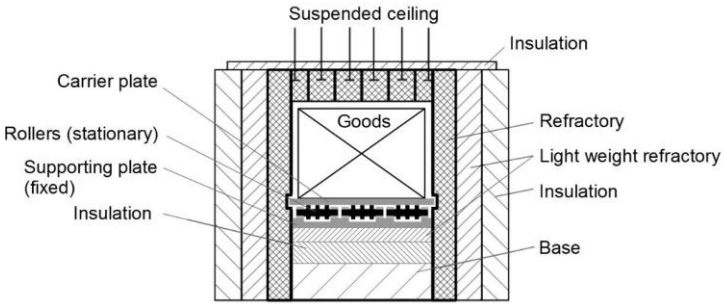

Figure 7-1 Concept of the new transportation system in Tunnel kiln with rollers and high temperature bearings [42]

7.2 Non-adiabatic Boundary Condition

When a carrier plate is used, the temperature under the carrier can become high. The approximation used in section 4.2, where the bottom is considered as an adiabatic boundary condition becomes invalid. From the bottom of the carrier plate, heat radiates to the insulation layer and base layer and finally to the ground. For a tunnel kiln with a kiln car, the heat is conducted through it and from its bottom, the heat is radiated to the floor. The radiated heat is conducted through the floor and then conducted into the ground. This change in the non-adiabatic

bottom has to be inserted into the ordinary equation of the last numerical layer of the kiln as given in (7-1)

$$\dot{M}_n c_n \frac{dT_n}{dx} = \left[\dot{Q}_{KC^{n-1}\rightarrow KC^n} - \dot{Q}_{KC^n\rightarrow Soil}\right]. \quad (7\text{-}1)$$

Figure 7-2 shows the non-adiabatic boundary condition under the bottom of the kiln car. The heat which is conducted through the different material layers of the kiln car is radiated from the bottom of the kiln car to the floor of the tunnel kiln '$\dot{Q}_{Rad,n\rightarrow floor}$'. The heat from the top of the floor is conducted through the floor construction (0.5 m) '$\dot{Q}_{Cond,Floor}$' and then conducted through the soil '$\dot{Q}_{Cond,Soil}$'. The thermal resistance network of the heat transfer with the non-adiabatic boundary condition is shown in **Figure 7-3**. The temperature of the soil beneath the tunnel kiln at a depth of 1 m, is assumed to be 15 °C. The temperature of soil below 1 m mentioned by the Deutscher Wetterdienst [43] when the air temperature is between 10 °C - 15 °C is between 5 °C and 10 °C.

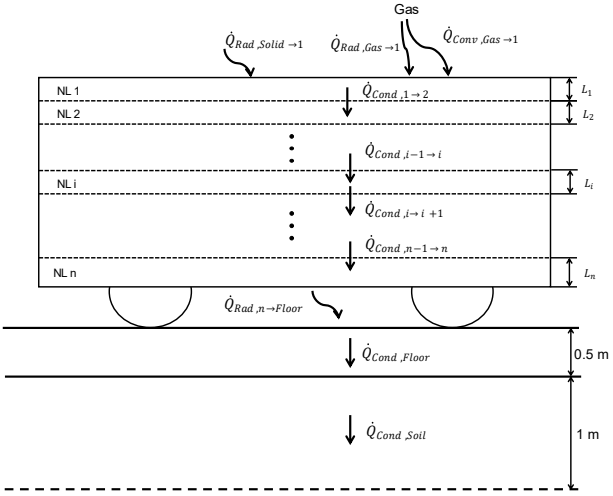

Figure 7-2 Heat conduction through the kiln car in the preheating zone with the bottom of the kiln car as a non-adiabatic boundary condition car as a non-adiabatic boundaryon

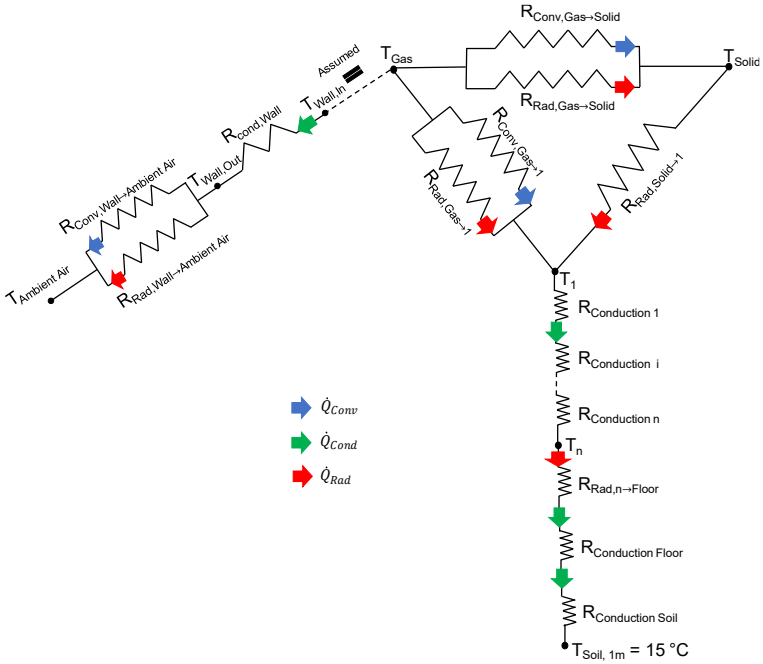

Figure 7-3 Thermal resistance network of heat transfer inside the preheating zone with non-adiabatic boundary condition

$$\dot{Q}_{KC^n \to Soil} = \dot{Q}_{Rad,n \to Floor} = \dot{Q}_{Cond,Floor} = \dot{Q}_{Cond,Soil} \tag{7-2}$$

$$\dot{Q}_{Rad,n \to Floor} = \alpha_{Rad,n \to Floor} \cdot A_{Floor} \cdot \left(T_n - T_{Floor,Top}\right) \tag{7-3}$$

$$\dot{Q}_{Cond,Floor} = \frac{\lambda_{Floor}}{L_{Floor}} \cdot A_{Floor} \cdot \left(T_{Floor,Top} - T_{Floor,Bottom}\right) \tag{7-4}$$

$$\dot{Q}_{Cond,Soil} = \frac{\lambda_{Soil}}{L_{Soil}} \cdot A_{Floor} \cdot \left(T_{Floor,Bottom} - T_{Soil,1\,m}\right) \tag{7-5}$$

The above equations from (7-2) to (7-5) represent the heat flow rate towards the bottom of the kiln car, where $T_{Floor,Top}$ means the temperature of the floor facing the bottom of the kiln car and $T_{Floor,Bottom}$ means the temperature of the floor on the soil. These temperatures are iteratively calculated from the temperatures of the

last numerical layer 'T_n' of the kiln car and the soil temperature '$T_{Soil,1\,m}$' at a depth of 1 m.

7.3 Reduction in the Kiln car Thickness with Non-adiabatic Boundary Condition

7.3.1 Kiln and Kiln Car Information

The reduction in the thickness of the kiln car leads to a reduced mass of the kiln car and hence a positive influence on the energy consumption of the tunnel kiln. The brick kiln and roof tile kiln which were described in sections 6.2 and 6.3 respectively are re-simulated with the non-adiabatic boundary conditions. When the thickness of the kiln car is reduced, mass flow rates of the supply air, LTR, HTR, rapid cooling air, and the fuel are changed accordingly to maintain the firing curve of the ware. The thickness of the kiln car is reduced from the initial thickness of 683 mm (100%) to a minimum value of 6.83 mm (1%) without reducing the mass flow rate of the ware. The thickness of the kiln car is reduced in steps of 25% from 100% to 1% to show the influence of a reduction in the mass flow rate of the kiln car on the fuel consumption without a change in the product quality by maintaining the firing curve. The internal construction of the kiln car remains the same as mentioned in Table 6-1 and only the thickness of each of the material layers is reduced correspondingly when the overall thickness of the kiln car is reduced.

7.3.2 Brick Kiln

Table 7-1 contains information regarding the outlet energy from the brick kiln for different thicknesses of the kiln car. The energy loss along with the produced bricks remains the same because of the unchanged production rate. The energy loss through the walls also remains the same. This is because of the same temperature difference between the gas inside the tunnel kiln and the outside ambient air. The energy loss through the HTR is reduced because of the reduced mass flow rate of the supply air to keep the capacity ratio ($\frac{\dot{m}_{Gas}c_{p,Gas}}{\dot{m}_{Solid}c_{Solid}+\dot{m}_{KC}c_{KC}}$) constant when the thickness of the kiln car is reduced. When the

thickness of the kiln car is at a minimum of 1%, the energy loss through the kiln car is reduced by 99.8 %. The reduction in the fuel consumption when the thickness of the kiln car is 1% is about 32% less and the energy lost through the non-adiabatic bottom of the kiln car increases to 60 kW from 10 kW. From section 6.7, when the thickness of the kiln car is reduced to 1% in an adiabatic case, the fuel savings was 40%. For a thickness of the kiln car between 10% to 25% which corresponds to 70 mm - 170 mm respectively, the energy savings are about 23% to 15%.

Table 7-1 Outlet energy from a brick tunnel kiln with kiln cars of various thickness

Thick-ness of Kiln car [mm]	Fuel Sav-ings [%]	Brick [kJ/s]	Flue gas [kJ/s]	Kiln car [kJ/s]	HTR [kJ/s]	LTR [kJ/s]	Wall Loss [kJ/s]	Bott-om Loss [kJ/s]
6.83 1%	32	79	267	0.4	103	106	153	60
68.3 10%	23	81	310	12	147	113	155	58
170.8 25%	15	81	325	80	166	128	153	46
341.5 50%	9.5	79	340	149	199	118	153	24
512.3 75%	6	81	350	177	224	128	152	14
683.0 100%	0	83	379	212	250	127	153	10

7.3.3 Roof Tile kiln

In the roof tile kiln, when the thickness of the kiln car is reduced to a value of 1% of the initial thickness, the energy required to maintain the firing curve is reduced by 34%. From section 6.7, when the thickness of the kiln car is reduced to 1% in an adiabatic case, the reduction in

fuel consumption is 35%. The wall loss and the energy through the roof tile and cassette remained almost the same for the cases with different thicknesses of the kiln car. The energy through the LTR and HTR was reduced by 25% because of the reduced mass flow rate of the supply air. For a thickness of the kiln car between 10% to 25% which corresponds to 70 mm - 170 mm respectively, the energy savings are about 23% to 18%.

Table 7-2 Outlet energy from a roof tile tunnel kiln with kiln cars of various thickness

Thick-ness of Kiln car [mm]	Fuel Sav-ings [%]	Roof tile [kJ/s]	Flue gas [kJ/s]	Kiln car [kJ/s]	HTR [kJ/s]	LTR [kJ/s]	Wall Loss [kJ/s]	Bott-om Loss [kJ/s]
6.83 1%	34	715	1186	5	108	641	256	103
68.3 10%	23	702	1291	231	79	847	257	89
170.8 25%	18	691	1315	553	79	834	256	41
341.5 50%	12	963	1378	770	188	829	254	18
512.3 75%	5	712	1410	1100	189	844	254	14
683.0 100%	0	715	1447	1428	138	846	255	13

7.4 Comparison of Kiln Car and Carrier Plate as Transport System

7.4.1 Carrier Plate Information

The Brick and Tile Research Institute Essen (Institut für Ziegelforschung Essen e.V.) conducts experiments with a carrier plate that has a thickness of 100 mm and a thermal conductivity of 1.5 W/m·K. The tunnel kiln producing bricks and roof tiles which were described in

section 6.2 and section 6.3 are re-simulated with the carrier plate as shown in **Figure 7-4**. The ceramic wares are kept on the carrier plate and the carrier plate moves through the tunnel kiln on ceramic rollers which are rotating along a fixed axis in the tunnel kiln. The thickness and conductivity of the carrier plate are considered to be the same as the carrier plate used in above mentioned institute.

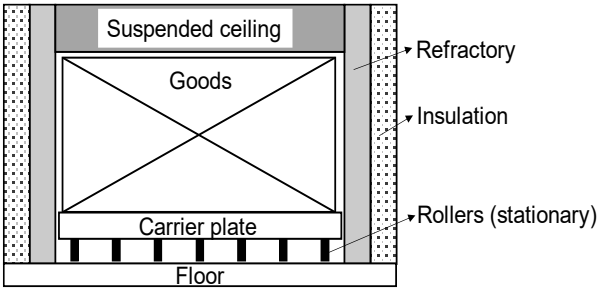

Figure 7-4 Carrier plate as a transportation system

7.4.2 Brick Kiln

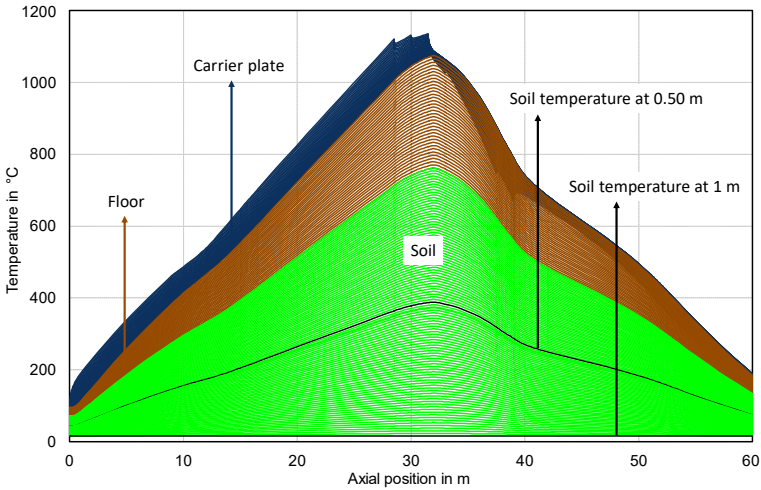

Figure 7-5 Temperature profiles of carrier plate ($\lambda = 1.5$ W/m·K), floor and soil along brick kiln

The temperature profile of the carrier plate along the tunnel kiln, when the firing curve of the brick is achieved, is depicted in **Figure 7-5**. The temperature profile of the 35 different numerical layers of the carrier plate is shown in blue whereas brown represents the temperature profile of the floor which has a thickness of 0.5 m. The green colour represents the temperature of the soil beneath the floor for a depth of 1 m. The carrier plate which has a thickness of 100 mm has a temperature difference between the top and bottom surface to be 50 K. In the cooling zone, the temperature of the carrier plate becomes less than the floor because of the heat loss to the cooling air. In the firing zone, the temperature of the top surface of the floor becomes more than 1000 °C and the bottom of the floor is around 750 °C and reduces to a temperature of approximately 200 °C at the end of the cooling zone. The temperature of the soil at a depth of 0.5 m is represented by a black line and the maximum temperature at this depth can reach almost 400 °C in the firing zone. At a depth of 1 m, the temperature of the soil remains constant and is 15 °C as seen in Figure 7-5.

The comparison of the outlet energy from the tunnel kiln producing bricks with the kiln car and carrier plate is given in **Table 7-3**. The energy consumption of the tunnel kiln with a carrier plate as a transportation system is almost 9% less than the kiln with kiln cars. This 9% is less than the 15% and 22% savings achieved when the thickness of the kiln car is reduced to 170.8 mm and 68.3 mm respectively, as given in Table 7-1. This is because the plate is made up of a single high conductive material rather than the kiln car which is made up of different material layers even when the thickness is reduced. There is no reduction in the HTR which suggest that because of the high conductivity of the carrier plate a lot of air is required in the cooling zone. This is because the carrier plate tends to heat the air more as compared to the kiln car and hence more amount of cooling is required.

Table 7-3 Comparison of the outlet energy of kiln car and carrier plate transportation system in brick kiln

TS	Fuel Savi-ngs [%]	Solid [kJ/s]	Flue gas [kJ/s]	TS [kJ/s]	HTR [kJ/s]	LTR [kJ/s]	Wall Loss [kJ/s]	Bott-om Loss [kJ/s]
Kiln car	0	83	379	212	250	127	153	10
Carrier plate	9	78	362	37	250	112	153	61

The influence of the conductivity of the carrier plate on the process is studied. **Table 7-4** contains information on the energy loss from the tunnel kiln producing bricks for carrier plates with different conductivity. When the conductivity is reduced from 1.5 W/m·K to 0.1 W/m·K, the amount of fuel required to maintain the firing curve is reduced by 14%. The energy losses thorough the HTR and bottom also decreased by 45% and 50% respectively. A reduction in the conductivity of the carrier plate caused an increase in the outlet energy through the carrier plate by 105%. This is due to the high residence time in the preheating and firing zone of approximately 33 hours and the reduction in the amount of supply air for cooling.

The temperature profile of the carrier plate with a conductivity of 0.1 W/m·K along the tunnel kiln, when the firing curve of the brick is recreated, is shown in **Figure 7-6**. As compared to the carrier plate with conductivity of 1.5 W/m·K, the maximum difference between the top and bottom surface of the carrier plate is higher and the value is around 650 K. The low thermal conductivity of the carrier plate causes a reduced flow of heat from the gas in the brick kiln to the floor. This has caused a reduced maximum temperature of the floor of 500 °C as compared to the 1100°C with the high conductivity carrier plate. The maximum temperature at a position 50 cm below the floor is also reduced to 150 °C from the 400°C. The maximum temperature of the floor and at position 50 cm below the floor is in the cooling zone of the tunnel kiln rather than in the firing zone when a high thermal

conductivity carrier plate is used. At the end of the cooling zone, the temperature difference in the lower conductivity carrier plate is 300 K which also explains the high energy loss through the lower conductivity carrier plate than the higher conductivity carrier plate.

Table 7-4 Outlet energy from a brick tunnel kiln for various conductivity of carrier plate

Conductivity [W/m·K]	Fuel Savings [%]	Solid [kJ/s]	Flue gas [kJ/s]	Kiln car [kJ/s]	HTR [kJ/s]	LTR [kJ/s]	Wall Loss [kJ/s]	Bottom Loss [kJ/s]
0.1	14	76	304	76	138	125	153	31
0.5	2	77	350	52	218	125	153	57
1	0	78	356	41	252	112	153	60
1.5	0	78	362	37	250	112	153	61

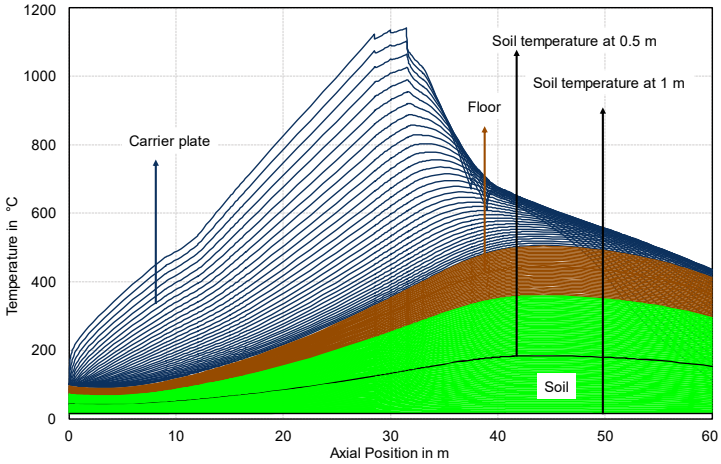

Figure 7-6 Temperature profiles of carrier plate ($\lambda = 0.1$ W/m·K), floor and soil along brick kiln

7.4.3 Roof Tile Kiln

The temperature profile of the carrier plate along the tunnel kiln is depicted in **Figure 7-7**. The temperature profile of the carrier plate in the roof tile kiln is different from that in the brick kiln. The main reason is the difference in the residence time of the carrier plate in both kilns. In the brick kiln, the residence time is 60 hours whereas in the roof tile kiln it is 16.5 hours. The temperature difference between the top and bottom of the carrier plate is high in the roof tile kiln as compared to that in the brick kiln. In the roof tile kiln, the difference in the temperature of the top of the carrier plate to the bottom of the carrier plate is 300 K at the start of the firing zone but in the brick kiln, it is 100 K as seen in Figure 7-5. This is because of the high velocity of the carrier plate in the roof tile kiln than in the brick kiln. In the cooling zone because of the small residence time of 6 hours, there arises a temperature difference between the top and bottom of the carrier plate of around 150 K whereas in the brick kiln it is around 50 K.

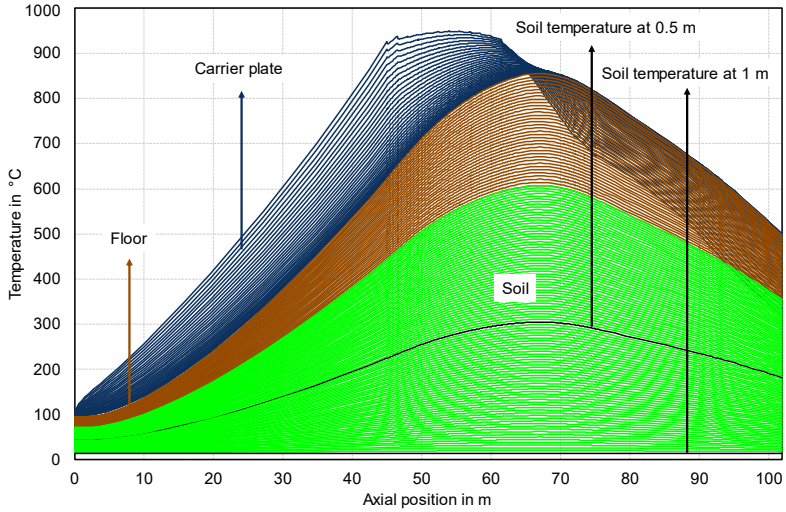

Figure 7-7 Temperature profiles of carrier plate (λ = 1.5 W/m·K), floor and soil along roof tile kiln

Table 7-5 Comparison of the outlet energy of kiln car and carrier plate transportation system in roof tile kiln

TS	Fuel Sav-ings [%]	Solid [kJ/s]	Flue gas [kJ/s]	TS [kJ/s]	HTR [kJ/s]	LTR [kJ/s]	Wall Loss [kJ/s]	Botto m Loss [kJ/s]
Kiln car	0	715	1447	1428	138	846	255	13
Carrier plate	3.5	713	1523	626	246	828	256	94

The amount of fuel used in the roof tile kiln with kiln car and carrier plate as transportation system is given in

Table 7-5. There is only a 3.5 % reduction in the energy consumption when carrier plate with a conductivity of 1.5 W/m·K. The outlet energy through the roof tile plus the cassette and the wall remained the same in both cases. The energy loss through the LTR remained the same but the loss through the HTR increased by 78%. The bottom loss increases from 13 kJ/s to 94 kJ/s, furthermore, the energy loss through the flue gas increased by 5%. The reason for the less effectiveness of the carrier plate as a transportation medium can be understood from the temperature profiles of the roof tile and the carrier plate which is shown in **Figure 7-8**.

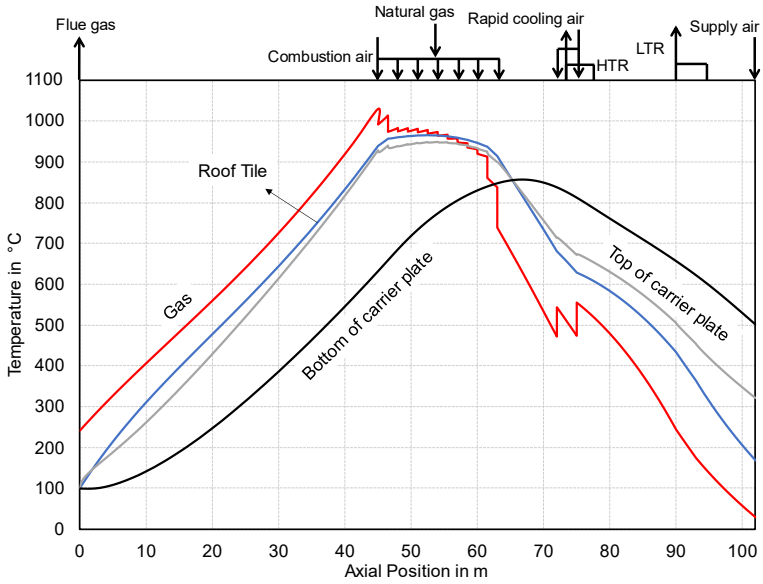

Figure 7-8 Temperature profile of roof tile along with the top and bottom profiles along the tunnel kiln

Initially, the temperature of the top of the carrier plate is higher than the roof tiles. Then in the preheating zone, the temperature becomes lower than the roof tiles as seen in Figure 7-8. The radiative heat transfer coefficient between the roof tiles is high as shown in Figure 6-10, because of the approximation of the heat transfer as two parallel plates. This causes the heat from the roof tile to radiate to the top of the carrier plate and since the conductivity of the carrier plate is high, the heat is conducted to the bottom of the plate which increases its bottom temperature. In the preheating zone, the heat which is supplied from the gas to the roof tile is lost to the carrier plate through radiation and this is the reason for the less energy savings achieved with the carrier plate. In the cooling, the temperature of the top of the carrier plate is higher than the roof tiles which means that the heat from the carrier plate will flow to the roof tiles. This cause problem in achieving the required cooling rate in the static cooling zone where the cooling rate has to be 66 K/h. Since the roof tile is receiving heat from the carrier plate, the amount of cooling air in the cooling zone in increased

which is extracted through the HTR. This is the reason for the increase in the energy loss through HTR of 78% compared to the roof tile kiln with a normal kiln car.

The effect of conductivity of the carrier plate on the tunnel kiln process is studied and the results are given in **Table 7-6**. When the conductivity of the carrier plate is reduced to 0.1 W/m·K, the bottom loss is reduced to 21 kJ/s from 94 kJ/s. The energy loss through the HTR is reduced by 44% which shows a reduced amount of cooling air is supplied in the cooling zone. The amount of fuel required to maintain the firing curve reduces by 20% when the conductivity of the kiln car is reduced to 0.1 W/m·K.

Table 7-6 Outlet energy from a roof tile tunnel kiln for various conductivity of carrier plate

Conductivity [W/m·K]	Fuel Savings [%]	Solid [kJ/s]	Flue gas [kJ/s]	Kiln car [kJ/s]	HTR [kJ/s]	LTR [kJ/s]	Wall Loss [kJ/s]	Bottom Loss [kJ/s]
0.1	20	683	1187	451	139	840	254	21
0.5	5	703	1262	685	292	851	252	67
1	0.5	715	1392	670	294	857	253	85
1.5	0	713	1523	626	246	828	256	94

The temperature profile of the carrier plate with a conductivity of 0.1 W/m·K along the roof tile kiln is depicted in **Figure 7-9**. Because of the lower conductivity of the carrier plate, the heat flow rate from the top plate to the bottom of the carrier plate is restricted. This is the reason for the bottom temperature of the carrier plate to remain the same in the preheating zone. The top temperature of the carrier plater is higher than the roof tile in the preheating zone which minimises the heat loss from the roof tile to the kiln car. The temperature difference between

the top and bottom of the low conductivity carrier plate is around 850 K whereas in a high conductivity carrier plate, it is 300 K at the start of the firing zone. In the high conductivity carrier plate at a position of 65 m, almost the entire plate is heated to a temperature of 850°C as seen in Figure 7-7. But in a low conductivity carrier plate, the maximum temperature reached by the bottom surface is 250°C.

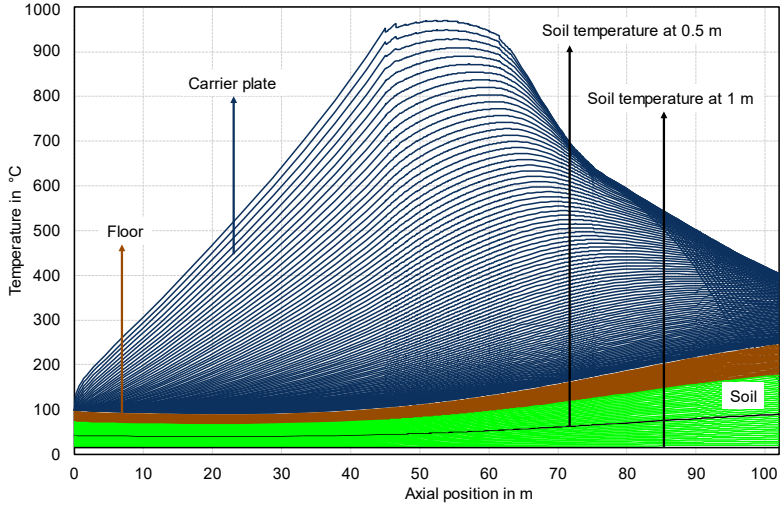

Figure 7-9 Temperature profiles of carrier plate (λ = 0.1 W/m·K), floor and soil along roof tile kiln

7.5 Kiln Car as Base Construction

7.5.1 Stationary Kiln Car Information

The idea of a supporting plate, insulation, and base under the rollers as seen in [42], requires the kiln cars which are currently in the tunnel kiln to be fully scraped. This leads to an enormous financial burden to the tunnel kiln owners which are predominantly family-owned small and medium-scale enterprises. The kiln car will be retained as the stationary base on which the ceramic rollers are supported. The carrier plates are pushed on the rollers which carry the ware along the tunnel kiln as shown in **Figure 7-10**. The tunnel kiln producing bricks and roof tiles which were described in sections 7.3.2 and section 7.3.3 are re-

simulated with stationary kiln cars along the tunnel kiln supporting the rollers and the carrier plate (dimensions same as from section 7.4). With the addition of the carrier plate ($\lambda = 1.5$ W/m·K) and the rollers in the tunnel kiln, the number of rows of bricks and roof tiles along the vertical direction is reduced from 14 to 11. This corresponds to a reduction in the mass flowrate of the brick and roof tile by 22%.

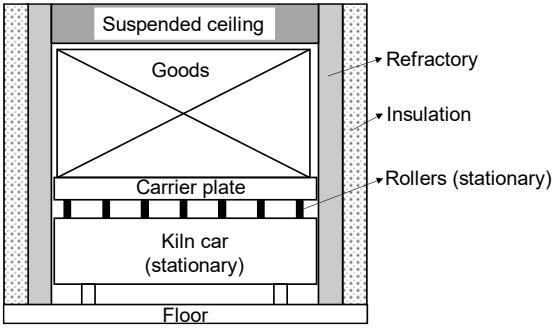

Figure 7-10 Carrier plate on rollers which are supported on kiln cars

7.5.2 Brick Kiln

The temperature profile of the carrier plate, the stationary kiln car, the floor, and the soil along the tunnel kiln, when the firing curve of the brick is achieved, is depicted in **Figure 7-11**. The temperature profile of the stationary kiln car is different from the temperature profile of the kiln car in a tunnel kiln where it is moving as seen in Figure 6-8. The maximum temperature in the 5th material layer of the stationary kiln car is 700 °C as compared to 300 °C in the moving kiln car. The 4th material layer in the moving kiln car also reaches a maximum temperature of 300 °C whereas in the stationary kiln car, it is about 750 °C. For the 3rd material layer, the maximum temperature in the stationary kiln car and moving kiln car are 850 °C and 500 °C respectively. In the 2nd material layer of the stationary kiln car, the maximum temperature difference is about 200 K with the highest temperature in the firing zone being about 1080 °C. The 2nd material layer in the moving kiln car has a maximum temperature difference of 500 K with a maximum temperature of approximately 950 °C. The 1st material layer in the stationary kiln car

has a maximum temperature difference of 50 K as compared to the 300 K in the moving kiln car.

The top and the bottom surface of the carrier plate tend to have a temperature difference of 100 K and the temperature of the carrier plate reduces more than the temperature of the 1st material layer of the stationary kiln car as seen in Figure 7-11. In the firing zone, the maximum temperature of the top of the floor is about 600 °C and at the end of the cooling zone the temperature is 100 °C. The temperature of the soil at a depth of 0.5 m in the firing zone reaches a temperature of more than 200 °C whereas the temperature at a depth of 1 m remains at a constant 15 °C.

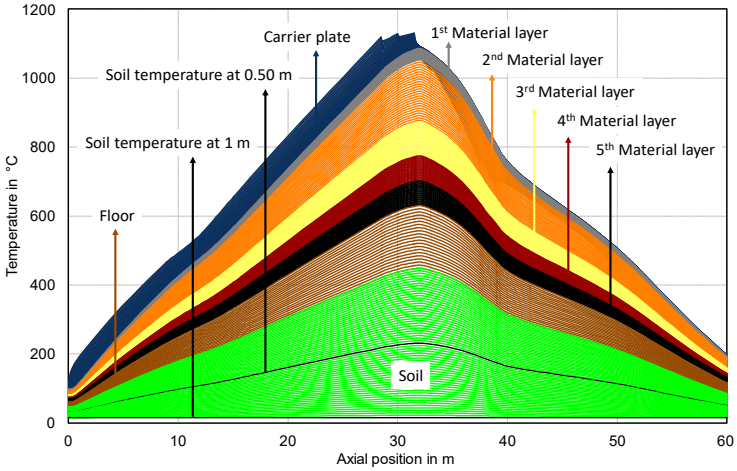

Figure 7-11 Temperature profiles of the carrier plate, kiln car (stationary), floor and soil along the brick kiln

7.5.3 Roof Tile Kiln

As seen in **Figure 7-12**, for a distance of 5 - 10 m inside the tunnel kiln, the temperature inside the stationary kiln does not increase and remains the same. This is because of the high velocity of the carrier plate in the roof tile kiln than in the brick kiln. The high temperature difference between the top and bottom of the carrier plate in the roof tile kiln than in brick kiln is also due to the low residence time of the

carrier plate. In a kiln with a moving kiln car, the maximum temperature difference in the first material layer is about 500 K as seen in Figure 6-9. But in the kiln with a stationary kiln car, the maximum temperature difference is about 50 K. For the second material layer, it is about 300 K in the moving kiln car and about 250 K in the stationary kiln car and both occur in the cooling zone of the kiln. At the outlet of the kiln, the third material layer in the moving kiln car has a maximum temperature of 300 °C and a maximum temperature difference of 150 K whereas in the stationary kiln car, the maximum temperature is about 450 °C and the maximum difference is 50 K. The fifth material layer, which is the bottommost layer in the kiln car has a maximum temperature of 120°C and 550°C in the moving kiln car and stationary kiln car respectively. The top temperature of the carrier plate reaches a maximum temperature of 950°C in the firing zone. In the cooling zone, the temperature of the upper surface of the carrier plate becomes lower than that of the material layers in the stationary kiln car.

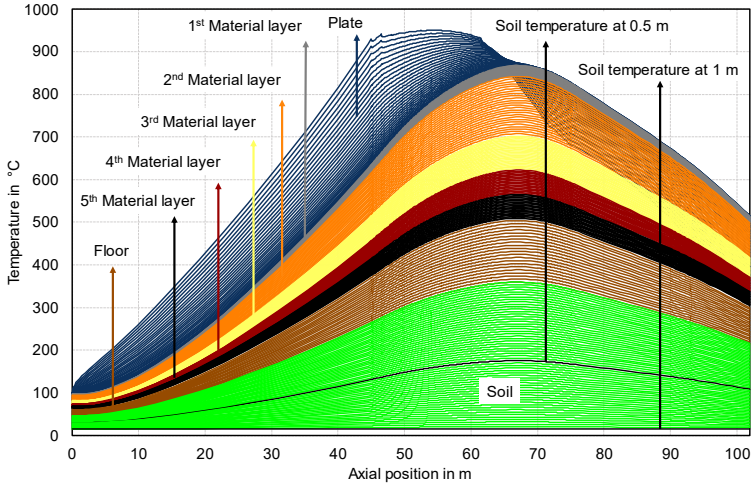

Figure 7-12 Temperature profiles of the carrier plate, kiln car (stationary), floor and soil along the roof tile kiln

In the kiln with the stationary kiln car, the floor gets a maximum temperature of 500°C in the rapid cooling zone. The temperature of the

soil beneath the tunnel kiln with the stationary kiln car also increases to a maximum temperature of 350°C and 150°C at a depth of 0.5 m.

7.6 Comparison of Transportation Systems

7.6.1 Kiln Information

The different kinds of transportation systems used for moving the ware along the tunnel kiln are the normal kiln car, the carrier plate ($\lambda = 1.5$ W/m·K) as kiln car (dimensions same as in section 7.4) and the carrier plate on the stationary kiln car. The tunnel kiln producing bricks and roof tile which were described in section 7.3.2 and section 7.3.3 are re-simulated for all the different types of transportation systems. The mass flow rate of the brick and roof tile is equal to the mass flow rate described in section 7.4 and the height of the tunnel kiln above the transportation system is equal in all the different cases and is 0.87 m.

7.6.2 Brick Kiln

The outlet energy of the tunnel kilns with various transportation systems is given in **Table 7-7**. The outlet energy of the bricks from all the tunnel kilns remains the same which is because of the same mass flow rate of the bricks. Energy loss through the gas and walls remains also the same in the various tunnel kiln. The energy loss through the HTR and LTR remains the same in all the different tunnel kilns showing that a reduction of the amount of cooling air is not achieved when the heavy kiln car is replaced with the carrier plate. The fuel consumption in the tunnel kiln with a carrier plate on the tunnel kiln floor reduces by 10 % whereas the energy loss through the bottom increases to 61 kJ/s from 10 kJ/s. In the tunnel kiln where the carrier plate is on the stationary kiln car, the energy savings is about 12 % and the bottom energy loss is 36 kJ/s compared to 10 kJ/s in a tunnel kiln with a normal kiln car as a transportation system.

As mentioned in section 7.4.2, when the conductivity of the carrier plate is reduced to 0.1 W/m·K the energy saving is 14% compared to a carrier plate with conductivity of 1.5 W/m·K. When a carrier plate of conductivity of 0.1 W/m·K is used the fuel consumption can be reduced

by 23% in kilns without stationary kiln cars and by 25% in kilns with stationary kiln cars.

Table 7-7 Comparison of the outlet energy of brick kilns with various transportation systems

TS	Fuel Savings [%]	Ware [kJ/s]	Flue gas [kJ/s]	TS [kJ/s]	HTR [kJ/s]	LTR [kJ/s]	Wall loss [kJ/s]	Bottom loss [kJ/s]
Kiln car	0	68	333	212	217	118	141	10
Carrier plate	10	63	314	35	211	111	140	61
Carrier plate on stationary kiln car	12	63	316	37	219	105	140	36

7.6.3 Roof Tile kiln

The outlet energy from the tunnel kilns with different transportation systems is given in **Table 7-8**. The carrier plate is considered to have a thermal conductivity of 1.5 W/m·K. In the tunnel kiln with the carrier plate, the energy loss through the HTR increases to 302 kJ/s from 86 kJ/s. This is because of the need for high cooling air to counteract the heat which is radiated from the carrier plate to the roof tile. The energy loss through the HTR also increases in the case when the carrier plate is on the stationary kiln car. The bottom loss increases in the case with carrier plate and carrier plate on kiln car to 93 kJ/s and 54 kJ/s respectively. The amount of fuel saved is 3% when the transportation system is carrier plate and 4% when the carrier plate is on the stationary kiln car.

When the conductivity of the carrier plate is changed to 0.1 W/m·K, as mentioned in section 7.4.3, the achieved energy saving is 20%. Therefore, when a carrier plate of conductivity 0.1 W/m·K is considered, the amount of fuel consumption can be reduced to 22%. When the carrier plate is on the stationary kiln car the fuel consumption reduces by 23%.

Table 7-8 Comparison of the outlet energy of roof tile kilns with various transportation systems

TS	Fuel Savings [%]	Ware [kJ/s]	Flue gas [kJ/s]	TS [kJ/s]	HTR [kJ/s]	LTR [kJ/s]	Wall loss [kJ/s]	Bottom loss [kJ/s]
Kiln car	0	553	120	1427	86	721	237	13
Carrier plate	3	560	125	624	302	637	238	93
Carrier plate on stationary kiln car	4	577	127	643	224	655	240	54

7.7 Reducing the Stack Height

7.7.1 Thickness of Kiln Car

The reduction in the thickness of the kiln car reduces the capability of the kiln car to transport the ware through the tunnel kiln. Hence the mass of ware on the kiln car has to be reduced. The reduction in the mass of the ware on the kiln car is achieved by reducing the number of vertical layers (stack) of the ware. To overcome the decreased production rate by reducing the stack height, the velocity of the kiln car should be increased such that the production rate remains the same. The kiln car thickness is kept a minimum of 1% which means a thickness of 6.83 mm. This thickness allows to study the effect of

reducing the stack height on the process without the influence of a heavy kiln car.

7.7.2 Brick Kiln

The brick kiln described in section 7.3.2 has a mass of the brick per unit area of the top surface of the kiln car of 678 kg/m^2. The total number of vertical layers of brick on the kiln car is 14 with a total height of 0.98 m. Two different stack heights were chosen to find the influence on the tunnel kiln process. The first case has a stack height of 0.87 m which corresponds to 11 layers of bricks on the kiln car. This case has a mass per unit area of the kiln car to be 532 kg/m^2. The second case has a stack height of 0.59 m where the number of layers of bricks is equal to 7. In this case, the mass per unit area of the kiln car is 339 kg/m^2. The first case where the number of layers is 11 and the second case where the number of layers is 7 can be considered as cases where the stack height is approximately 75% and 50% of the initial stack height respectively. The velocity of the kiln car should be increased by approximately 28% and 100% to keep the production rate constant when the stack height is reduced to 75% and 50%.

The influence of the change in the stack height without changing the production rate on the tunnel kiln process is shown in **Figure 7-13**. When the stack height is reduced to 75% and 50% of the initial stack height, the maximum temperature achieved by the bricks reduces to 1050°C and 900°C respectively. The exit temperature of the bricks increases to 180°C and 225°C when the stack height is 75% and 50% respectively. The decrease in the temperature of the brick between 9 m and 12 m is because the endothermic reactions are programmed to occur at these locations. The temperature of the heated cooling air entering into the firing zone when the stack height is 75% and 50% is 650°C and 500°C respectively. When the stack height is 100% the temperature of the heated cooling air entering the firing zone was 750°C.

When the stack height is reduced, the area of the bricks for heat exchange reduces which means that A_{Solid} in the equation (6-2) also reduces. When the area of heat exchange reduces, the rate of change

of temperature of the gas with respect to the distance also reduces. When the rate of change of the temperature of the gas reduces, the temperature of the gas reduces in the cooling zone, and the temperature increase of the cooling air along the cooling zone also reduces. This is the reason for the reduced temperature of the heated cooling air entering the firing zone when the stack height is reduced. When this temperature reduces, the temperature achieved by the combustion of natural gas also reduces. This causes a reduction in the maximum temperature achieved by the combustion gas in the firing zone ultimately leading to a reduced temperature of the bricks in the firing zone.

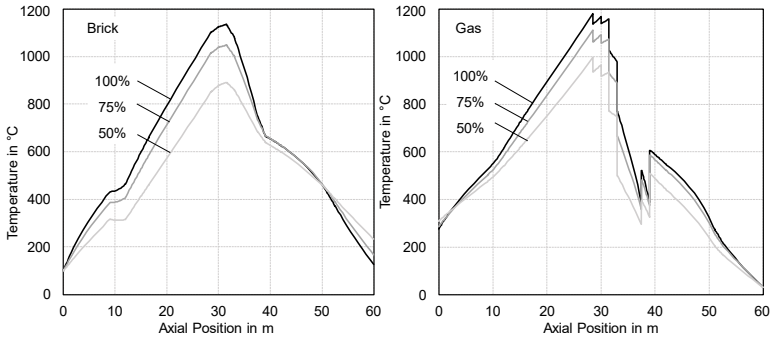

Figure 7-13 Temperature profile of brick (right) and gas (left) for different stack heights

The changed temperature profile of the brick, when the stack height is changed, should be brought back to the firing curve. This is achieved by increasing the fuel supply in the firing zone and the mass flow rate of the cooling air in the cooling zone accordingly. **Figure 7-14** shows the change in the mass flow rate of the fuel and the various inlets and outlets of cooling air to achieve the firing curve with respect to the case when the stack height is 100%. The amount of fuel required to increase the temperature of the brick in the firing zone increases by 25% and 80% when the stack height is reduced to 75% and 50% respectively. The amount of rapid cooling air also increases similarly as compared to the mass flow rate of the fuel in both cases. The mass flow rates of the supply air, LTR, and HTR increase also in a similar for both cases

when the stack height is reduced. The mass flow rates of supply air, LTR, and HTR increase by more than 100%, to reduce the temperature of the brick in the cooling zone to overcome the negative effect caused by the reduced area of brick for heat exchange.

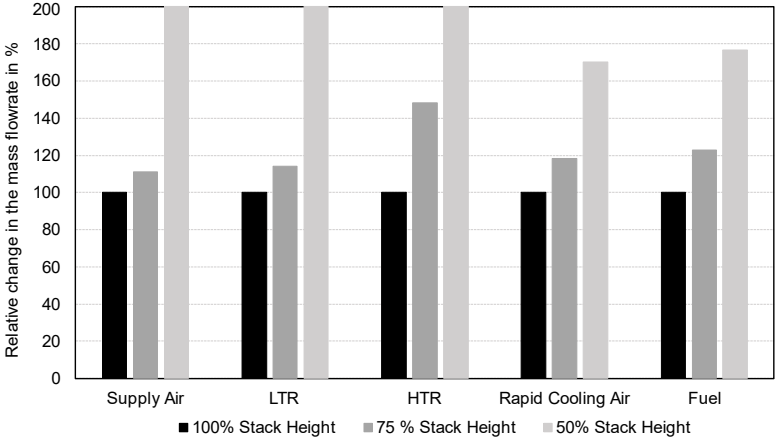

Figure 7-14 Change in the mass flow rate of various inlets and outlets to maintain the firing curve of the brick when the stack height is changed

7.7.3 Roof Tile kiln

The roof tile kiln in section 7.3.3 has a mass of roof tiles per unit area of the kiln car to be 317 kg/m^2. There are 14 layers of roof tiles and cassette on the kiln car with a total height of the stack to be 0.98 m. When the stack height is approximately 75% of the initial stack height, the mass per square meter of roof tile on the kiln car becomes 249 kg/m^2. The height of the stack is 0.87 m and the number of layers reduces to 11. When the stack height is 50%, the height of the stack is 0.49 and the number of layers is 7. The mass of the roof tiles per unit area of the top surface of the kiln car is 158 kg/m^2.

The temperature profile of the roof tiles and gas, when the stack height is reduced, are shown in **Figure 7-15** for a constant production rate. The maximum temperature of the roof tiles achieved in the firing zone when the stack height is reduced to 75 % and 50%, is 950°C and 810°C respectively. The temperature of the heated cooling air from the cooling

zone that is entering the firing zone when the stack height is 100% is almost 720°C. When the stack height is reduced to 75% and 50% of the initial height, the temperature of the heated cooling air reduces to 680°C and 550°C respectively. The area of the roof tiles for heat exchange reduces when the height of the stack is reduced. This results in a reduced rate of change in the temperature of the gas along the cooling zone, leading to a reduced temperature of the heated cooling air at the end of the firing zone.

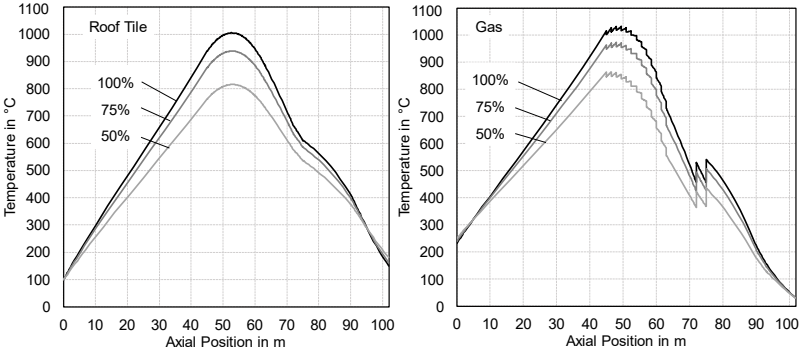

Figure 7-15 Temperature profiles of roof tile (right) and gas (left) for different stack heights

Figure 7-16 shows the change in the mass flow rate of fuel and the mass flow rates of the various inlets and outlets of the cooling air to achieve the firing curve relative to the case when stack height is 100%. The amount of fuel and supply air increase by 10% and 15% respectively when the stack height is reduced to 75%. When the stack height is reduced to 50%, the amount of fuel and supply air increases by 35% and 25% respectively. The mass flow rate from the HTR increases by more than 200% when the stack height is reduced to 50%.

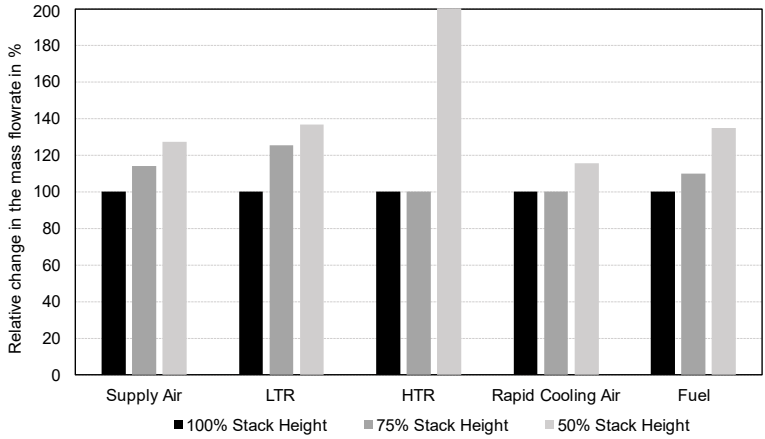

Figure 7-16 Change in the mass flow rate of various inlets and outlets to maintain the firing curve of the roof tiles when the stack height is changed

When the stack height is reduced by 75% and 50% to maintain the production rate constant, the velocity of the kiln car is increased by 30% and 100% in both the brick kiln and roof tile kiln. This causes a reduced residence time in all the different zones of the tunnel kiln correspondingly. The reduced residence time means the heating rate in the preheating zone will be high and the cooling rate in the cooling zone will also be high. The time spent by the ware in the firing zone at a temperature of 1100°C for brick and 950°C for roof tile also reduces. As seen in section 6.1, for the ware to have its desired physical properties, the total residence time in the tunnel kiln is 60 hours and 16.5 hours for brick and roof tile respectively. Because of the reduced residence time and the increased heating and cooling rate, the desired product quality will not be achieved when the stack height is reduced and the velocity is increased to maintain the production rate.

8 Conclusion

The model takes into account the heat transfer between all the different mediums in the tunnel kiln. Between the gas and the ware and furniture, the convective and radiative heat transfer are considered along with the transient conduction in the ware. Between the ware and the kiln car, the radiative heat transfer is considered and the conduction of the heat through the kiln car is also modeled. The convective and radiative heat transfer between the kiln car and the gas are also added to the model. The heat lost through the kiln walls to the outside ambient air from the gas is calculated in the model to obtain the temperature of the outer walls of the tunnel kiln. The model is validated with the experimental result from a roof tile producing tunnel kiln. The model can be extended to other tunnel kilns producing ceramics such as sanitary wares and vitrified pipes.

The model can be used to gain insights into which kind of heat transfer is dominant between each flow in the tunnel kiln. In the roof tile producing tunnel kiln, the radiation between the kiln car and the roof tile is much higher than between the kiln car and the bricks. The temperature profiles of the kiln car in the brick tunnel kiln are different from that in the roof tile tunnel kiln. This is due to the high residence time in the brick kiln compared to the roof tile kiln. The percentage of the energy coming out with the kiln car to the total outlet energy is about 30% and 20% for the roof tile and brick tunnel kiln respectively. The model can be used by the manufacturer of the kiln car to design kiln cars depending upon the residence time of the kiln car. The aim of the design should be to minimize the heat absorption in the preheating and firing zone without reducing the stability. This will help the kiln car manufacturers understand the influence of different designs of kiln cars on the process for tunnel kilns which require different residence times.

For achieving the goal of a carbon-neutral tunnel kiln process, there is no single way but a combination of a number of measures. The measures include changing the composition of the raw material for ceramic production to remove the process emissions, improving the thermal efficiency of the kiln by using preheated combustion air,

increasing the area covered by one roof tile, and reducing the mass of the brick. The model can be used to create a carbon-neutral tunnel kiln by incorporating the measures. The model can also be applied to an existing tunnel kiln, to find out the influence of each measure on the process before any costly retrofitting is done on the tunnel kiln.

Further works which can be done to improve the model are listed below.

- The temperature of the gas is considered homogeneous in the vertical direction. But in reality, the temperature is non-homogeneous in the vertical direction with a temperature of more than 150K, especially in the preheating zone. As seen in **Figure A-2** from Appendix I, the vertical simulated temperature distribution of the different layers of the roof tiles are not matching the experimental result as shown in Figure 5-2. From the experimental result, it can be seen that the temperature difference between the top and bottom layers of the roof tile is more than 150 K in the preheating zone. The difference minimizes at the end of the firing zone and then to the cooling zone. In the simulation, the maximum temperature difference between the top and bottom of the roof tiles in the preheating zone is 50 K and almost 0 K in the rapid and static cooling zone.
- In an industrial tunnel kiln, when the parameters in the tunnel kiln process are changed like the change in the production rate, the firing curve of the ware remains the same. This is achieved by adjustment of the mass flow rate of fuel, cooling air, HTR, and LTR automatically by the control systems. In the model, when a process parameter is changed, the firing curve of the ware is recreated by adjusting the mass flow rate of all the inlets and outlets manually. **Figure 8-1** shows which parameters has to be changed manually for a tunnel kiln to obtain the firing after a change in the process parameter. This makes the recreation of the firing curve with the model challenging. Firstly, the behaviour of the model to the change in the mass flow rate of each parameter has to be understood by the user. Then the recreation of the firing curve with the understanding of the behaviour of

each parameter change is time-consuming. Machine learning is efficient at finding patterns and understanding the behaviour of the model. Therefore, machine learning can be used to understand the patterns in the change in the temperature profile of ware when the mass flow rate of any kiln parameter is changed. The aim of using machine learning is to automate the process of finding the mass flow rate of the inlets and outlets as shown in Figure 8-1, to create the firing curve when any process parameter is changed.

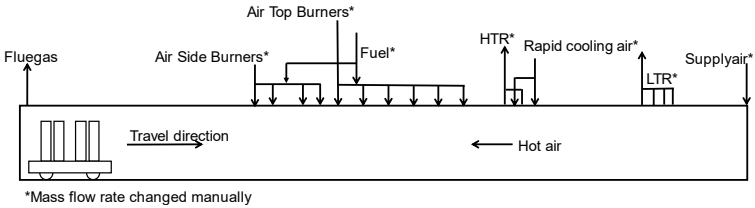

Figure 8-1 Schematic of a tunnel kiln

References

[1] J. Bender, J. Hadley, J. Hellerstein, C. Hohman, Encyclopedia of occupational health and safety, Geneva: International Labor Organisation, 2011.

[2] U. Rajarathnam, V. Athalye, S. Ragavan, S. Maithel, D. Lalchandani, S. Kumar, E. Baum, C. Weyant, T. Bond, Assessment of air pollutant emissions from brick kilns, Atmospheric Environment. 98 (2014) 549–553. https://doi.org/https://doi.org/10.1016/j.atmosenv.2014.08.075.

[3] Z. Zhang, Energy efficiency and environmental pollution of brickmaking in China, Energy. 22 (1997) 33–42. https://doi.org/10.1016/S0360-5442(96)00078-3.

[4] I. González, E. Galán, A. Miras, Fluorine, chlorine and sulphur emissions from the Andalusian ceramic industry (Spain)—Proposal for their reduction and estimation of threshold emission values, Applied Clay Science. 32 (2006) 153–171. https://doi.org/https://doi.org/10.1016/j.clay.2005.07.005.

[5] R. Geres, J. Lausen, S. Weigert, Roadmap für eine treibhausgasneutrale Ziegelindustrie in Deutschland, München, 2021. https://ziegel.de/sites/default/files/2021-03/Ziegel_24_110321_Web_200dpi_1.pdf.

[6] P.E. Jewkes Stephen, Binnie Isla, Gas price surge pushes Europe's ceramics industry to breaking point, Reuters. (2021). https://www.reuters.com/world/europe/gas-price-surge-pushes-europes-ceramics-industry-breaking-point-2021-10-27/.

[7] N. Soussi, W. Kriaa, H. Mhiri, P. Bournot, Reduction of the energy consumption of a tunnel kiln by optimization of the recovered air mass flow from the cooling zone to the firing zone, Applied Thermal Engineering. 124 (2017) 1382–1391. https://doi.org/10.1016/j.applthermaleng.2017.06.111.

[8] E. Mancuhan, E. Alpman, K. Küçükada, Mathematical Modeling and Simulation of the Preheating Zone of a Tunel Kiln, Journal of Thermal Science and Technology. 31 (2011) 79–86.

[9] S. Kaya, K. Küçükada, E. Mançuhan, Model-based optimization of heat recovery in the cooling zone of a tunnel kiln, Applied Thermal Engineering. 28 (2008) 633–641. https://doi.org/10.1016/j.applthermaleng.2007.04.002.

[10] S. Kaya, E. Mançuhan, K. Küçükada, Modelling and optimization of the firing zone of a tunnel kiln to predict the optimal feed locations and

mass fluxes of the fuel and secondary air, Applied Energy. 86 (2009) 325–332. https://doi.org/10.1016/j.apenergy.2008.04.018.

[11] E. Specht, Temperature Measurement of Gases, in: Heat and Mass Transfer in Thermoprocessing., Vulkan Verlag, 2017: pp. 345–346.

[12] G.M. Santos, Study of thermal behavior of a tunnel kiln used in red ceramic industry, Federal University of Santa Catarina, 2001.

[13] F.N. Mônica, S.P.G. Marcos, O.N. Angela, Numerical Simulation of Flow and Heat Transfer Through a Tunnel Kiln, in: 18th International Congress of Mechanical Engineering, 2005: pp. 6–11.

[14] A.H. Tehzeeb, M. Bhuiyan, N. Jayasuriya, Evaluation of Brick Kiln Performances Using Computational Fluid Dynamics (CFD), Energy and Environmental Engineering Journal. 1 (2012) 1–8.

[15] P. Meng, Solid-Solid Recuperation to Improve the Energy Efficiency of Tunnel Kilns, Otto von Guericke University Magdeburg, 2011.

[16] A.G.T. Al-Hasnawi, H.A. Refaey, T. Redemann, M. Attalla, E. Specht, Computational Fluid Dynamics Simulation of Flow Mixing in Tunnel Kilns by Air Side Injection, Journal of Thermal Science and Engineering Applications. 10 (2018). https://doi.org/10.1115/1.4038840.

[17] H.A.. Rafaey, E.. Specht, M.R.. Salem, Influence of fuel distribution and heat transfer on energy consumption in tunnel kilns, International Journal of Advances in Engineering and Technology. 6 (2015) 281–293.

[18] T. Redemann, Entwicklung innovativer Tunnelofenkonzepte zum Brennen von keramischem Gut anhand eines mathematischen Prozessmodells, Otto-von-Guericke-Universität Magdeburg, 2019. https://opendata.uni-halle.de//handle/1981185920/32794.

[19] S. Vogt, K. Nover, The application of computer models for the design and optimization of tunnel kilns in the heavy clay industry, ZI, Ziegelindustrie International/Brick and Tile Industry International. 44 (1991) 549–556.

[20] V.G. Abbakumov, G. Aschinadse, Konvektiwny teploobmen w tunnelnych petschach (Convective heat transfer in tunnel kiln), Ogneupory. 40 (1972) 20–27.

[21] K. Elgeti, Ein neues Verfahren zur Brechnung des Strahlungsaustauches zwischen einem Gas und einer grauen Wand, Brennstoff-Wärme-Kraft. 14 (1962) 1–6.

[22] R. Jeschar, Das Temperaturfeld einer beidseitig im Gegenstrom beheizten ebenen Platte, Arch. Eisenhüttenw. 37 (1966) 193–200.

[23] V.G. Abbakumov, The heat resistance of various types of setting in tunnel-kiln cars, Refractories. 7 (1966) 18–23. https://doi.org/10.1007/BF01281868.

[24] V. De Paulo Nicolau, A.P. Dadam, Numerical and experimental thermal analysis of a tunnel kiln used in ceramic production, Journal of the Brazilian Society of Mechanical Sciences and Engineering. 31 (2009) 297–304. https://doi.org/10.1590/s1678-58782009000400003.

[25] R. Oba, P. Talita Sauter, N. Vicente De Paulo, Numerical Simulation of Tunnel Kilns Applied To White Tile With Natural Gas, in: 21st Brazilian Congress of Mechanical Engineering, 2011.

[26] R. Oba, T.S. Possamai, V.P. Nicolau, Thermal analysis of a tunnel kiln used to produce roof tiles, Applied Thermal Engineering. 63 (2014) 59–65. https://doi.org/10.1016/j.applthermaleng.2013.10.063.

[27] B. YU, Dynamic Modeling of a Tunnel Kiln, Heat Transfer Engineering. 15 (1994) 39–53. https://doi.org/10.1080/01457639408939823.

[28] Xu, Zhongsheng, Energy saving ways of the refractory industrial tunnel kiln (in Chinese), Refractories. 3 (1984) 51–53.

[29] H. Hagens, R. Jeschar, P. Jeschke, H. Kainer, THEORETICAL INVESTIGATIONS ON THE THERMAL BEHAVIOR OF TUNNEL KILN CARS., CFI Ceramic Forum International. 64 (1987) 145–153.

[30] H. Hagens, H. Kainer, J. Sommerer, The Role of Tunnel Kiln Car in the Brick and Tile Industry, InterCeram: International Ceramic Review. 1 (1985) 25–27.

[31] H. Hagens, H. Kainer, J. Sommerer, The Role of the Tunnel Kiln Car in the Brick and Tile Industry - Part II, InterCeram: International Ceramic Review. 2 (1986) 19–22.

[32] Y. Zhang, J. Wang, T. Redemann, E. Specht, Thermal behavior of kiln cars while traveling through a tunnel kiln, Advances in Mechanical Engineering. 7 (2015) 1687814015588468. https://doi.org/10.1177/1687814015588468.

[33] CP, Kiln car construction, (2015). https://grabcad.com/library/kiln-car-study-1 (accessed November 13, 2022).

[34] M. Zhu, CFD analysis of a gas flow through a roof tile setting in tunnel kiln with focus on convective heat transfer., Otto-von-Guericke-Universität Magdeburg, 2018.

[35] E. Pohlhausen, Der Wärmeaustausch zwischen festen Körpern und Flüssigkeiten mit kleiner reibung und kleiner Wärmeleitung, ZAMM - Zeitschrift Für Angewandte Mathematik Und Mechanik. 1 (1921) 115–121. https://doi.org/10.1002/zamm.19210010205.

[36] E. Specht, 3.2.3 Nusselt Functions, in: Heat and Mass Transfer in Thermoprocessing, Vulkan Verlag, 2017: pp. 81.

[37] VDI e.V, ed., F2 Heat transfer by free convection, in: VDI Heat Atlas, Second Edi, Springer, Düsseldorf, 2010: p. 669.

[38] S.W. Churchill, A comprehensive correlating equation for laminar, assisting, forced and free convection, AIChE Journal. 23 (1977) 10–16. https://doi.org/10.1002/aic.690230103.

[39] E. Specht, Heat and Mass Transfer in Thermoprocessing, Vulkan Verlag, 2017.

[40] E. Specht, Radiation exchange between two walls, in: Heat and Mass Transfer in Thermoprocessing, Vulkan Verlag, 2017: pp. 341–343.

[41] M.V. Vasić, L. Pezo, J.D. Zdravković, Z. Bačkalić, Z. Radojević, The study of thermal behavior of montmorillonite and hydromica brick clays in predicting tunnel kiln firing curve, Construction and Building Materials. 150 (2017) 872–879. https://doi.org/10.1016/j.conbuildmat.2017.06.068.

[42] T. Redemann, E. Specht, Roadmap for Energy Efficient Firing of Ceramics, in: V. Scherer, N. Fricker, A. Reis (Eds.), 13th European Conference on Industrial Furnaces and Boilers, Algarve, 2022.

[43] Deutsche Wetterdienst, Bodentemperatur, (2023). https://www.dwd.de/DE/leistungen/bodentemperatur/bodentemperatur.html (accessed March 30, 2023).

Appendix I - Temperature profiles of different roof tile layers on the kiln car

The model developed in section 4, considers the roof tiles to be a single mass flow rate. This means that the temperature of the roof tiles in different layers on the kiln car will have a uniform temperature in the vertical direction. Figure 4-2 shows the heat transfer between the roof tiles where it is considered as a single entity and gas and kiln car. **Figure A-1** shows the heat exchange between 16 different layers of roof tile and cassette with the gas and the kiln car in the preheating zone.

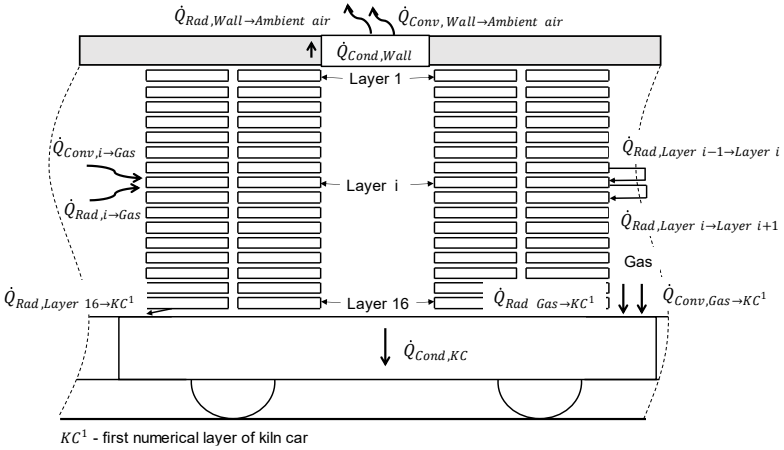

Figure A-1 Heat transfer in the preheating zone with different layers of roof tiles

Here the gas is assumed to have a uniform temperature in the vertical direction. Except for the roof tiles and cassettes on the top and bottom of the stack on the kiln car, each other layer gains heat ($\dot{Q}_{Rad,Layer\ i-1\rightarrow Layer\ i}$) from the layer which is above it and losses heat ($\dot{Q}_{Rad,Layer\ i\rightarrow Layer\ i+1}$) to the layer below it by radiation. The bottommost layer of the losses heat to the first numerical layer kiln car ($\dot{Q}_{Rad,Layer\ 16\rightarrow KC^*}$) in addition to the heat received from the second last layer ($\dot{Q}_{Rad,Layer\ 15\rightarrow Layer\ 16}$) by radiation. The radiative heat exchange between the top roof tile and cassette, to the top wall is neglected to

reduce the complexity. Each layer of roof tile and cassette gains heat from the gas by convection ($\dot{Q}_{Conv,Gas\rightarrow Layer\ i}$) and by radiation ($\dot{Q}_{Rad,Gas\rightarrow Layer\ i}$).

The equation (4-3) is for the case with the 16 layers of roof tiles and cassette as a single entity and hence only one ordinary differential equation. In the case when each layer's temperature profile is to be simulated, each layer is represented by its ordinary differential equation. The total number of ordinary differential equations representing the roof tiles and cassettes is equal to the number of layers which is 16. The ordinary differential equations for the first layer, $i^{th,}$ and last layer are equation (A-1), (A-2) and (A-3) respectively.

$$\dot{m}_{Layer\ 1}c_{Layer\ 1}\frac{dT_{Layer\ 1}}{dx} = \dot{Q}_{Gas\rightarrow Layer\ 1} - \dot{Q}_{Layer\ 1\rightarrow Layer\ 2} \quad \text{(A-1)}$$

$$\dot{m}_{Layer\ i}c_{Layer\ i}\frac{dT_{Layer\ i}}{dx} = \dot{Q}_{Gas\rightarrow Layer\ i} + \dot{Q}_{Layer\ i-1\rightarrow Layer\ i} - \dot{Q}_{Layer\ i\rightarrow Layer\ i+1} \quad \text{(A-2)}$$

$$\dot{m}_{Layer\ 16}c_{Layer\ 16}\frac{dT_{Layer\ 16}}{dx} = \dot{Q}_{Gas\rightarrow Layer\ 16} + \dot{Q}_{Layer\ 15\rightarrow Layer\ 16} - \dot{Q}_{Layer\ 16\rightarrow KC^1} \quad \text{(A-3)}$$

The ordinary differential equation of the first numerical layer of the kiln car is also changed and is rewritten as equation (A-4).

$$\dot{M}_1 c_1 \frac{dT_1}{dx} = \dot{Q}_{Gas\rightarrow KC^1} + \dot{Q}_{Layer\ 16\rightarrow KC^1} - \dot{Q}_{KC^1\rightarrow KC^2} \quad \text{(A-4)}$$

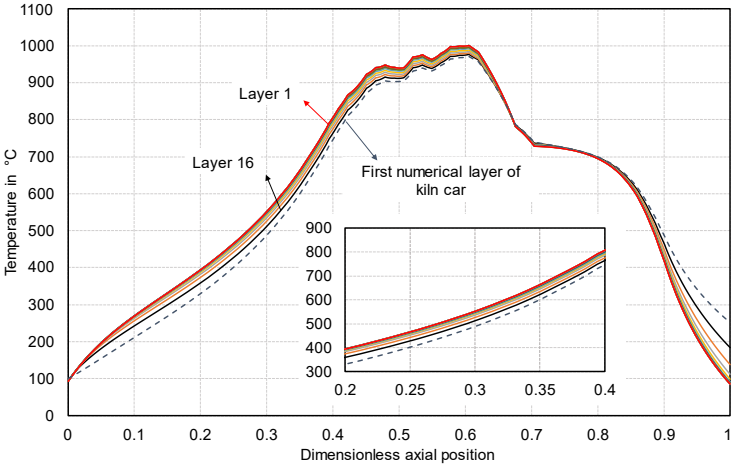

Figure A-2 Simulated temperature profiles of different layers of roof tiles along the tunnel kiln

Figure A-2 shows the simulated temperature profiles of the different layers of the roof tiles. Layer 1 and Layer 16 refer to the topmost and bottommost layers of roof tiles respectively. The maximum temperature difference between the top and bottom layers in the preheating zone and firing zone is about 50 K. In the cooling zone, the difference ranges from 0 K to 100 K. In reality, as seen in Figure 5-2, the difference in the preheating zone and firing zone can be more than 100 K whereas in the cooling zone, the maximum difference is about 50 K. In the program, the gas is assumed to have a uniform temperature along the vertical direction which is not the case in an industrial setting. In the preheating zone of the industrial tunnel kiln, the vertical difference in the temperature of the gas is more than 100 K. The vertical difference in temperature of the gas reduces in the firing zone because of the high-speed burners and in the cooling zone because of many locations for injection and extraction of air.

List of publications

1. Alex, D. M.; Redemann, T.; Specht, E.: Development of Process Model for the Manufacturing of Sanitary Ware in Tunnel Kiln. 12th European Conference on Industrial Furnaces and Boilers, Porto (Online), 2020
2. Alex, D. M.; Redemann, T.; Specht, E.: Process Modelling of a Sanitary Ware Tunnel Kiln. American Ceramic Society Bulletin, Vol. 100, No. 2, 2021
3. Alex, D. M.; Redemann, T.; Specht, E.: Effect of kiln car on the tunnel kiln process. 13th European Conference on Industrial Furnaces and Boilers, Algarve, 2022
4. Alex, D. M.; Redemann, T.; Specht, E.: Energy Optimization of A Roof Tile Producing Tunnel Kiln by Examining the Kiln Car Physical Properties. 9th International Conference on Fluid Flow, Heat and Mass Transfer (FFHMT'22), Niagara Falls, 2022, DOI: 10.11159/ffhmt22.177
5. Alex, D. M.; Redemann, T.; Specht, E.: Effect of kiln car weight on the tunnel kiln process. Thermal Science and Engineering Progress, Vol. 41, DOI: 10.1016/j.tsep.2023.10186